

UNCLASSIFIED

AD NUMBER
AD437951
NEW LIMITATION CHANGE
TO Approved for public release, distribution unlimited
FROM Distribution authorized to U.S. Gov't. agencies only; Administrative/Operational Use; MAR 1964. Other requests shall be referred to Army Signal Corps, Washington, DC.
AUTHORITY
USAEC ltr, 5 Jan 1971

THIS PAGE IS UNCLASSIFIED

**UNCLASSIFIED**

**4 3 7 9 5 1**

**AD**

---

**DEFENSE DOCUMENTATION CENTER**

FOR

**SCIENTIFIC AND TECHNICAL INFORMATION**

**CAMERON STATION, ALEXANDRIA, VIRGINIA**



**UNCLASSIFIED**

NOTICE: When government or other drawings, specifications or other data are used for any purpose other than in connection with a definitely related government procurement operation, the U. S. Government thereby incurs no responsibility, nor any obligation whatsoever; and the fact that the Government may have formulated, furnished, or in any way supplied the said drawings, specifications, or other data is not to be regarded by implication or otherwise as in any manner licensing the holder or any other person or corporation, or conveying any rights or permission to manufacture, use or sell any patented invention that may in any way be related thereto.

# High-Frequency Oscillography with Electrostatically Deflected Ink Jets

by  
Richard G. Sweet

March 1964

Technical Report No. 1722-1

Prepared under  
Signal Corps Contracts  
DA 36(039) SC-87300 and  
DA 36(039) AMC-03761(E)

437951

437951

017 1722-1

NC

**SYSTEMS TECHNIQUES LABORATORY**  
**STANFORD ELECTRONICS LABORATORIES**  
STANFORD UNIVERSITY • STANFORD, CALIFORNIA

**DDC AVAILABILITY NOTICE**

**Qualified requesters may obtain copies of this report from DDC. Foreign announcement and dissemination of this report by DDC is limited.**

SEL-64.004

HIGH-FREQUENCY OSCILLOGRAPHY WITH  
ELECTROSTATICALLY DEFLECTED INK JETS

by

Richard G. Sweet

March 1964

Reproduction in whole or in part  
is permitted for any purpose of  
the United States Government.

Technical Report No. 1722-1

Prepared under  
Signal Corps Contracts DA 36(039) SC-87300  
and DA 36(039) AMC-03761(E)

Systems Techniques Laboratory  
Stanford Electronics Laboratories  
Stanford University                      Stanford, California

## ABSTRACT

This report describes a method of forming, charging, and electrostatically deflecting a high-speed jet of small, fluid droplets, and the application of this technique to a high-frequency oscillograph in which the recorded trace is written directly by a jet of ink.

In a typical experimental model of the ink-jet oscillograph, a jet of ink, 0.0035 cm in diameter, is divided into a regular succession of droplets that are formed at a rate of 100,000/sec. The droplets are electrically charged, as they form, in proportion to the amplitude of the signal to be recorded. A record of the input signal is made by intercepting the droplets on a moving strip of paper after they have passed through a constant deflecting field. The mark made by each droplet is an independent sample of the input drop-charging signal. The oscillograph combines 1) a frequency response that exceeds that obtainable with mirror-galvanometer systems employing expensive photo-sensitive recording paper, with 2) the instant visibility, contrast, resolution, permanence, and economical operation of moving-pen or -stylus recorders.

We have constructed experimental oscillographs that produce traces with amplitudes up to 2 cm peak-to-peak; this 2-cm span may be traversed in as little as 10  $\mu$ sec. The amplitude accuracy of the record is typically  $\pm 5$  percent and is limited by spurious deflections of the ink droplets during flight caused by aerodynamic drag and mutual electrostatic repulsion between adjacent charged droplets. A flow of air is established in the space traversed by the ink droplets, decreasing the variation in aerodynamic force on different droplets. An analysis of distortion phenomena indicates that fidelity decreases as parameters of the system are changed to give higher maximum trace amplitude or higher drop-formation frequency.

The rate at which ink is delivered to the paper may be reduced, independent of the rate at which it issues from the nozzle, by intercepting a fraction of the ink in transit. This feature extends the usefulness of the recording technique to very low writing speeds, where the record would otherwise be blurred by a surplus of ink.

CONTENTS

	Page
I. INTRODUCTION . . . . .	1
II. DESCRIPTION OF OSCILLOGRAPH AND EXPERIMENTAL RESULTS . . . .	3
A. Ink-Drop Formation and Charging . . . . .	6
1. Drop Formation . . . . .	6
2. Drop Charging . . . . .	8
3. Ink and Ink-Supply System . . . . .	8
4. Ink-Drop Gun . . . . .	9
B. Ink-Drop Deflection . . . . .	11
C. Paper Transport and Ink Interception . . . . .	15
D. Frequency and Transient Response . . . . .	16
E. Distortion . . . . .	17
1. Effect of Parameter Variation on Distortion . . . . .	19
2. Reduction of Distortion Resulting from Aerodynamic Forces . . . . .	21
F. Control of Ink Delivery Rate . . . . .	23
1. Interception of Surplus Ink . . . . .	25
2. Proportioning Ink Flow to Instantaneous Writing Speed . . . . .	25
G. Experimental Test Setup . . . . .	28
H. Record Characteristics . . . . .	31
1. Trace Characteristics . . . . .	31
2. Fidelity . . . . .	32
3. Accuracy . . . . .	32
4. Representative Oscillograms . . . . .	36
III. EVALUATION OF OSCILLOGRAPH AND COMPARISON WITH OTHER TECHNIQUES . . . . .	43
A. Comparison with Conventional Systems . . . . .	43
B. Other Fluid-Jet Systems and Related Techniques . . . . .	44
C. Multiple-Channel Potential . . . . .	45
D. Environmental Considerations . . . . .	45
1. Temperature . . . . .	45
2. Pressure and Humidity . . . . .	46
3. Shock and Vibration . . . . .	46

E. Problem Areas . . . . .	46
1. Stability of Drop-Formation Process . . . . .	46
2. Air-Flow-System Size . . . . .	47
3. Nozzle Clogging . . . . .	47
4. Stability of Deflection Sensitivity . . . . .	47
IV. CONCLUSIONS AND RECOMMENDATIONS FOR FURTHER WORK . . . . .	48
A. Summary of Oscillograph Characteristics . . . . .	48
B. Potential of Ink-Jet Technique as a Practical Recording Method . . . . .	49
C. Applications to Other Fields . . . . .	50
APPENDIXES	
A. Analysis of Ink-Drop Formation and Deflection . . . . .	52
B. Experimental Oscillograph with Air Flowing Collinearly with Ink Jet . . . . .	91
C. Experimental Oscillograph with Rotating Nozzle . . . . .	96
D. Ink-Drop Rate Control System . . . . .	103
REFERENCES . . . . .	106

## ILLUSTRATIONS

Figure	Page
1. Ink-jet oscillograph . . . . .	4
2. Representative oscillograms . . . . .	5
3. Ink-drop formation . . . . .	7
4. Ink-supply system . . . . .	9
5. Ink-drop gun . . . . .	10
6. Ink-drop gun, exploded view . . . . .	11
7. Ink-drop gun and deflection system . . . . .	13
8. Ink drops in flight. . . . .	14
9. Oscillograms showing effect of nozzle vibration . . . . .	14
10. Paper transport, disassembled . . . . .	15
11. Oscillograms showing influence of chart speed on record readability . . . . .	17
12. Oscillograms with small integral number of samples per signal period . . . . .	18
13. Oscillograms showing effect of jet length on record fidelity .	19
14. Oscillograms showing effects of mutual repulsion between ink drops . . . . .	20
15. Effect of air flow on ink-drop wake . . . . .	22
16. Air-flow supply system . . . . .	23
17. Experimental oscillograph with air-flow system . . . . .	24
18. Oscillograms showing effect of air flow across ink stream . .	24
19. Interception of surplus ink . . . . .	26
20. Oscillograms made with various fixed ink-drop rates . . . . .	27
21. Comparison of oscillograms made with fixed and signal-controlled ink-drop rates . . . . .	28
22. Block diagram of complete oscillograph and test setup . . . .	29
23. Experimental recording system . . . . .	30
24. Oscillograms for evaluating fidelity of basic system . . . . .	33
25. Oscillograms for evaluating fidelity of system with air flowing across ink stream . . . . .	34
26. Deflection linearity . . . . .	35
27. Representative low-frequency oscillograms . . . . .	37-39
28. Representative high-frequency oscillograms . . . . .	40-41
29. Oscillograms demonstrating maximum high-frequency performance	42

30. Jet profile showing drop-formation process . . . . .	55
31. Variation of jet instability factor $I$ with disturbance wavelength . . . . .	56
32. Relation between jet diameter, drop diameter, and drop spacing	57
33. Envelope of jet profile showing transition from linear growth to exponential growth of disturbance . . . . .	60
34. Drop-charging configuration . . . . .	63
35. Representation of drop stream as a transmission line . . . . .	63
36. Compensation for transient overshoot . . . . .	64
37. Breakdown gradient for air between plane-parallel electrodes .	66
38. Open-circuit response of distributed RC transmission line to unit-step input voltage . . . . .	67
39. Deflection-system geometry . . . . .	70
40. Aerodynamic-drag coefficient for sphere . . . . .	76
41. Drops in flight for sine-wave record, showing reduction in aerodynamic drag near peaks . . . . .	77
42. Fringing of deflection field . . . . .	79
43. Nozzle and charging-electrode dimensions for numerical example	84
44. Nozzle profile showing calculated ink-pressure components . .	85
45. Experimental oscillograms for numerical example . . . . .	87
46. Diagram of oscillograph with air flowing collinearly with ink-drop stream . . . . .	91
47. Experimental oscillograph with air flowing collinearly with ink-drop stream . . . . .	92
48. Experimental oscillograph, partially disassembled . . . . .	92
49. Closeup of experimental oscillograph . . . . .	93
50. Oscillograms showing effect of air velocity . . . . .	95
51. Oscillograph with rotating nozzle and cylindrical record surface . . . . .	96
52. Raster presentation made by rotating-nozzle oscillograph . . .	97
53. Experimental oscillograph with rotating nozzle . . . . .	97
54. Experimental oscillograph with outer paper guide removed . . .	98
55. Paper transport and inner paper guide . . . . .	99
56. Rotating ink-drop gun . . . . .	100
57. Rotating ink-drop gun with charging electrode and cover plate removed . . . . .	101
58. Oscillogram made with rotating-nozzle oscillograph . . . . .	102
59. Block diagram of ink-drop-rate control system . . . . .	104

ACKNOWLEDGMENT

The author wishes to express his appreciation for the encouragement and advice given by Dr. Raymond Cumming, under whom this investigation was undertaken. The assistance of Messrs. Peter Leal, C. K. Liu, and Richard McMaster, who helped with the design and testing of the experimental systems, and of Mr. Herschel Berkheiser, who constructed much of the experimental apparatus, is also gratefully acknowledged.

## I. INTRODUCTION

This report describes and analyzes a method of forming, charging, and electrostatically deflecting a high-speed jet of small fluid drops, and describes the application of the technique to a high-frequency oscillograph in which the recorded trace is written directly by a jet of ink. The technique offers a method of extending direct-writing oscillography well into the kilocycle frequency range, without the use of light-sensitive recording paper or other expensive or inconvenient writing materials.

The breakup of fluid jets into drops was studied in the 19th century, and the fact that drops of uniform size could be formed by applying small, regularly spaced disturbances to a cylindrical jet was well known. Analyses of the phenomena involved were presented by Lord Rayleigh in several classic papers; these are all contained in or referred to in his "Theory of Sound" [Ref. 1].

The author became aware of these early studies through a popular description of the mechanism by which a fluid jet breaks up into discrete drops, given by C. V. Boys in 1890 and recently republished [Ref. 2]. Boys demonstrated that vibration of the nozzle from which a fluid jet issues results in synchronous division of the jet into drops of uniform size and spacing; it is this phenomenon that is the basis of the oscillograph described here.

The Stanford project was initiated after preliminary experiments verified our predictions that drop-formation frequencies of the systems described by Boys could be increased by decreasing the jet diameter and increasing the jet velocity; that the drops were uniform in size and could be accurately charged, independently, by electrostatic induction; and that useful and precise deflections of the charged drops could be obtained with realizable electrostatic fields.

The techniques described here may have applications in fields other than oscillography. The capability of producing very small fluid drops of precise size in synchronism with an electrical signal, and

accurately controlling their trajectory on a "drop-by-drop" basis should prove useful in many situations. Appropriate fluids would include any moderately conductive, low-viscosity liquid or molten solid.

## II. DESCRIPTION OF OSCILLOGRAPH AND EXPERIMENTAL RESULTS

The configuration of the experimental oscillograph is illustrated by Fig. 1. The parameter values given in the figure and in the remainder of this chapter are for illustration and are typical for systems that have been constructed.

A high-speed jet of ink is divided into a succession of droplets that are electrically charged in proportion to the amplitude of the signal to be recorded. An instantly visible and permanent record of the input signal is made by intercepting the droplets, after they have passed through a constant deflecting field, on a moving strip of paper. A typical drop-formation frequency of 100 kc results in a transient response time for full deflection of 10  $\mu$ sec. A deflection of 1 cm at the record typically requires a signal-input potential of 350 v. Some sample oscillograms made with experimental systems are reproduced in Fig. 2.

The configuration resembles that of a cathode-ray tube with the electrons replaced by a stream of ink drops. It is important, however, to emphasize one essential difference: the transverse field through which the ink stream passes is constant; the signal controls the charge of the particles (drops) in the "beam". Since the charge on each drop constitutes a distinct sample of the input signal, the frequency response is determined by the rate at which charged particles are generated, and is not limited by transit time through the deflection system.

Associated with each projected drop is a turbulent wake of disturbed air extending back along its line of flight. This wake affects the trajectory of subsequent drops if they follow approximately the same path, and results in distortion of the recorded waveform. This distortion is substantially reduced by directing a stream of air, as shown in Fig. 1, across the space traversed by the ink stream. The air flow changes the direction of the drop wake so that interference with following drops does not occur.

The ink flow may be rapidly interrupted or modulated by deflecting the stream to a collector, interposed between nozzle and paper. The collector is positioned so that a deflection greater than that

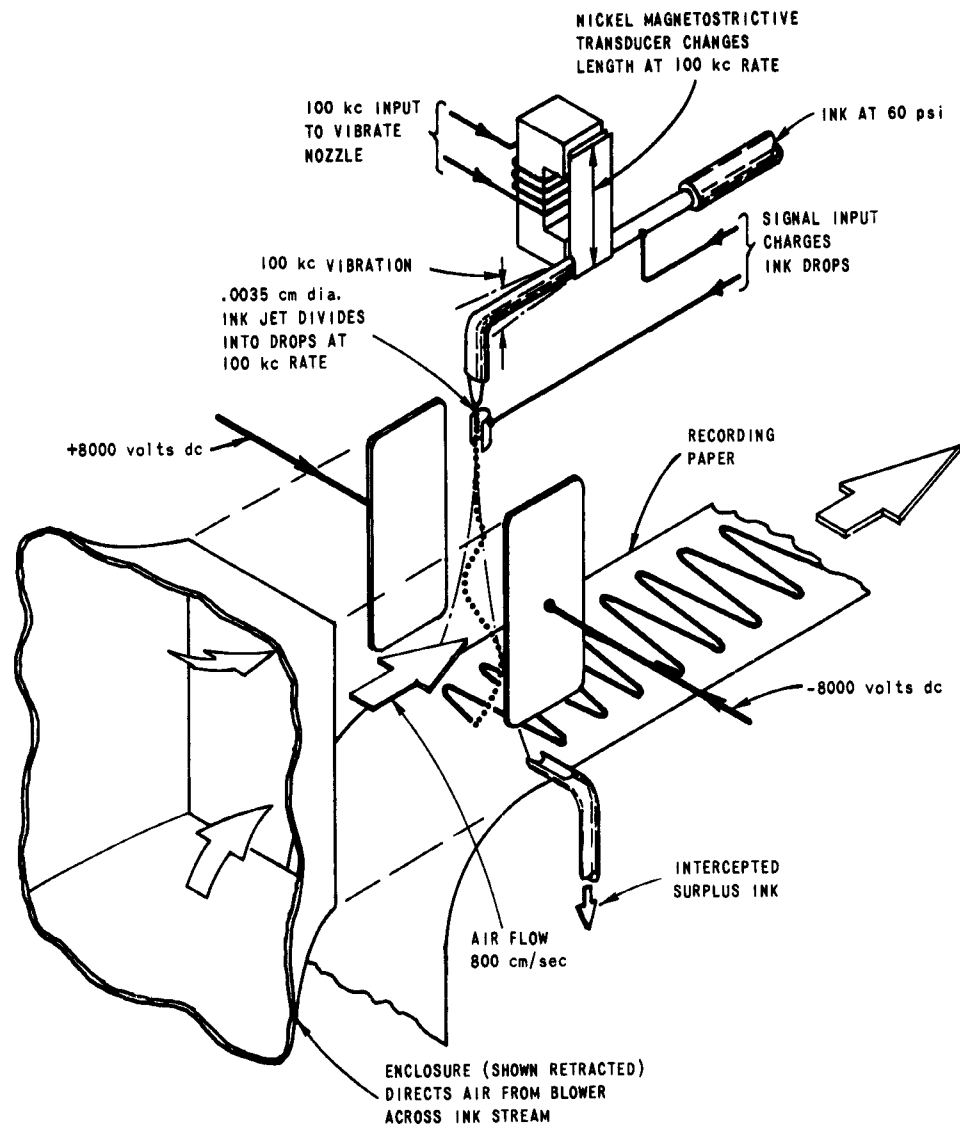
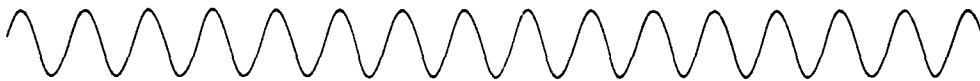


FIG. 1. INK JET OSCILLOGRAPH.



a. 2.5-cps sine wave



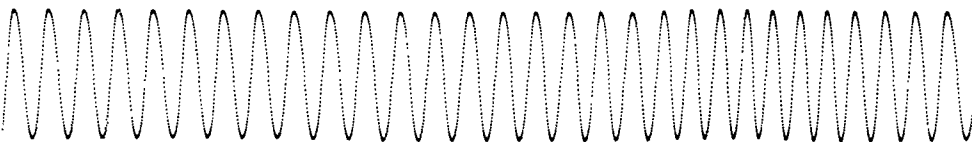
b. 10-cps sawtooth



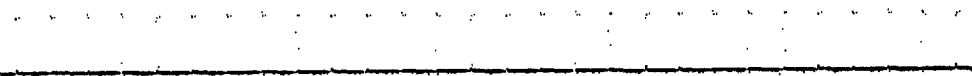
c. 200-cps square wave



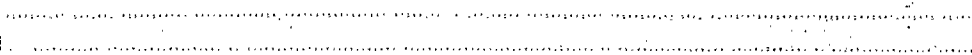
d. 1000-cps damped sine wave



e. 1000-cps sine wave



f. 30- $\mu$ sec pulses, 2000 pps



g. 10,000-cps sine wave

FIG. 2. REPRESENTATIVE OSCILLOGRAMS.

corresponding to the maximum recorded signal is required for interception. By intercepting an appropriate fraction of the ink in transit, good trace characteristics may be attained at very low writing speeds, where the record would otherwise be blurred by excess ink.

#### A. INK-DROP FORMATION AND CHARGING

Drops are formed from a cylindrical jet, 0.0035 cm in diameter, which emerges from a nozzle supplied with an electrically conducting ink under pressure. The initial jet velocity is determined by the ink pressure; a typical value of 2200 cm/sec corresponds to a pressure of about 60 psi. Surface tension forces, which cause the jet to break up into drops a few millimeters from the nozzle, are synchronized by vibrating the nozzle along the jet axis at a frequency of 100 kc. The resulting velocity modulation of the emerging jet synchronizes the drop formation to the nozzle vibration, decreases and establishes exactly the distance from the nozzle at which the drops form, and makes the drop size and spacing precisely uniform. Each drop is charged, as it forms, in proportion to the instantaneous input-signal voltage.

An analysis of the drop-forming and -charging processes is given in Sections 1 and 2 of Appendix A.

##### 1. Drop Formation

Typical drop formation is illustrated by the photograph of Fig. 3, taken through a microscope with stroboscopic illumination synchronized to a submultiple of the nozzle vibration frequency. The stability of the process is evidenced by the sharpness of the picture, which is the superposition of approximately 100 images exposed over a total time interval of 1/5 sec.

At the instant of formation, each drop has a "tail" extending to the point of jet separation. With proper operation, surface tension causes the tail and body to coalesce and form a single drop that ultimately assumes a spherical form. Initially, the shape of the drop vibrates about this equilibrium figure; the variation in shape of successive drops in Fig. 3 is due to this phenomenon.



1.0 mm

FIG. 3. INK-DROP FORMATION.

At certain amplitudes and frequencies of nozzle vibration, a portion of the drop tail may separate and form an extra small "satellite" drop (Plateau's spherule) for each nozzle vibration cycle. If the drop is charged, this separation process is aided by electrostatic forces that act to oppose coalescence of the tail and body of the drop. Satellite drops cannot be allowed during recorder operation; their formation modifies the deflection sensitivity of the system and their high charge-to-mass ratio, when a signal is applied, causes them to collect on the charging electrode or deflection plates of the oscillograph.

Experimentally, we have found that drops of uniform size may be formed at frequencies corresponding to jet division into intervals equaling 3.5 to 10 jet diameters. The tendency for satellite drop formation is most serious near the extremes of this range, and at maximum drop charge. The relationship between nozzle vibration amplitude and the other parameters involved in the drop formation process is very critical with respect to satellite formation. The optimum vibration amplitude is best determined by making the adjustment while carefully observing the process with stroboscopic illumination.

It turns out that distortion is minimized by maximizing the drop-to-drop spacing; the most satisfactory drop spacing for the experimental systems is between six and eight jet diameters. It follows that the drop formation frequency is directly proportional to the jet velocity and inversely proportional to the jet diameter.

## 2. Drop Charging

Ink drops are charged by electrostatic induction. The input-signal voltage is applied between the nozzle and a charging electrode which surrounds the jet at the point of drop formation. This induces a charge proportional to the input signal on the continuous conducting column of ink which extends from the nozzle to the point at which drops are formed. As drops separate from this fluid column, they carry with them a sample of this induced charge which is equal to the product of the input voltage at the instant of drop detachment, and the capacitance between the charging electrode and the separating drop. Because the drops are of uniform size, the resulting charge-to-mass ratio is proportional to the input signal.

The resistance of the column of ink extending from the nozzle must be low enough so that the flow of induced charges (current) does not produce appreciable voltage drop between the nozzle and drop separation point. Ink volume resistivities of less than 5000 ohm-cm are typically required.

## 3. Ink and Ink-Supply System

The best ink for the system is one that combines (in addition to good marking qualities) high surface tension, low viscosity, and high conductivity. We have tried a number of fountain-pen inks in various colors, washable and permanent, and found them all satisfactory. Schaeffer's\* "Scrip", washable black, has been used for most of the experimental work; its fluid properties are similar to those of water and its specific resistivity is 130 ohm-cm.

In the experimental system, ink and rinse water are supplied from reservoirs pressurized by a nitrogen cylinder and a two-stage gas-pressure regulator. A filter capable of screening suspended particles large enough to obstruct the nozzle is a necessity, and is included between the fluid control valves and the nozzle. Figure 4 is a photograph of the main components of the ink-supply system.

---

\* W. A. Schaeffer Pen Company, Fort Madison, Iowa.

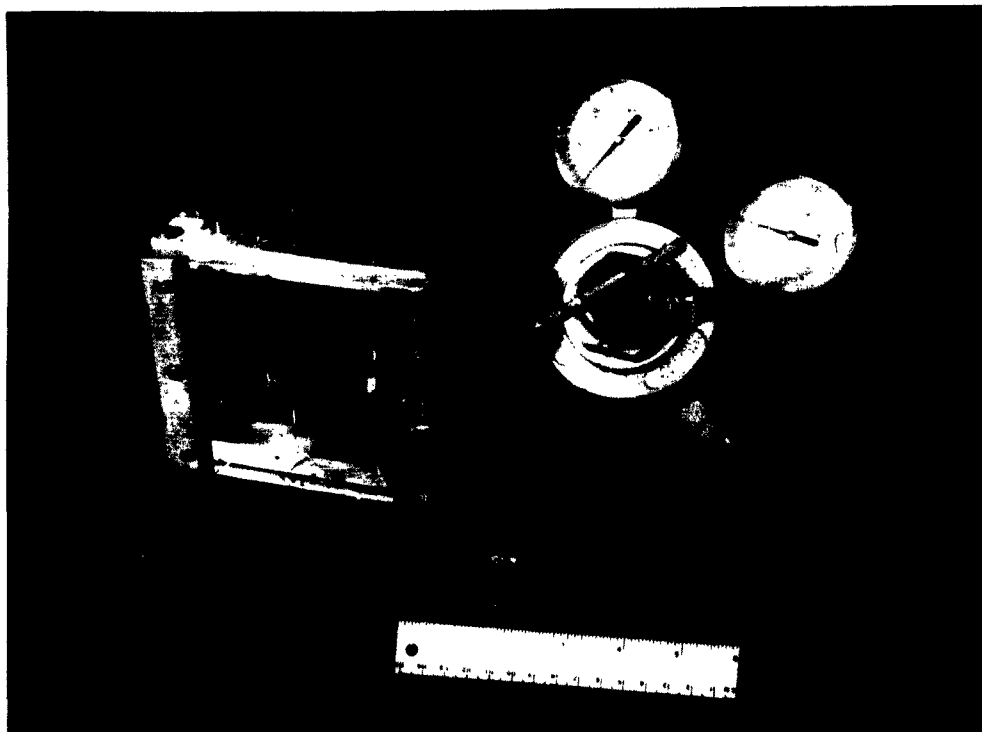


FIG. 4. INK-SUPPLY SYSTEM.

#### 4. Ink-Drop Gun

Figure 5 is a photograph of an experimental "ink-drop gun". The main components are shown in the exploded view of Fig. 6. The ink-drop charging electrode (in the left foreground) surrounds the jet at the drop-formation point with two parallel plates having a spacing of 0.050 cm. The charging electrode is pivoted so that it can be swung aside and the drop-formation process can be viewed directly with a microscope in conjunction with stroboscopic illumination.

The jet-forming nozzle is also located in the left foreground of Fig. 5, just to the right of the charging electrode, and points to the left. It consists of a tiny piece of glass tubing cemented into the end of a length of stainless-steel, hypodermic-needle tubing.

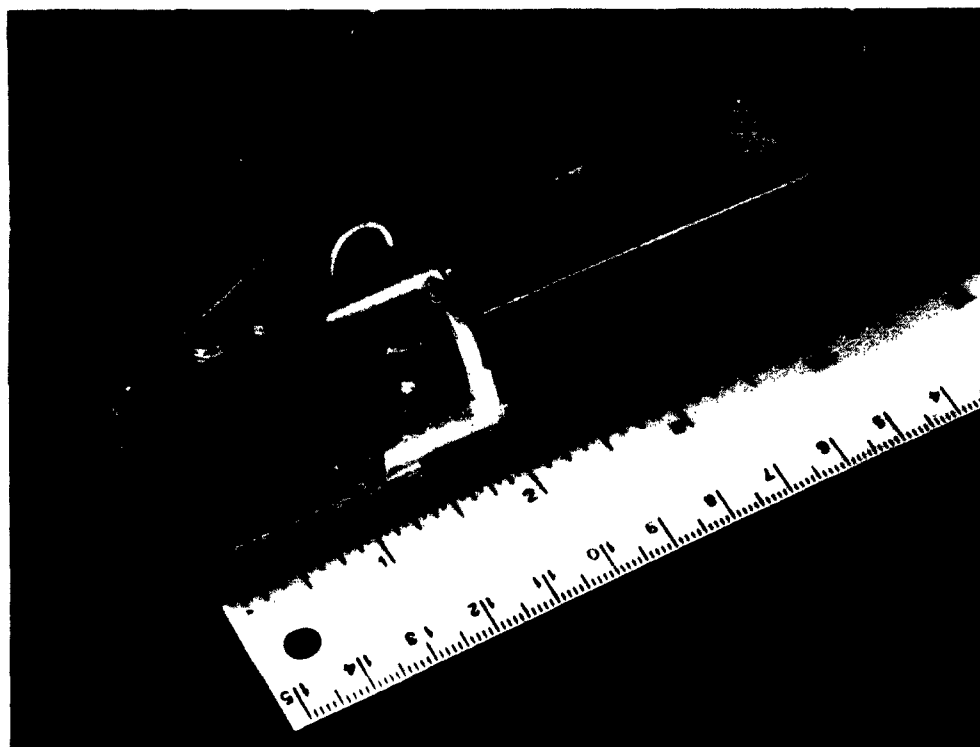


FIG. 5. INK-DROP GUN.

Nozzles are fabricated by drawing soft-glass capillary tubing down to an inside diameter of approximately 0.012 cm. A second drawing operation forms a pointed tip on a piece of this tubing. A short piece of tubing, with pointed tip, is broken off and cemented into the stainless steel tubing. Finally, the pointed tip is ground back until the desired exit diameter is realized.

Axial vibration of the nozzle is produced by magnetostrictive action that changes the length of a strip of nickel brazed to the supply tube. The nickel is magnetized at the desired vibration frequency by the ferrite core and coil visible in Fig. 6. The amplitude of the required vibration is so small that mechanical resonance of the system is not required; adequate amplitude can be attained at most frequencies between 20 and 200 kc with less than 2-w input into the transducer.

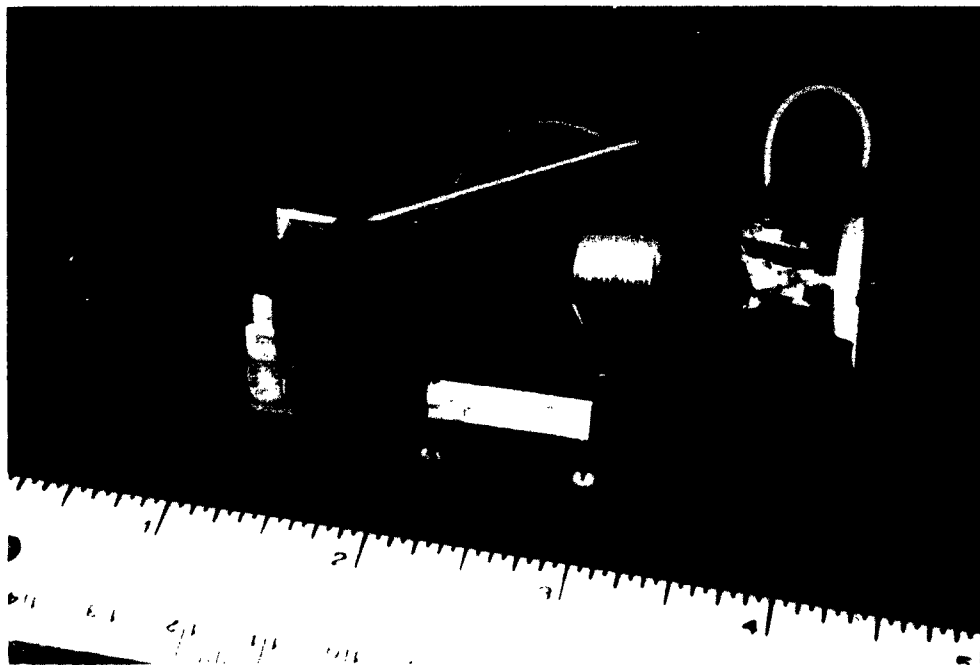


FIG. 6. INK-DROP GUN, EXPLODED VIEW.

The nozzle and transducer are supported by the cylindrical phenolic insulators visible in Fig. 6 just below the nickel transducer. The nozzle is insulated from the ink supply (except for the high-resistance path through the ink itself) by supplying the ink through a length of small-diameter plastic tubing. The input-charging voltage between nozzle and charging electrode may be single-ended (either side grounded), or push-pull, balanced to ground.

#### B. INK-DROP DEFLECTION

Ink is deflected by a dc electrostatic field, established perpendicular to the jet axis. The field exerts a constant transverse force, proportional to its charge, on each drop. If the field is assumed constant in magnitude and direction throughout the space traversed by the ink drops, and non-uniform forces due to other causes are neglected, the trajectory of each drop is parabolic, with a curvature and ultimate

deflection exactly proportional to the drop charge (deflection forces neglected here are discussed in Section E). Since there is no component of electrical force along the jet axis, perpendicular to the record surface, the transit time is independent of deflection. The mark made by each drop on the record surface is thus a permanent record of the magnitude and polarity of the input signal at the instant that drop was formed and charged. Equations for drop deflection are derived in Section 3 of Appendix A.

For a given trace amplitude, fidelity of the record increases as the magnitude of the deflection field is increased. A field of 16 kv/cm is typical for the experimental system; values much greater than this result in corona or sparking.

Since each ink drop is independently charged, the time required for a transition from zero to full deflection is determined only by the time interval between the formation of successive drops. A transient response time of 10  $\mu$ sec for a 1-cm deflection (typical for this system) corresponds to a minimum pen or stylus-tip acceleration of  $4 \cdot 10^{10}$  cm/sec<sup>2</sup> ( $4 \cdot 10^7$  g's) in a conventional direct-writing system. The actual acceleration of the drops in the ink-jet system is much less than this; for a typical charging point-to-paper transit time of 2 msec, the transverse acceleration required for 1-cm deflection is  $5 \cdot 10^5$  cm/sec<sup>2</sup> (500 g's). The necessary acceleration is determined only by the deflection amplitude and ink-drop flight time, and not by the required transient-response time.

Figure 7 shows the portion of the experimental oscillograph that includes the deflection plates and ink-drop gun. The deflection-plate spacing, which is adjustable, is set at 1.0 cm; the potential for this spacing is typically 16 kv between plates. The record paper (not shown) passes beneath the plates and is spaced 0.5 cm from the bottom of the plates. The distance from nozzle to record surface is adjustable; a typical value is 3.5 cm. For the representative parameters given here, the deflection sensitivity of the oscillograph with respect to the drop-charging voltage is approximately 350 v/cm.

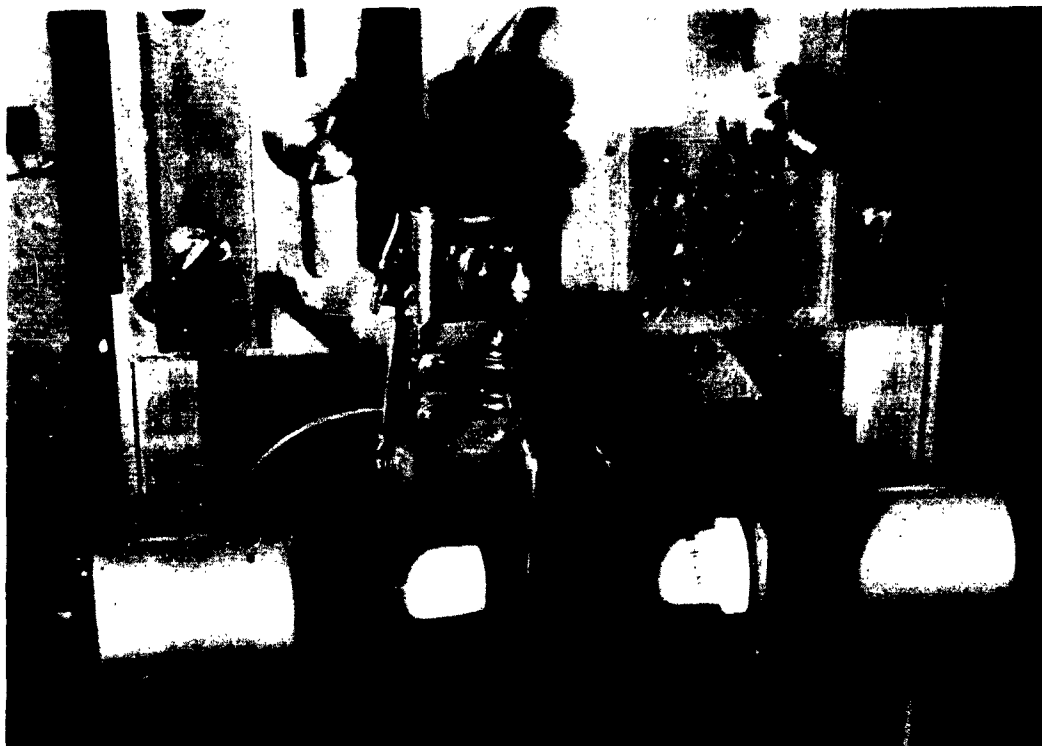
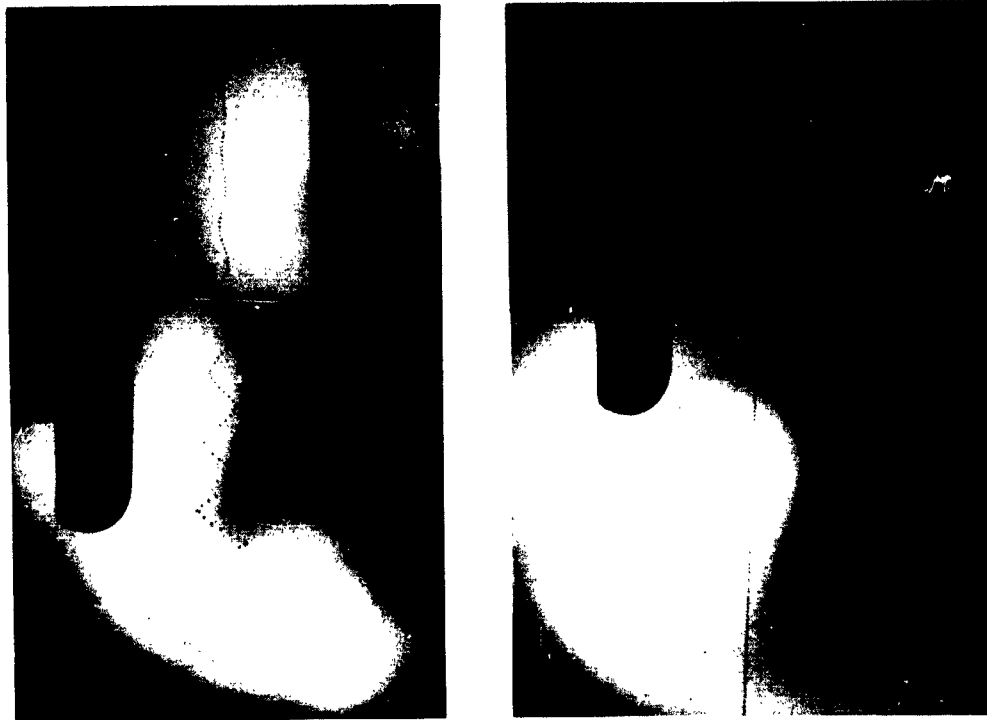


FIG. 7. INK-DROP GUN AND DEFLECTION SYSTEM.

Deflection of the ink drops in flight is illustrated by the photographs of Fig. 8, taken with stroboscopic illumination. In Fig. 8a the applied signal is a 3700-cps sine wave; in Fig. 8b it is a 150- $\mu$ sec rectangular pulse. The drop-formation frequency for these photographs is 62 kc.

Proper operation of the oscillograph depends on the ink drops being uniform in size and initial velocity. Figure 9 compares records made with and without nozzle vibration. With no vibration, the random variation in drop size results in a corresponding random variation in deflection sensitivity. The 2000-cps input signal is the same for both records.



a. Sine wave signal

b. Pulse signal

FIG. 8. INK DROPS IN FLIGHT.



a. Input signal: 2000-cps sine wave  
No nozzle vibration



b. Input signal: 2000-cps sine wave  
Nozzle vibration frequency: 80 kc

FIG. 9. OSCILLOGRAMS SHOWING EFFECT OF NOZZLE VIBRATION.

### C. PAPER TRANSPORT AND INK INTERCEPTION

Figure 10 shows the paper transport, disassembled to show internal details. Paper enters at the bottom, foreground, makes a 90-deg turn, is engaged by the rubber-tired drive wheel and an idler (the idler is not visible), makes a second 90-deg turn, and emerges at the top. For slow chart speeds, power is not supplied to the motor in the photograph; its shaft and drive wheel are turned by coupling it to a second low-speed motor, which is not shown.

A test record is made by running the motor continuously at the desired speed and feeding a short length of paper manually to the point where it is picked up by the rubber-tired drive wheel and idler. Chart speeds as high as 1500 cm/sec can be obtained with the transport for paper lengths of about a foot; the length of paper that will feed without tearing is limited by the high acceleration involved.

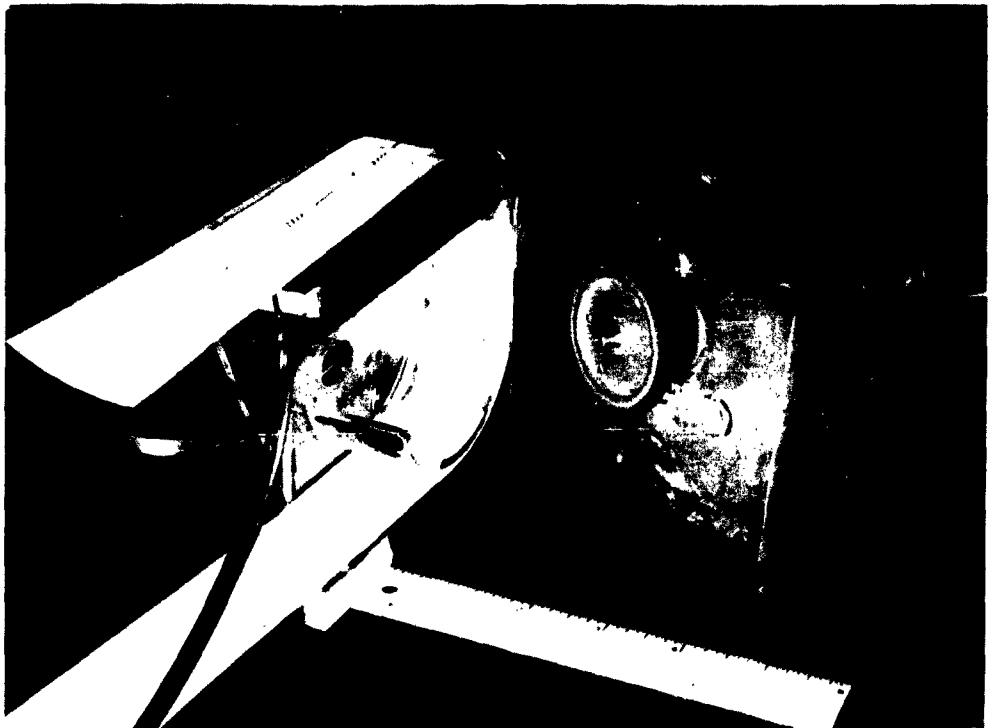


FIG. 10. PAPER TRANSPORT, DISASSEMBLED.

Ink may be intercepted before striking the paper by deflecting it into the glass tube visible in Fig. 10 overhanging the rear edge of the chart. Ink collected in this fashion drains into the plastic dish in the background. With no paper in the system, ink collects in the reservoir below the position occupied by the paper and drains via the plastic tubing in the foreground of the photograph.

The transport described here provides a simple and convenient means for evaluating the experimental recording system. The poor speed calibration and difficulties involved in handling long records make it less suitable for actual, continuous, data recording.

#### D. FREQUENCY AND TRANSIENT RESPONSE

The minimum transient-response time of the oscillograph is typically 10  $\mu$ sec; it is equal to the reciprocal of the drop-formation frequency. The response to a step input exhibits an overshoot as analyzed in Section 2 of Appendix A; it may be effectively eliminated by equalizing the input signal with a simple RC network. The experimentally determined overshoot is typically 20 percent, with a decay time constant of approximately 20  $\mu$ sec.

High frequencies are recorded as a regular sequence of samples of the input signal, taken at the ink-drop-formation rate. According to Shannon's sampling theorem for sampled-data systems [Ref. 3], the frequency response of the oscillograph extends to one-half the sampling frequency, provided the input signal is band-limited to this value.

The discontinuous sampling process and presentation make the interpretation of records difficult for high frequencies, and the usable frequency response may be considerably lower than theory indicates. The observer's visualization of the input waveform depends on the relative time and amplitude scales, as illustrated by Fig. 11, which shows the same record on different time scales. The 5-kc-sine wave input signal for each of the three traces is identical, and each record contains 14 samples (ink drops) per cycle.

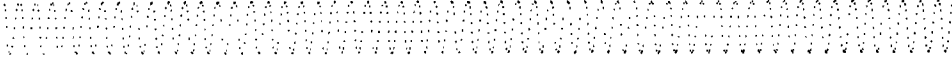
If a repetitive signal waveform is sampled once per period, at a frequency differing slightly from the signal frequency, the resulting record is a reproduction of the input on a greatly reduced time scale.



a. Input signal: 5000-cps sine wave  
Chart speed: 250 cm/sec



b. Input signal: 5000-cps sine wave  
Chart speed: 520 cm/sec



c. Input signal: 5000-cps sine wave  
Chart speed: 1300 cm/sec

FIG. 11. OSCILLOGRAMS SHOWING INFLUENCE OF CHART SPEED ON RECORD READABILITY.

The concept is analogous to that involved in sampling oscilloscopes. Figure 12 shows records made by sampling a 101-kc sawtooth signal at a 100-kc rate, and records of sine waves that nearly equal the sampling frequency or its submultiples.

From the foregoing, it may be concluded that the frequency response of the recorder is best specified in terms of sampling frequency and corresponding transient response times (typically 100 kc and 10  $\mu$ sec); the maximum, usable, signal-input frequency is then determined by the particular application. The response capability of the system is most efficiently utilized in recording signals having frequency components that decrease in amplitude with increasing frequency, in order to limit the size of the gaps or discontinuities in the recorded trace.

#### E. DISTORTION

Record fidelity is limited by spurious deflections and transit-time variations that result in distortion along both the time and amplitude axes of the record. The distortion is caused by non-uniformities in the deflecting field, and by aerodynamic and mutual electrostatic forces acting on the drops during flight.



a. Input signal: 16.03-kc sine wave  
 Ink-drop rate: 80 kc  
 Samples per signal period: 5



b. Input signal: 40.06-kc sine wave  
 Ink-drop rate: 80 kc  
 Samples per signal period: 2



c. Input signal: 80.3-kc sine wave  
 Ink-drop rate: 80 kc  
 Samples per signal period: 1



d. Input signal: 101-kc sawtooth  
 Ink-drop rate: 100 kc  
 Samples per signal period: 1

FIG. 12. OSCILLOGRAMS WITH SMALL INTEGRAL NUMBER OF SAMPLES PER SIGNAL PERIOD.

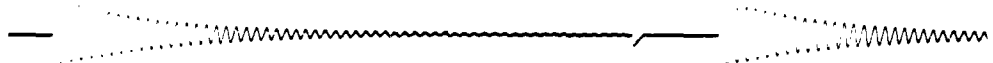
Nonuniformities in the deflection forces are due mainly to fringing of the electric field at the exit end of the deflection system. For a given deflection-plate spacing, distortion resulting from this effect decreases with increasing nozzle-to-record spacing.

Aerodynamic distortion is associated with the turbulent wake of disturbed air extending back along the line of flight of each drop. This wake affects the trajectory of subsequent drops following approximately the same path, and results in a nonuniform deceleration of the drops which is a function of their position in the waveform being recorded. Distortion from this source increases with increasing nozzle-to-record spacing.

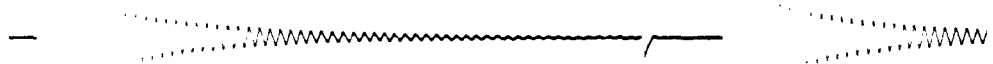
Mutual electrostatic forces vary as the square of the drop charge. An increase in nozzle-to-record spacing decreases the distortion from this source, because less charge is then required for a given deflection. An analysis of these phenomena is given in Section 4 of Appendix A.

1. Effect of Parameter Variation on Distortion

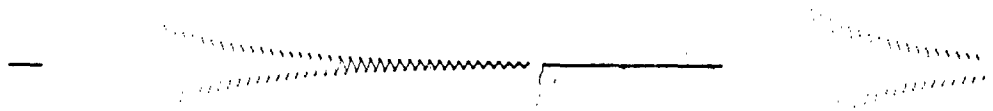
Figure 13 compares three records taken at different jet lengths (drop-separation point-to-record spacing) and input voltages, for the basic system (no air flowing across the jet). Other parameters were not varied. At points of corresponding deflection amplitude, the traces recorded with a 1.8-cm jet exhibit distortion that was due mainly to



a. Input signal: 3570-cps damped sine wave  
Jet length: 1.8 cm  
Deflection sensitivity: 1200 v/cm



b. Input signal: 3570-cps damped sine wave  
Jet length: 2.5 cm  
Deflection sensitivity: 500 v/cm



c. Input signal: 3570-cps damped sine wave  
Jet length: 3.7 cm  
Deflection sensitivity: 180 v/cm

FIG. 13. OSCILLOGRAMS SHOWING EFFECT OF JET LENGTH ON RECORD FIDELITY.

mutual electrostatic repulsion; the longer, 3.8-cm jet resulted in distortion caused predominately by aerodynamic forces. The records illustrate the existence of an optimum jet length somewhere between these two extremes.

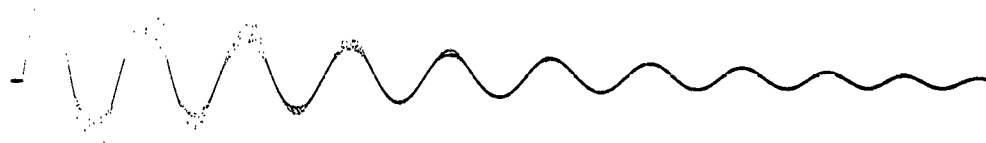
If deflection field and drop charge are changed so as to keep their product constant, the deflection sensitivity of the oscillograph does not change. Distortion that is due to mutual electrostatic forces increases, however, with increasing drop charge, as demonstrated by the records reproduced in Fig. 14.



a. Input signal: 330-cps damped sine wave  
Maximum peak-to-peak input amplitude: 300 v  
Deflection field: 14,400 v/cm



b. Input signal: 330-cps damped sine wave  
Maximum peak-to-peak input amplitude: 450 v  
Deflection field: 9600 v/cm



c. Input signal: 330-cps damped sine wave  
Maximum peak-to-peak input amplitude: 900 v  
Deflection field: 4800 v/cm

FIG. 14. OSCILLOGRAMS SHOWING EFFECTS OF MUTUAL REPULSION BETWEEN INK DROPS.

Both the analysis in Appendix A and experimental results indicate that, for the basic configuration with optimum parameters, the product of maximum deflection and drop-formation frequency is approximately constant for different systems having the same percentage distortion.

## 2. Reduction of Distortion Resulting from Aerodynamic Forces

The most promising method of improving the system fidelity appears to be through some means of reducing the distorting effects of air resistance. The effects of mutual electrostatic forces between drops and deflection-field fringing may then also be reduced by using a lower maximum drop charge and achieving the desired deflection by increasing the jet length.

An obvious method of reducing aerodynamic distortion involves modifying the fluid characteristics of the atmosphere through which the drops travel. Unfortunately, the dielectric properties of the atmosphere must also be considered, since they determine the achievable deflection field. A rough vacuum is not an appropriate solution, since a high field cannot be established in low-pressure air; a good vacuum is difficult to maintain, particularly if an ink with a volatile solvent is used. The moderate performance improvement that could be obtained by replacing the air with some other gas does not justify the resulting increase in system complexity.

Aerodynamic interaction between drops in flight may be reduced by providing a relative motion between the jet-forming nozzle and the air through which the drops travel. Several approaches have been applied to actual experimental systems; the most satisfactory is described here. It incorporates a stream of air that is directed across the space traversed by the ink drops, in a direction perpendicular to the jet axis. A system utilizing air flowing collinearly with the jet, and a system incorporating a nozzle rotating in still air have been constructed, and are briefly described in Appendixes B and C.

The principle of the system utilizing air flowing across the jet is illustrated in Fig. 15a. The air flows in a direction that is mutually perpendicular to the jet and deflection axes, and parallel to the movement of the record paper. As shown in Fig. 15b, the drop wake

is displaced toward the downstream direction of the air flow, where it does not interfere with the following drops. This method does not reduce the maximum aerodynamic drag force; its effectiveness is due to equalization of the drag force on all drops, regardless of trajectory. The air flow deflects the drops in a direction parallel to the record movement, as shown in Fig. 15; this deflecting force is constant for all drops and does not result in distortion.

The effectiveness of this system depends on the establishment of an air flow of sufficient velocity that does not vary along the deflection axis, and that is nonturbulent. A turbulent flow exerts nonuniform forces on the drops and results in random deflections at the record surface. The minimum effective air velocity depends somewhat on the ratio of drop diameter to drop spacing; a value equal to one-third the initial jet velocity is typically required.

Figure 16 is a photograph of the experimental air-supply system. Air is supplied at the left, through a vacuum-cleaner hose, by a vacuum cleaner connected as a blower. The wooden box is a settling chamber that contains transverse silk screens to smooth the air flow. The air then accelerates in the convergent section, which has a smooth, polished, inner surface, to the required exit velocity. An essentially nonturbulent flow can be obtained across the 2.5-by-5.0-cm rectangular output for air

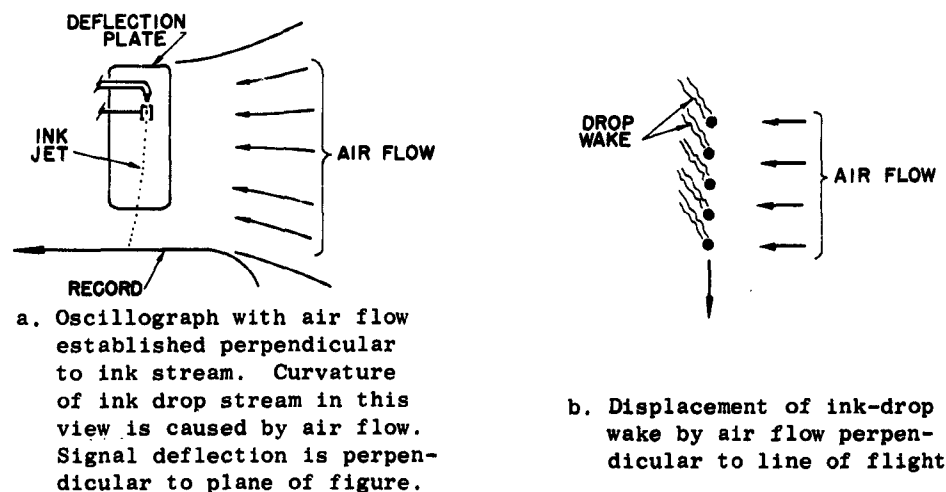


FIG. 15. EFFECT OF AIR FLOW ON INK-DROP WAKE.

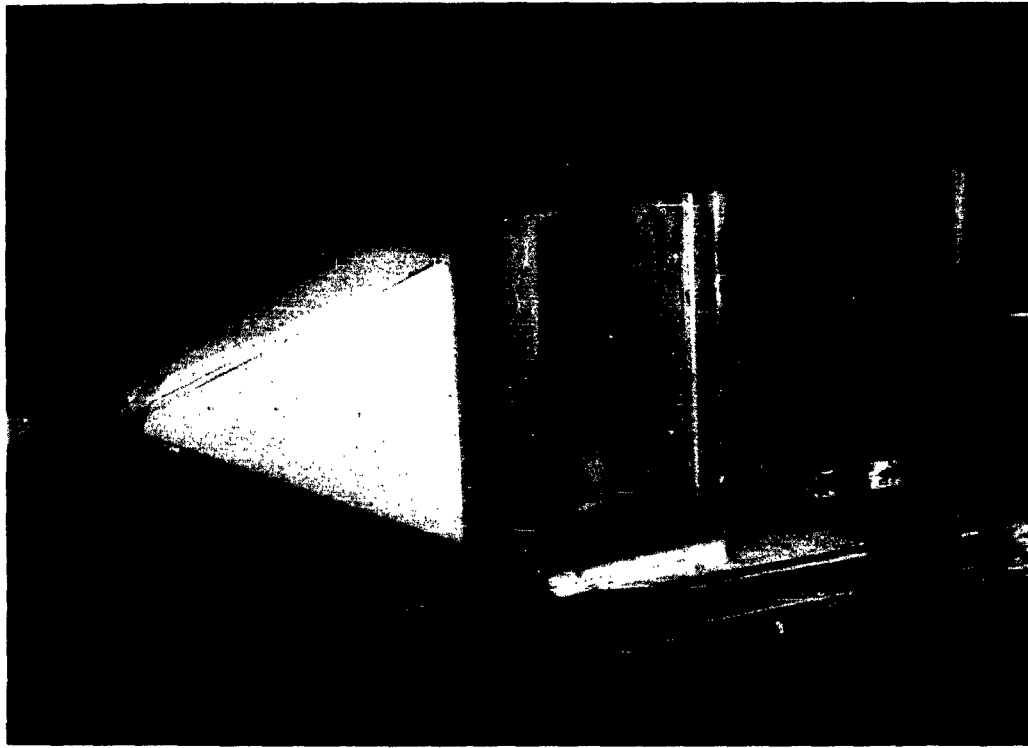


FIG. 16. AIR-FLOW SUPPLY SYSTEM.

velocities up to about 1100 cm/sec. The close-up view of Fig. 17 shows the relative configuration of the air outlet and the other oscillograph components. No attempt was made to minimize the size of the air-supply system, and considerable reduction in its dimensions is almost certainly feasible.

The effectiveness of the system in reducing distortion is evidenced by the two recordings, made with and without air flow, reproduced in Fig. 18. The input signal was the same for both records.

#### F. CONTROL OF INK DELIVERY RATE

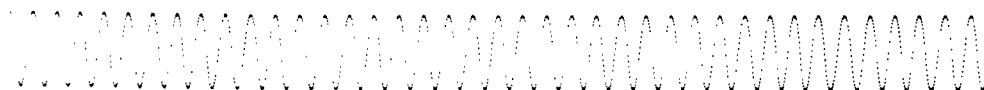
For good trace characteristics over a wide range of writing speeds, some method of varying the rate of ink delivery to the paper is required. Variation by modification of the jet velocity and diameter is possible



FIG. 17. EXPERIMENTAL OSCILLOGRAPH WITH AIR-FLOW SYSTEM.



- a. Input signal: 2000-cps sine wave  
Initial jet velocity: 2200 cm/sec  
No air flow



- b. Input signal: 2000-cps sine wave  
Initial jet velocity: 2200 cm/sec  
Air velocity transverse to ink stream: 650 cm/sec

FIG. 18. OSCILLOGRAMS SHOWING EFFECT OF AIR FLOW ACROSS INK STREAM.

but is inconvenient, and it can provide control of flow rates over only a limited range. A more versatile method, described here, maintains a constant nozzle flow rate and controls the amount of ink used in the actual recording by intercepting the surplus ink during its transit from nozzle to paper.

#### 1. Interception of Surplus Ink

By applying to the charging electrode a voltage that exceeds the maximum signal voltage, the ink drops may be deflected into a collector that prevents them from reaching the paper. The quantity of ink forming the recorded trace may thus be reduced by charging the ink drops with a pulse train that is amplitude-modulated by the signal to be recorded. The width of each pulse is just sufficient to charge one ink drop; the frequency of the pulse train is made proportional to the desired ink delivery rate. Ink drops charged by the pulse peaks strike the paper, forming the record trace; ink drops having a charge corresponding to the pulse baseline voltage have a trajectory lying beyond the limits of the signal-drop trajectories, and these are intercepted by a collector interposed between charging point and paper. Figure 19 illustrates the ink-drop trajectories associated with a sinusoidal-signal input, for a record using one-third of the ink issuing from the nozzle. Corresponding signal and drop-charging waveforms are also shown.

In order to avoid deflections corresponding to the rising and falling portions of the pulses, signal sampling (drop separation) must not occur during the transition intervals. The pulses are therefore synchronized with the drop-forming signal (nozzle-vibration-transducer input) and phased so that drop separation does not occur during the transitions between pulse peak and baseline.

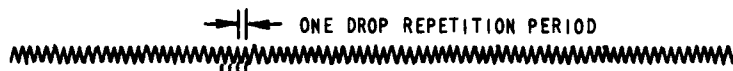
Records made with various fixed ink-drop rates, using this technique, are illustrated in Fig. 20.

#### 2. Proportioning Ink Flow to Instantaneous Writing Speed

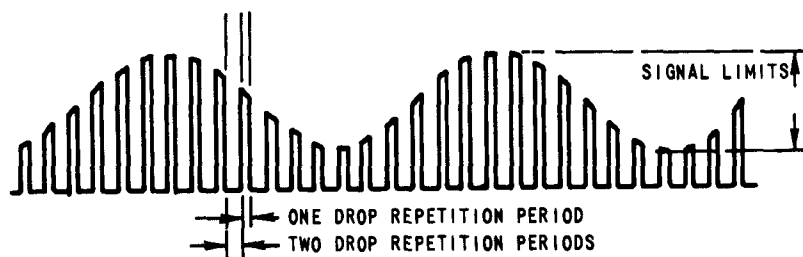
Ideally, the ink delivery rate should be proportional to the instantaneous writing speed, as determined by the chart velocity and the derivative of the input signal. Experimental circuits have been constructed that approximate this condition by electronically controlling



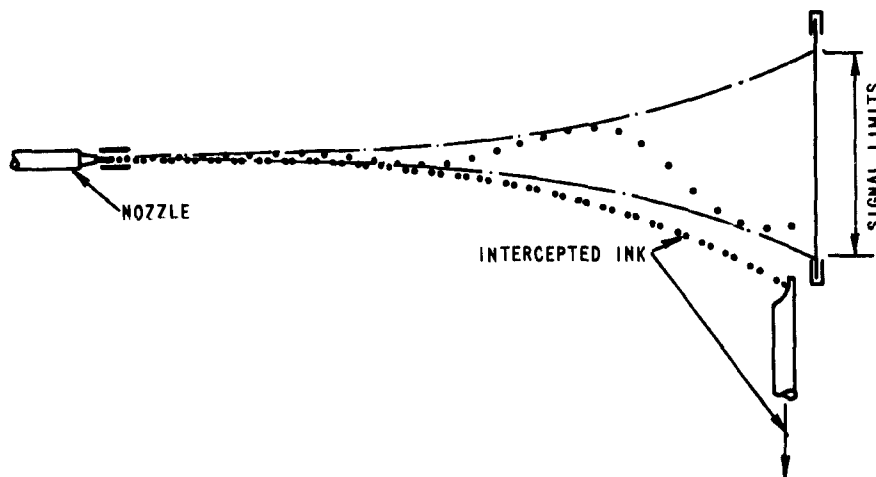
a. Signal waveform



b. Nozzle-vibrator input



c. Drop-charging voltage waveform  
for interception of two-thirds of ink

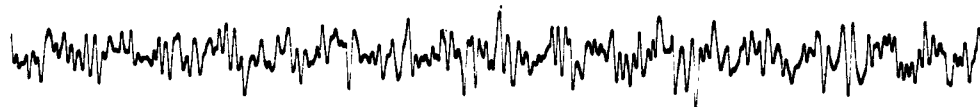


d. "Snapshot" showing ink-drop trajectories

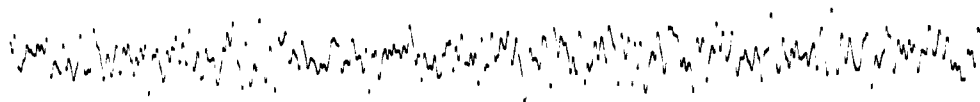
FIG. 19. INTERCEPTION OF SURPLUS INK.



a. Ink-drop rate at record: 100 kc



b. Ink-drop rate at record: 50 kc



c. Ink-drop rate at record: 20 kc



d. Ink-drop rate at record: 10 kc



e. Ink-drop rate at record: 4.2 kc

FIG. 20. OSCILLOGRAMS MADE WITH VARIOUS FIXED INK-DROP RATES.

For all records:

Input signal: white noise, band limited,  
20 - 500 cps

Drop-formation  
frequency at nozzle: 100 kc

the frequency of the drop-charging pulse train. A minimum pulse-repetition frequency is provided, proportional to the chart speed; this basic frequency is increased, as the signal is recorded, by an amount proportional to the instantaneous signal derivative. Figure 21 compares a record made by this technique with records made at fixed ink-drop rates. This method of controlling the ink-drop rate is described in more detail in Appendix D.



a. Input signal: 1000-cps damped sine wave  
Ink-drop rate at record: 50 kc



b. Input signal: 1000-cps damped sine wave  
Ink-drop rate at record: 4.2 kc



c. Input signal: 1000-cps damped sine wave  
Ink-drop rate at record controlled by  
instantaneous signal derivative:  
Maximum drop rate: 50 kc  
Minimum drop rate: 4.2 kc

FIG. 21. COMPARISON OF OSCILLOGRAMS MADE WITH FIXED AND SIGNAL-CONTROLLED INK-DROP RATES.

#### G. EXPERIMENTAL TEST SETUP

Figure 22 is a block diagram for a typical, complete recording system. Included in the block diagram are means for illuminating the drop stream with a stroboscope in synchronism with the drop formation and for applying an input signal synchronized with this illumination. Operation of the system may then be monitored by direct observation of the drop stream.

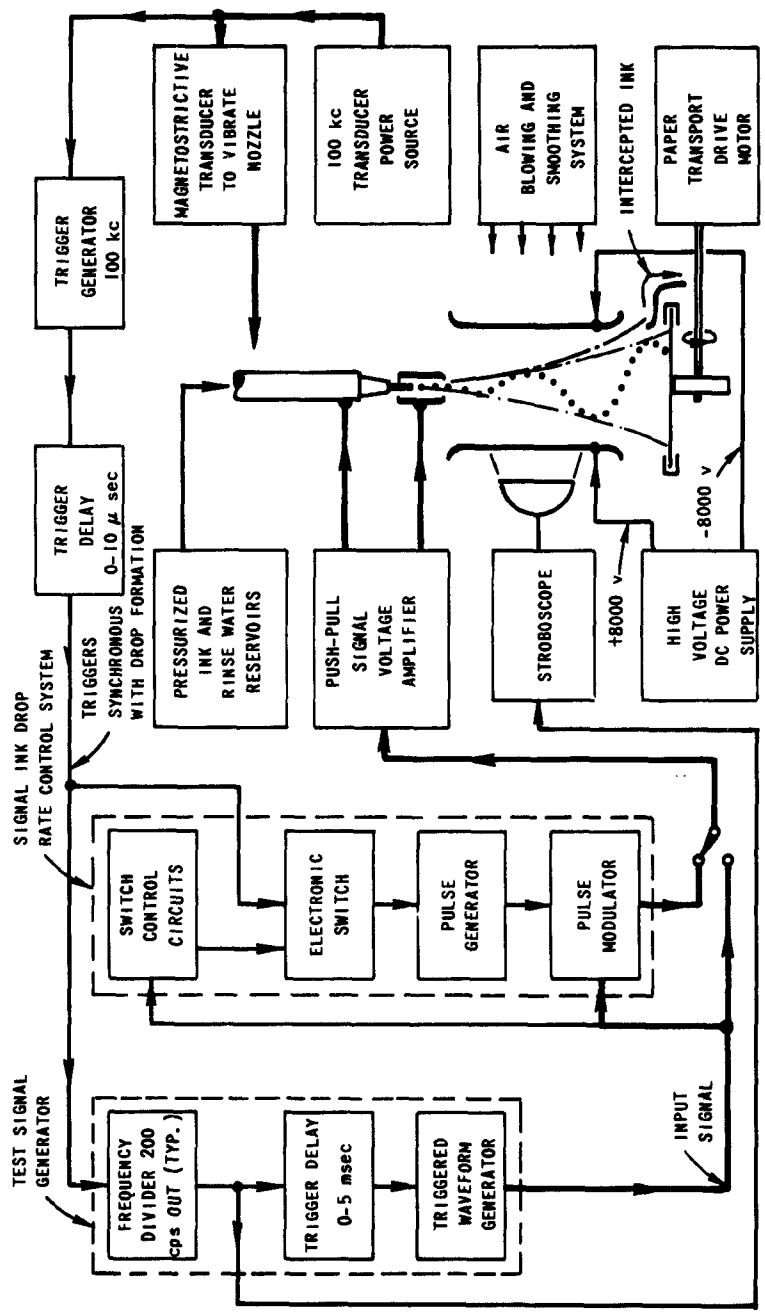


FIG. 22. BLOCK DIAGRAM OF COMPLETE OSCILLOGRAPH AND TEST SETUP.

Many of the electronic functions are provided with available laboratory test equipment. The signal-drop-rate control circuits and the test-signal generator were constructed specifically for this application.

Figure 23 is a photograph showing an overall view of the experimental setup. Visible from left to right are the gas cylinder and regulator for supplying the ink pressure, ink and rinse-water reservoirs, ink and water valves, air-supply hose (the source of air is a vacuum cleaner connected as a blower, under the bench), air-flow smoothing system, stroboscope for illuminating the ink stream, and the basic ink-jet recording system. Light from the stroboscope shines through a window in the side of the convergent section of the air-flow system and is reflected from a small mirror inside to backlight the drop stream for observation.



FIG. 23. EXPERIMENTAL RECORDING SYSTEM.

## H. RECORD CHARACTERISTICS

### 1. Trace Characteristics

Excellent traces may be made on a wide variety of surfaces. A smooth, relatively nonabsorbent surface results in maximum contrast and resolution, and minimum spreading, except for records having an excess quantity of ink per unit length of trace. The records reproduced in this report were made on paper having a hard, smooth coating that was somewhat water repellent.\* The following comments are for records made on this paper with fountain-pen ink (Schaeffer's "Scrip").

At high writing speeds, each ink drop produces a distinct circular dot on the recording paper. As the writing speed is decreased, the dots overlap, and a continuous trace results. A further decrease in writing speed, at the same ink-flow rate, results in a broadening of the trace, with a consequent loss of detail, and finally, at very low speeds, the ink forms puddles on the paper.

The size of individual dots is determined by the drop size and the ink and paper characteristics. Typically, a 0.0075-cm-diameter drop, striking at normal incidence, results in a nearly perfect, circular dot of 0.020-cm diameter. The line of flight for a drop deflected from the jet axis is not perpendicular to the paper at impact, and the drop may "skid" when it hits, resulting in a mark that is somewhat egg-shaped. This effect does not significantly reduce the resolution of the record.

If the marks made by individual drops overlap, the impact of drops arriving at the record surface on the wet ink on the paper may result in splashing. The effect is most serious at high jet velocities and is evidenced by a broadening of the trace and subsidiary small marks made at short distances from the primary impact point.

If the ink dots do not overlap on the record, traces dry in a few seconds. Denser traces, made at slower speeds, take proportionally longer to dry, unless blotted.

Quantitative data relating to the effects just discussed has not been taken; some idea of their importance may be obtained by examining the record reproductions which accompany the following paragraphs.

---

\* Gubelman Charts, Newark, N.J.; Paper type GCK-5.

## 2. Fidelity

Typical fidelity of the basic configuration (no air flowing across the jet) is illustrated by the records of Fig. 24. The jet length for these records is 2.5 cm and the drop-formation frequency is 125 kc.

By increasing the jet length and directing a stream of air across the jet, the fidelity may be improved, as shown by the records of Fig. 25. The jet length for these records is 3.8 cm, and air flows across the jet at a velocity of 840 cm/sec. As before, the drop-formation rate is 125 kc.

Peak-to-peak amplitude for these records is plotted against input voltage in Fig. 26. Maximum deviation from a linear characteristic is about  $\pm 5$  percent of full-scale amplitude, which sets a corresponding limit on the amplitude accuracy obtainable from the record. Full-scale amplitude is taken as 1.0 cm (peak-to-peak) for the basic system, and 2.0 cm for the system with air flowing across the jet.

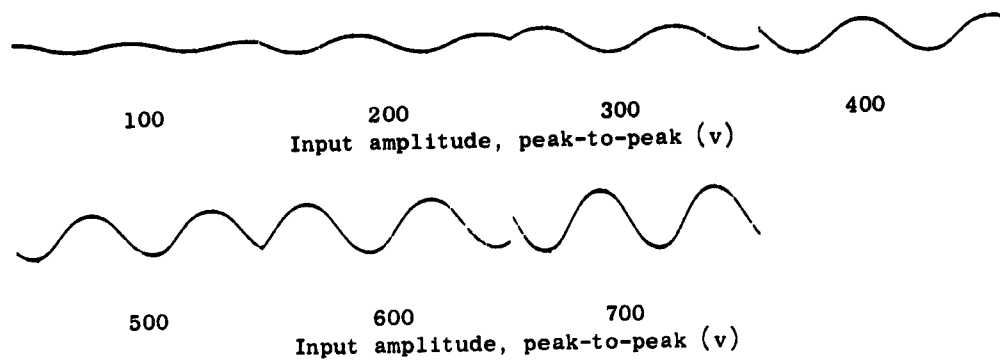
Variations in drop transit time from charging point to paper result in errors along the time axis of the record. For the maximum peak-to-peak amplitudes in the examples just given, spurious displacements along the time axis are approximately  $\pm 40$   $\mu$ sec for the basic system, and  $\pm 25$   $\mu$ sec for the system with air flowing across the jet.

## 3. Accuracy

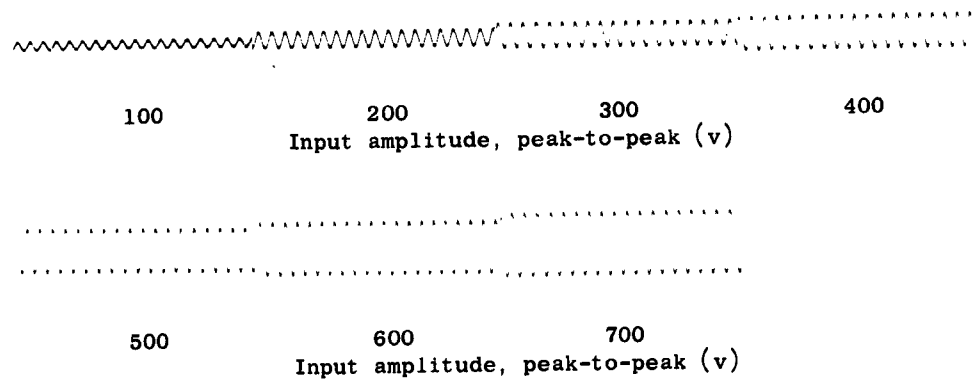
The accuracy with which an oscillogram represents the input signal depends on the distortion (just discussed) inherent in the recording process, trace definition, and stability of the deflection sensitivity with time.

Under most conditions, the trace definition is such that its position may be determined with an accuracy limited only by the resolution of the observer's eye. If the eye is capable of determining a trace displacement of 0.02 cm, this sets a typical accuracy limit of 2 percent for a 1-cm deflection (2 cm peak-to-peak). Since percentage distortion increases with deflection amplitude, there is an optimum, maximum, trace amplitude for best accuracy.

The stability of the deflection sensitivity of the laboratory system has not been evaluated. There is no evident limit to the



a. Input signal: 300-cps sine wave



b. Input signal: 3000-cps sine wave

For all records:

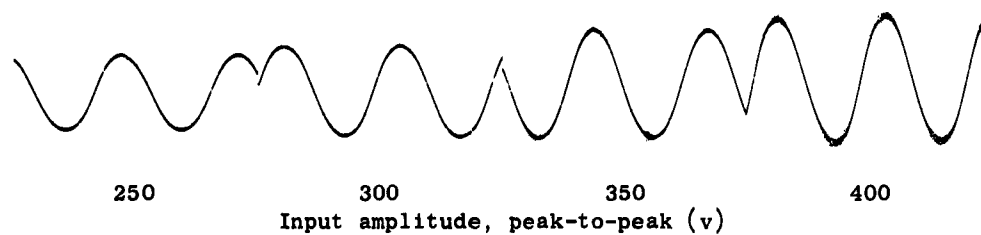
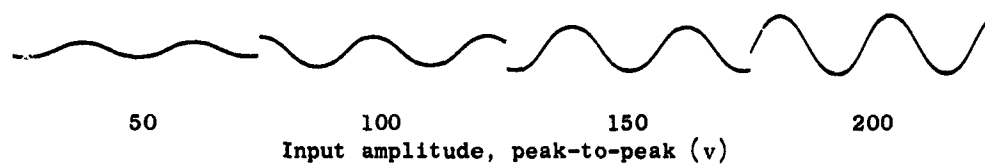
Drop rate: 125 kc

Jet length: 2.5 cm

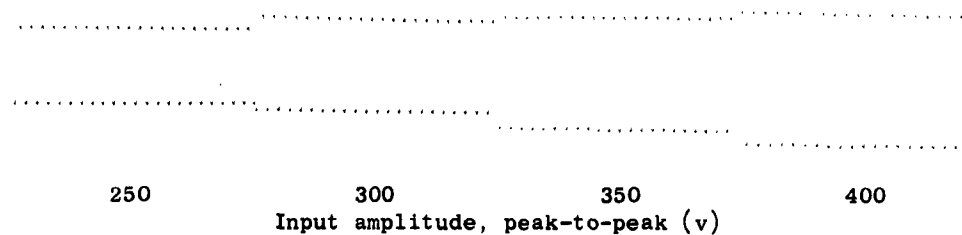
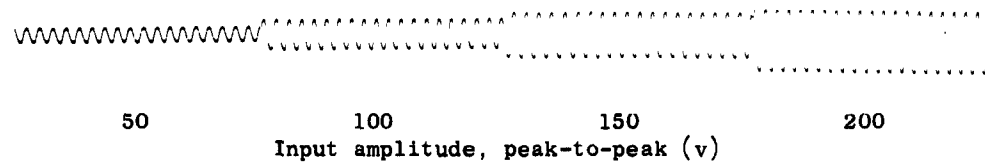
Initial jet velocity: 2300 cm/sec

Air velocity: zero

FIG. 24. OSCILLOGRAMS FOR EVALUATING FIDELITY OF BASIC SYSTEM.



a. Input signal: 300-cps sine wave



b. Input signal: 3000-cps sine wave

For all records:

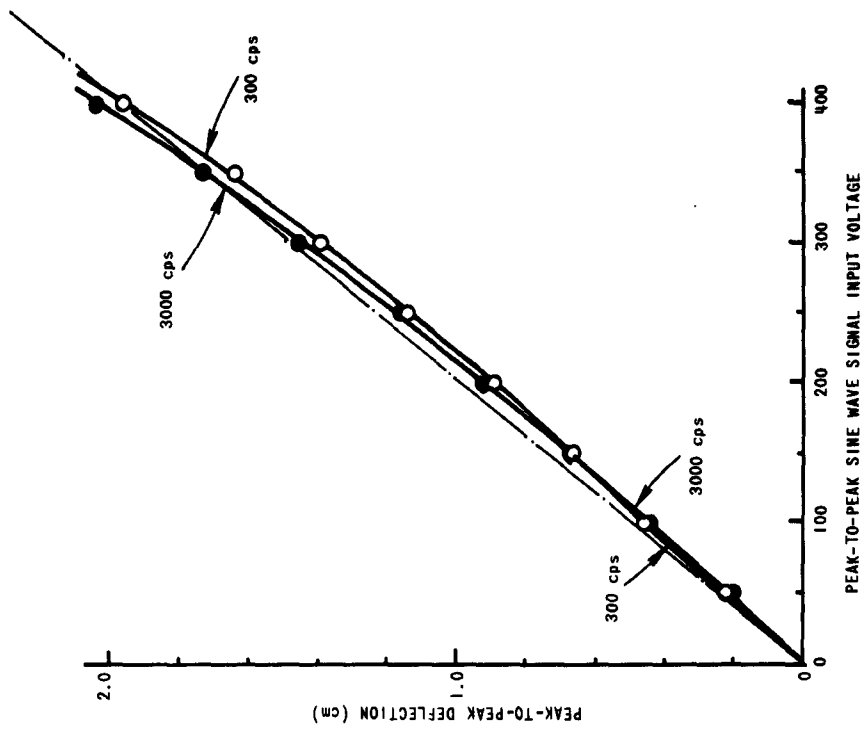
Drop rate: 125 kc

Jet length: 3.7 cm

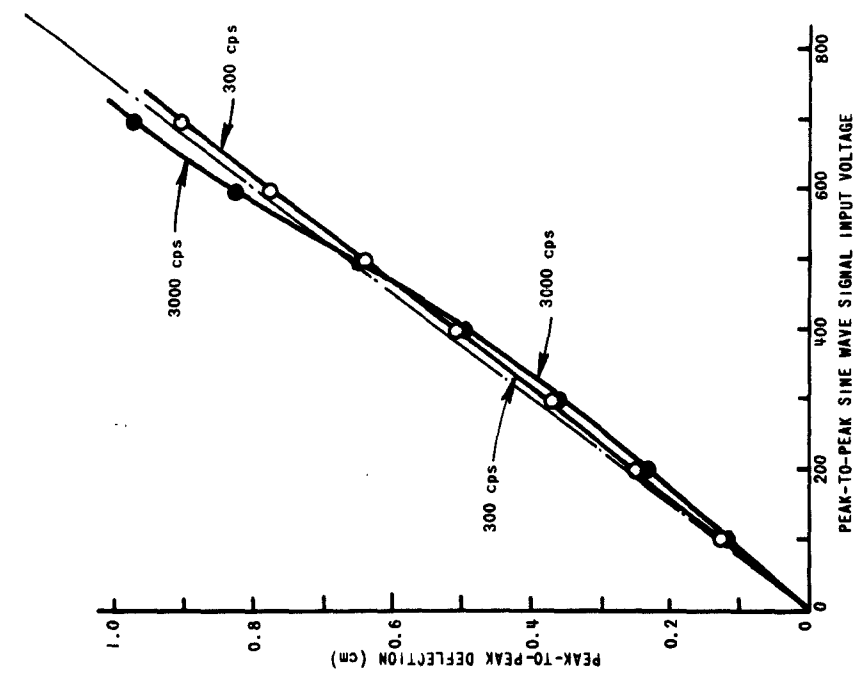
Initial jet velocity: 2300 cm/sec

Air velocity: 840 cm/sec

FIG. 25. OSCILLOGRAMS FOR EVALUATING FIDELITY OF SYSTEM WITH AIR FLOWING ACROSS INK STREAM.



a. No air flow



b. Air flow across ink stream

FIG. 26. DEFLECTION LINEARITY.

stability that can be maintained, but a large number of parameters enter into the deflection equation, and all must be controlled. Particularly critical are the ink fluid properties (viscosity and surface tension), which are temperature-sensitive. Since there are no friction or wear processes involved in the basic system, drift in characteristics as a result of aging is not a problem.

#### 4. Representative Oscillograms

Oscillograms for a wide variety of signals are reproduced in Figs. 27, 28, and 29. The illustrations are full size, as are all other records reproduced in this report. Typical deflection sensitivity is 350 v/cm; this varies somewhat from record to record since the same configuration was not used for all recordings. The deflection field was approximately 16 kv/cm. All records were made with air blown across the ink stream.

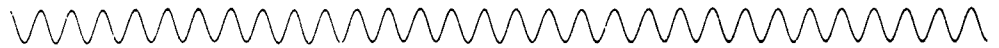
For the oscillograms reproduced in Fig. 27, the rate at which ink is delivered to the record surface is controlled by the instantaneous-input-signal derivative. The excellent definition of these relatively low-frequency recordings results from the diversion and interception of excess ink which would otherwise blur the recorded trace. Chart speed is 2.5 cm/sec for the 1.0- and 5.0-cps records, and is 54 cm/sec for the remaining traces.

Oscillograms made at higher chart speeds, with no ink diversion, are reproduced in Fig. 28. The records demonstrate the high-frequency performance of the oscillograph. Chart speed may be determined from the given signal data. Ink-drop repetition rates between 62 and 125 kc are represented. Initial jet diameters lie between 0.0024 and 0.0038 cm.

If records of smaller amplitude are acceptable, the frequency response may be increased by increasing the ink-drop-formation frequency. Oscillograms made with a 174-kc ink-drop rate are reproduced in Fig. 29 and demonstrate the highest frequency response attained with the experimental system. Chart speed for these records is 1000 cm/sec.



a. 1.0-cps sine wave



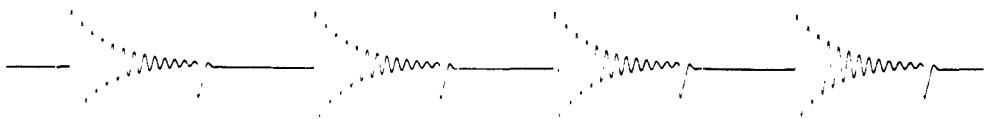
b. 5-cps sine wave



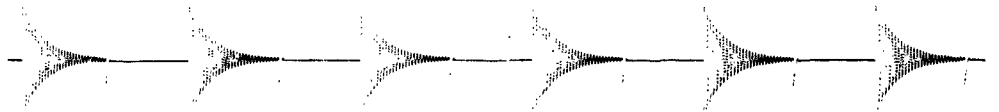
c. 50-cps sine wave



d. 500-cps sine wave

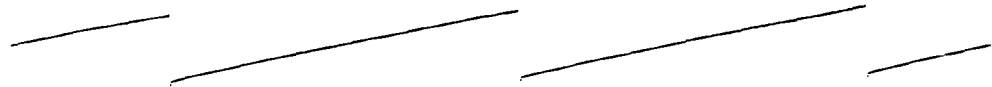


e. 330-cps damped sine wave



f. 1000-cps damped sine wave

FIG. 27. REPRESENTATIVE LOW-FREQUENCY OSCILLOGRAMS .



g. 10-cps sawtooth



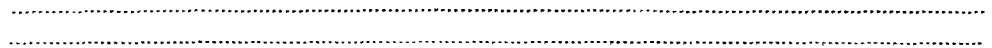
h. 100-cps sawtooth



i. 30-cps square wave



j. 200-cps square wave



k. 500-cps square wave

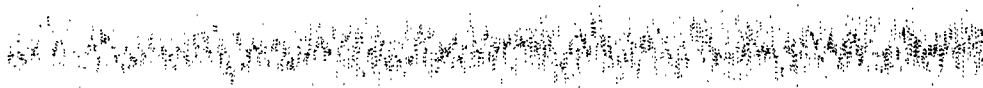
FIG. 27. (continued)



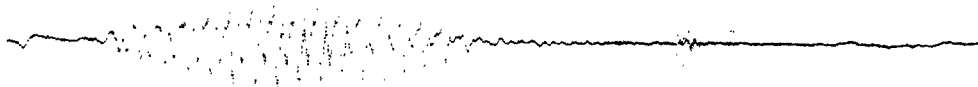
l. Band-limited white noise, 20 - 100 cps



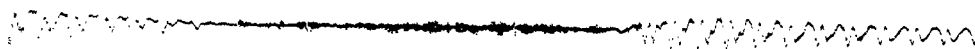
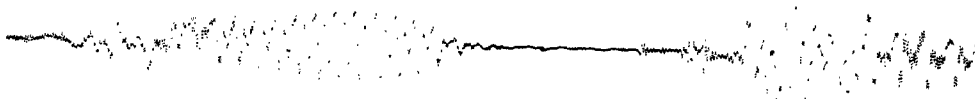
m. Band-limited white noise, 20 - 500 cps



n. Band-limited white noise, 20 - 2000 cps

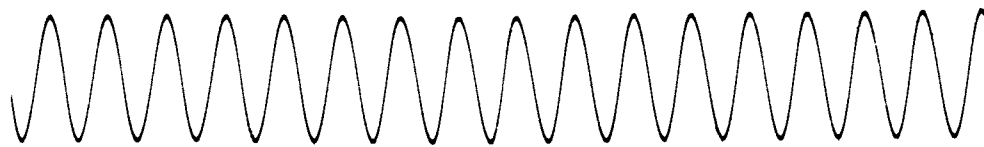


o. Voice recording of the words "ink jet"

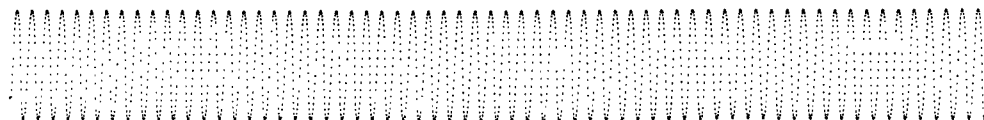


p. Voice recording of the word "frequency"

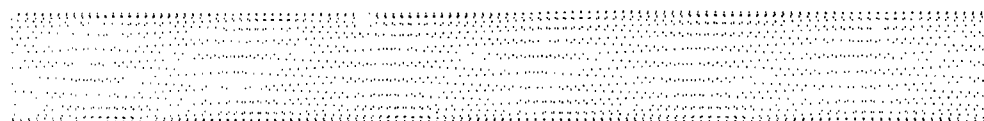
FIG. 27. (continued)



a. 500-cps sine wave



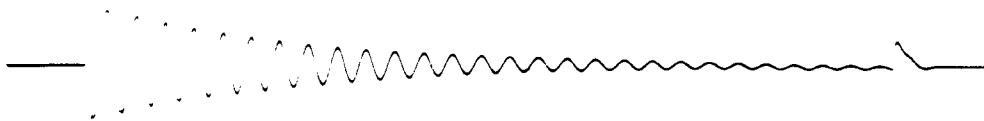
b. 2000-cps sine wave



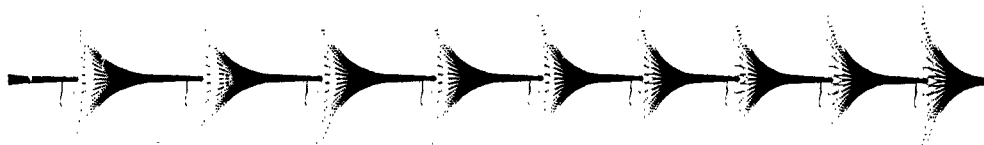
c. 4000-cps sine wave



d. 6700-cps sine wave

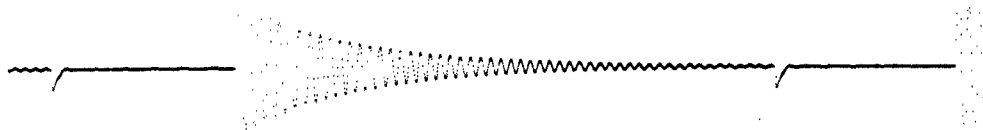


e. 1000-cps damped sine wave



f. 3570-cps damped sine wave, 20-msec period

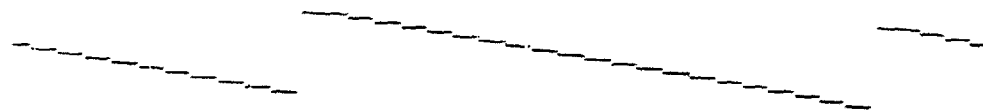
FIG. 28. REPRESENTATIVE HIGH-FREQUENCY OSCILLOGRAMS.



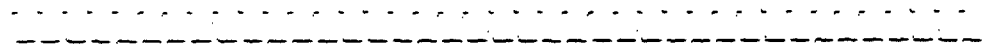
g. 3570-cps damped sine wave



h. 8750-cps damped sine wave



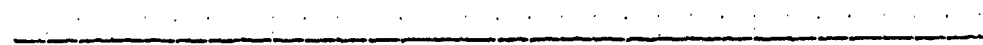
i. 90-cps staircase, 500  $\mu$ sec/step



j. 100- $\mu$ sec pulses, 2000 pps



k. 30- $\mu$ sec pulses, 2000 pps



l. 12- $\mu$ sec pulses, 2000 pps

FIG. 28. (continued)



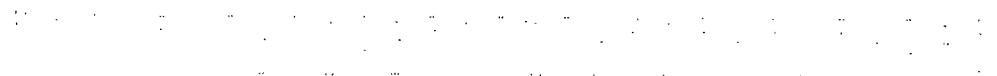
a. 2000-cps sawtooth



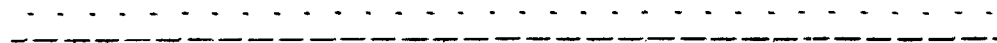
b. 5000-cps sine wave



c. 10,000-cps sine wave



d. 19,300-cps sine wave



e. 50- $\mu$ sec pulses, 2000 pps



f. 7- $\mu$ sec pulses, 5000 pps

FIG. 29. OSCILLOGRAMS DEMONSTRATING MAXIMUM HIGH-FREQUENCY PERFORMANCE.

### III. EVALUATION OF OSCILLOGRAPH AND COMPARISON WITH OTHER TECHNIQUES

This chapter briefly describes the characteristics of other oscillograph techniques, so that they may be compared with the ink-jet system described in this report. The advantages and shortcomings of the ink-jet system are also discussed.

#### A. COMPARISON WITH CONVENTIONAL SYSTEMS

The conventional pen-and-ink or stylus recorders have the advantage of producing high-contrast, permanent traces on a recording medium that is low in cost. However, these recorders are limited in frequency response to, at best, several hundred cycles. The ultimate in mechanical systems is obtained only by using optical techniques so that the mass of the moving parts may be reduced to an absolute minimum. The writing in this instance is done by an intense spot of light directed onto a photosensitive material from a tiny mirror, which rotates in response to the input signal. Oscillographs using this principle are presently manufactured by a number of concerns in a wide variety of configurations, including some very sophisticated systems with large numbers of independent channels. With natural frequencies as high as 8000 cps, these mirror-galvanometer systems are capable of reasonably flat response to 5000 cps with several-inches deflection. Even though spot velocities are over 100,000 cm/sec, readable traces are produced on print-out papers, papers that require no chemical processing. These papers are satisfactory for many applications, but under severe conditions they still lack the high contrast and permanence of image that are obtained with ink traces. The traces do not appear instantly, requiring from a fraction of a second to several seconds to appear with "latensification". Also, the inherent cost of all photosensitive papers is considerably higher than papers that can accept ink traces. Permanent, high-contrast records are possible with photographic materials that require processing; however, this type of operation necessitates inevitable delays and uncertainties.

An ideal solution would be a system that would produce traces on inexpensive paper at frequencies not limited by a mechanically resonant

device that causes the deflection. The oscillograph described in this report has demonstrated, on a laboratory scale, an approach to this ideal. The experimental system is inferior to conventional recorders only in the characteristics of accuracy and maximum achievable deflection amplitude. Although considerable further development is required to produce a manufacturable system suitable for field service, having the reliability and convenience of oscillographs now in use, we believe that this definitely can be done.

#### B. OTHER FLUID-JET SYSTEMS AND RELATED TECHNIQUES

Surface-tension effects in liquid cylinders and jets were studied in the 19th century, and the fact that drops of uniform size could be formed by applying small, regularly spaced disturbances to a cylindrical jet was well known [Refs. 1, 2]. At least one early experimenter, C. V. Boys, electrostatically deflected liquid drops formed this way, using a piece of electrified sealing wax [Ref. 2]. A laboratory demonstration model of a cathode-ray oscillograph, developed by H. M. Waage, utilizes water drops as "electrons" [Ref. 4]. Laboratory studies of the mechanisms involved in cloud and rain formation have prompted an interest in methods of producing small water drops having controllable diameter and electrostatic charge. Some of the techniques that have been used in these investigations [Refs. 5, 6] are quite similar to those employed in the oscillograph.

A number of direct writing oscillographic techniques utilizing electrostatic and magnetic deflection of fluid streams, drops, or mists have been patented [Refs. 7 - 11]. In all of these systems, the configuration is such that the frequency response is limited by the transit time required for the fluid to traverse the deflecting field. To the author's knowledge none of these systems have been produced commercially.

Liquid-jet oscillographs in which the jet is mechanically deflected are manufactured commercially in Europe [Refs. 9, 12]. In these systems, developed by Dr. Rune Elmqvist of Sweden, a 0.001-cm diameter jet is formed by a small nozzle mounted in a galvanometer movement similar to that used in mirror-galvanometer oscillographs. The galvanometer coil and attached nozzle rotate to produce an angular deflection of the jet

proportional to the input signal. Ink is intercepted on a moving chart spaced a few centimeters from the nozzle. Frequency response of these systems extends to 1.0 kc for a peak-to-peak deflection of 1.8 cm.

#### C. MULTIPLE-CHANNEL POTENTIAL

The technique described in this report is particularly appropriate to multiple-channel systems. Fidelity is highest for relatively low deflections, and the excellent trace resolution makes possible good readout accuracies with peak-to-peak deflection amplitudes of as little as 1 or 2 cm. In view of this, a multiplicity of records is easily accommodated on a strip of record paper of reasonable size. The number of separate traces may be increased by allowing overlap of adjacent traces, or even using superimposed traces. This is possible, since the jets may be arranged to cross each other without interference. Colored inks may be used for trace identification.

The small size and simplicity of the portion of the system that launches and charges the ink drops results in attractive configurations for multiple-channel systems. For superimposed channels using a common deflection system, the transducer for synchronizing ink-drop formation may be common to several channels. Systems with channels placed side by side may use a common electrical source for the transducer power and for the dc deflection potential. If ink of the same color is used for each channel, the ink-supply system may be common to all channels.

#### D. ENVIRONMENTAL CONSIDERATIONS

The following environmental factors have not been evaluated in the experimental system, which has been tested only in laboratory environments. The discussion therefore gives only a qualitative idea of their effect on system operation and calibration.

##### 1. Temperature

Temperature affects the important ink properties of viscosity and surface tension and thus the critical process of drop formation. Viscosity also affects the jet velocity and hence the drop size and deflection sensitivity. Storage temperature may be limited by the

freezing temperature of the ink. It should be possible to provide automatic compensation for the effects of temperature variation on drop formation and deflection sensitivity, or to stabilize the ink characteristics by warming the ink to some controlled temperature that is higher than any ambient temperature at which operation is contemplated.

## 2. Pressure and Humidity

The maximum deflection field that may be established is determined by barometric pressure and humidity. Recorded amplitude, for a given percentage distortion, is approximately proportional to the deflection field attainable. Performance of the system is thus reduced at high altitudes.

## 3. Shock and Vibration

The portion of the system that launches and deflects the ink drops may be quite rugged. Electrostatic drop-deflection forces for full deflection are typically several hundred g's; vibration and shock amplitudes, which are small compared with this, can be tolerated during operation. The configuration chosen for the present experimental system is poor in terms of susceptibility of vibration; the nozzle, which is located on the end of a long, unsupported tube, is easily shaken sufficiently at low frequencies to produce spurious deflections. Although the mounting must be flexible at the drop-formation frequency, it should be stiff at lower frequencies, where externally introduced vibration is more likely to be encountered.

## E. PROBLEM AREAS

This section discusses those areas of most concern in applying this technique to a practical recording instrument.

### 1. Stability of Drop-Formation Process

Operation of systems in which a portion of the ink is deflected from the record depends on maintaining a precise phase relationship between the drop-charging pulses and the time of separation of the ink drops from the conducting ink column that extends from the nozzle. The stability of the experimental systems that have been tested, while

adequate for laboratory evaluation, should be improved for a system appropriate for field use. Parameters affecting this stability should be determined and appropriately controlled so that aging or changes in the environment can be accommodated without the requirement for frequent realignment of the system.

The phenomena involved in the formation of "satellite" drops (a small drop in addition to the main drop produced for each vibration cycle) require further investigation. This has been one of the most serious problems encountered in the experimental systems, and was discussed in Section A of Chapter II.

#### 2. Air-Flow-System Size

The undistorted deflection amplitude that can be attained depends on the uniformity with which a flow of air can be maintained across the ink stream. The performance of the experimental air-supply system is adequate, but a great reduction in size is desirable for a practical, portable system. No experimental work has been done to determine the reduction in size that might be attained.

#### 3. Nozzle Clogging

This problem has occasionally caused some difficulty in experimental systems. Clogging due to dirt may be prevented by observing suitable precautions in cleaning components before assembly and including an appropriate final filter. Clogging caused by ink drying in the tip may be prevented by a suitable rinsing system. It should be noted that ink-jet recording systems using the Elmqvist system are presently manufactured by companies in Germany and Sweden and that nozzle stoppage in these systems is not a problem, despite the very small nozzle diameter of 0.001 cm.

#### 4. Stability of Deflection Sensitivity

The stability of the deflection sensitivity is determined by the stability of all the factors entering into the expression for deflection amplitude. No attempt to control all these quantities precisely has been made in the experimental work. Although no fundamental limitations are evident, the large number of interrelated factors that must be controlled may result in a practical limitation to system accuracy.

#### IV. CONCLUSIONS AND RECOMMENDATIONS FOR FURTHER WORK

This chapter summarizes the characteristics of the oscillograph described in this paper, and discusses its potential as a practical recording method that can compete with established techniques. The techniques resulting from this project may have application to other fields, which are briefly discussed.

##### A. SUMMARY OF OSCILLOGRAPH CHARACTERISTICS

The oscillograph described in this report uses an ink jet to form rectilinear records of input signals having frequency components extending to 10 kc or more. The oscillograms reproduced in Figs. 27 to 29 of Chapter II demonstrate the performance obtained with an experimental system. For instantaneous writing speeds up to about 2500 cm/sec the trace is continuous and equivalent, in definition and contrast, to the best traces made with conventional, low-speed, pen or stylus techniques. At higher writing speeds, the trace is a discontinuous series of dots, each representing an independent sample of the input waveform. The spacing between successive dots represents time intervals of 10  $\mu$ sec for the typical drop-repetition frequency of 100 kc.

The deflection sensitivity of the basic system, without amplifiers, is typically 350 v/cm. The input impedance may be several megohms or more, in parallel with a few picofarads.

The deflection characteristic of the oscillograph is not quite linear; the deviation from linearity is a function of the input-signal waveform and results in a limit to the amplitude accuracy obtainable. Records may also have phase or time errors that are waveform-dependent. The experimental system has a deflection characteristic that departs from linearity by less than  $\pm 5$  percent of maximum amplitude and has a timing accuracy of the order of  $\pm 25$   $\mu$ sec. These figures are for a system capable of a peak-to-peak deflection of 2.0 cm and an ink-drop-formation frequency of 125 kc. Better accuracy may be attained in a system having either a lower drop-repetition frequency or a lower maximum trace amplitude. Conversely, percentage error increases as the system parameters

are varied to increase either the drop-repetition frequency or the maximum trace amplitude.

The physical size of the system is determined mainly by the size of the air-flow enclosure required to direct a nonturbulent flow of air across the ink jet. The experimental air enclosure and blower occupy about 2 cu ft, but this volume is unnecessarily bulky. No attempt has been made to determine the size reduction possible. The remainder of the system may be quite compact and rugged; the basic components for producing and deflecting the ink jet typically occupy about a 2-in. cube, exclusive of ink supply, power supplies, and amplifiers.

#### B. POTENTIAL OF INK-JET TECHNIQUE AS A PRACTICAL RECORDING METHOD

A requirement exists for a high-frequency recorder having the convenience and operating economy of conventional low-frequency, direct-writing systems. The experimental system has demonstrated a performance capability that would fill this need and be valuable in a wide variety of practical applications.

The experimental system requires frequent critical adjustments, is inconvenient to operate, and is sensitive to changes in environment. Straightforward engineering solutions to these problems are evident, and it seems probable that a reasonably compact system, having a number of separate channels, could be economically produced and would be suitable for field use.

Additional investigation or development is needed in order to:

1. Increase the stability of the drop-formation process
2. Increase the stability of the factors affecting deflection sensitivity
3. Decrease the size of the air-flow system
4. Design a suitable ink supply and a nozzle-rinsing system
5. Fabricate nozzles of precise size efficiently.

The development effort required is considerable, because of the many diverse problems involved. It should be noted, however, that a different type of ink-jet oscillograph has been successfully commercialized in Europe by manufacturers of the Elmqvist system [Refs. 7 and 10], and that many of the problems involved in the application of tiny, high-speed ink jets to recording systems have been solved in these instruments.

A practical system must have characteristics acceptable to those who use oscillographs. It is evident that the record amplitude and accuracy obtainable with the ink-jet system are appropriate to a wide range of recording problems; however, these characteristics are somewhat inferior to those of other currently available systems. The acceptance of this unconventional technique will thus depend to some extent on the willingness of users to reduce their requirements for trace amplitude and accuracy in order to obtain the frequency response, economy, resolution, and convenience inherent in the ink-jet system.

#### C. APPLICATIONS TO OTHER FIELDS

The techniques described in this report may be used to form, charge, and deflect drops of any low-viscosity conducting fluid. The following paragraphs summarize the significant properties of drop streams produced in this way, and list some possible areas of application.

The drop stream is formed by dividing a cylindrical fluid jet into equal sections which then form a series of drops. Initially, each drop has a velocity equal to the jet velocity. The sections into which the jet is divided are restricted to lengths of approximately three to ten jet diameters. It follows that high drop-formation frequencies require small jets and high jet velocities. Drop-repetition frequencies up to at least 250,000 per second can be achieved, using a jet velocity on the order of 2500 cm/sec, and a jet diameter of 0.002 cm. The resulting drops are about 0.004 cm in diameter. Larger drops can be produced at lower rates. The drop size is precisely determined by the fluid flow rate and the drop-repetition frequency.

The initial size, velocity, and spacing of the drops in the stream are stable and uniform, and the charge of each drop is precisely proportional to the charging potential at the instant of drop formation. An electrical signal is easily derived that is synchronous with the instant of drop formation and charging. The trajectories of drops thus formed and projected through a constant electrostatic field are a precise function of the drop charge. Since the deflection field is constant, arrays of jets may be used with a common deflection field, and the drops associated with each jet may have charges and trajectories

determined by separate, independent, electrical inputs. Streams of drops may be turned "on" or "off" by catching them with a "collector" arranged to intercept drops having specific trajectories.

This report is concerned only with the application of these concepts to high-speed oscillography, and no attempt is made here to ascertain the value of the technique to other fields. It seems likely, however, that extensions of the technique could be applied to high-speed printing and facsimile systems; and to printing or labeling on rough or irregular surfaces.

More general applications include the precise high-speed control of any kind of low-volume fluid flow. The technique can be used to accurately dispense or deposit any solid substance that can be dissolved in a conducting-fluid vehicle, or that is sufficiently fluid and conductive when molten. It should also be of value in studies or applications involving mists, sprays, or fluid-atomization processes.

## APPENDIX A. ANALYSIS OF INK-DROP FORMATION AND DEFLECTION

This appendix presents theoretical relations for the processes of drop formation, evaporation, and charging; and drop deflection by both electrostatic and aerodynamic forces. The derivations involve a number of simplifying approximations, but a rough agreement with experimental results is obtained. The relations may be used to predict approximate performance; they are particularly useful in determining the effects of varying system parameters.

Rational cgs units are employed in the analysis. Electrical quantities are expressed as volts, amperes, and coulombs. Symbols used in the analysis are listed at the end of this appendix, together with appropriate units and conversion factors. A numerical example is given in Section 6 to illustrate the use of the relations and to give an idea of typical magnitudes of the quantities involved.

### 1. Ink-Drop-Stream Formation

The production of a uniform stream of drops involves the formation of a cylindrical jet and the impression of regularly spaced disturbances upon the jet as it forms. Division of the jet at regular intervals, through growth of the disturbances, results in the formation of a series of uniform, spherical drops.

#### a. Jet Formation

A free jet, initially cylindrical in form, is produced by supplying ink, under pressure, to a nozzle with a circular cross section. The required ink pressure is given by

$$P_i = 32\mu_i d_{jo}^2 v_{jo} \int_{l_1}^{l_2} \frac{dl}{d_n^4} + \frac{2\sigma_i}{d_{jo}} + \frac{\rho_i v_{jo}^2}{2} \quad (1)$$

where  $P_i$  is the pressure on the ink in the supply reservoir  
 $v_{jo}$  is the free-jet velocity  
 $d_{jo}$  is the free-jet diameter  
 $d_n$  is the inside diameter of the nozzle or supply tubing  
 $\ell$  is length along the nozzle or supply tubing  
 $\mu_i$  is the ink viscosity  
 $\sigma_i$  is the ink surface tension  
 $\rho_i$  is the ink density

The pressure loss due to friction  $P_f$  in the nozzle and supply tubing is given by the first term of Eq. (1), which is a consequence of the Hagen-Poiseuille law for laminar flow,

$$P_f = \frac{32\mu_i v_p \ell}{d_n^2} \quad (2)$$

This expression applies to uniform pipe flow, with fluid velocity  $v_p$ , for Reynolds numbers not exceeding 2000, which is the case in this application. The first term of Eq. (1) shows that, for a given flow rate, the pressure drop across an incremental distance along the direction of flow is inversely proportional to the fourth power of the diameter. Usually most of the friction loss occurs near the nozzle exit, where the diameter is small and the fluid velocity is high.

The internal pressure of the free cylindrical jet resulting from surface tension is given by the second term of Eq. (1). The third term gives the pressure required to provide the kinetic energy of the jet and is the predominate term if the nozzle is efficient.

#### b. Drop Formation

A free cylindrical jet is in unstable equilibrium, because of surface-tension forces, and must break up into drops. This breakup normally occurs through the growth of minute, random variations in the diameter and results in a random variation in drop size. If regularly spaced varicosities are introduced in a cylindrical jet at suitable intervals, these will grow and "pinch off" the stream at regularly spaced intervals, resulting in drops of uniform size and spacing.

The instability of a fluid cylinder was studied by Rayleigh [Ref. 1], who showed that a small sinusoidal variation of diameter (varicosity) impressed along the length of the cylinder grows exponentially with time according to

$$\Delta d_j = \Delta d_{j0} \exp[I(8\sigma_i/\rho_i d_{j0}^3)^{1/2} t] = \Delta d_{j0} \exp(t/T_j) \quad (3a)$$

where  $\Delta d_j$  = peak variation in jet diameter, resulting from the growing sinusoidal disturbance

$\Delta d_{j0}$  = initial peak variation in jet diameter, resulting from the impressed disturbance

$I$  = "instability factor," which is a function of the ratio of the wavelength of the disturbance to the jet diameter

$T_j$  = time constant for the growing disturbance; this is the time required for the amplitude of the disturbance to increase by the factor  $e$ , or

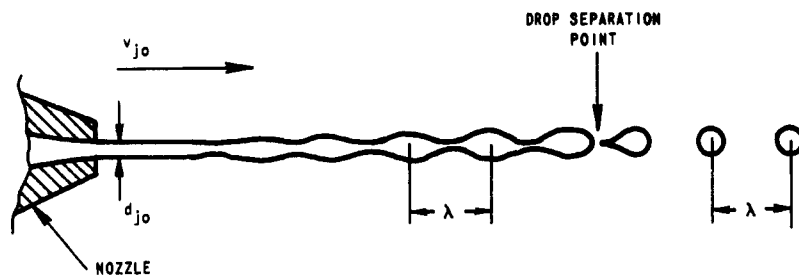
$$T_j = (1/I)(\rho_i d_{j0}^3/8\sigma_i)^{1/2} \quad (3b)$$

The relations (3) may be clarified by referring to Fig. 30. Distance is expressed as the product of initial jet velocity and time  $v_{j0} t$ , and is measured from the initial disturbance point at which  $\Delta d_{j0}$  is given.

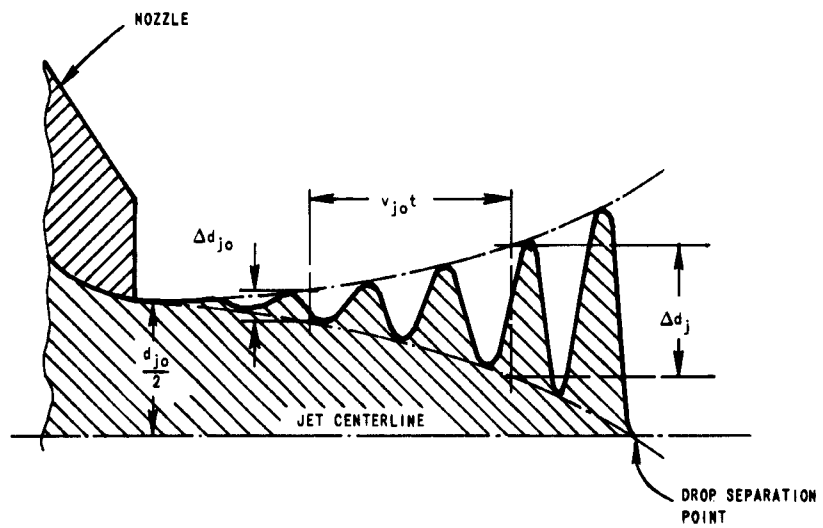
The relationship between the jet instability factor  $I$  and  $\lambda/d_{j0}$ , as derived by Rayleigh, is plotted in Fig. 31. It is evident that the wavelength  $\lambda$  of the disturbance measured along the jet axis must exceed  $\pi d_{j0}$  for growth of the disturbance to occur. The maximum rate of growth occurs for  $\lambda = 4.5d_{j0}$ . The relationship between the frequency of drop formation and disturbance wavelength is given by

$$f_d = v_{j0}/\lambda \quad (4)$$

where  $f_d$  is the drop-formation rate. The system frequency response is proportional to  $f_d$ ; since the minimum  $\lambda$  is equal to  $\pi d_{j0}$ ,  $f_d$  cannot exceed  $v_j/\pi d_{j0}$ .



a. Drop formation



b. Jet profile with magnified radial scale

FIG. 30. JET PROFILE SHOWING DROP-FORMATION PROCESS.

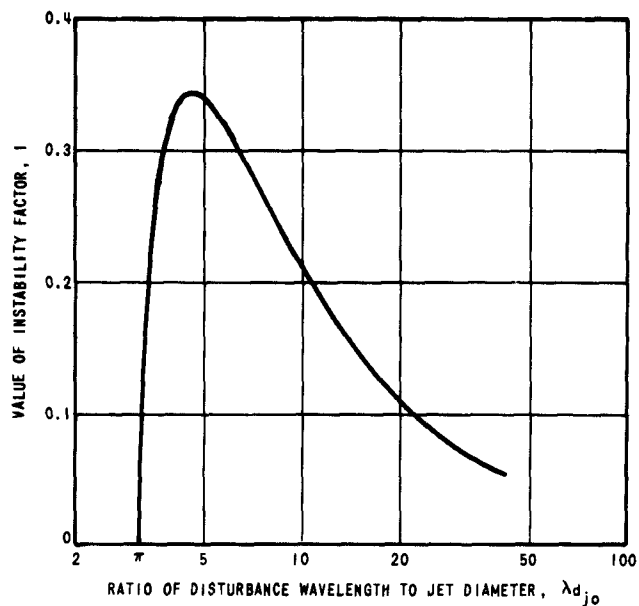


FIG. 31. VARIATION OF JET INSTABILITY FACTOR  $I$  WITH DISTURBANCE WAVELENGTH.

The drop mass  $m_d$  equals the mass of the cylindrical section of jet which forms one drop:

$$m_d = \frac{\rho_i \pi d_{j_0}^2 \lambda}{4} = \frac{\rho_i \pi d_d^3}{6} \quad (5)$$

where  $d_d$  is the drop diameter. Additional useful relationships between  $d_d$ ,  $d_{j_0}$ , and  $\lambda$  are given in Fig. 32.

The value of surface tension appropriate to Eq. (3) may be quite different from that determined from static measurements, unless the liquid is pure [Ref. 13]. A surface-active agent in dilute solution will affect the static surface tension, but time is required for the solute to migrate and form a concentration at a freshly formed surface. The migration time is typically many milliseconds; this is a long time compared to the jet surface lifetime between nozzle tip and the drop separation point. Rayleigh, for example, found that small jets formed with a soapy solution behaved no differently from those of pure water. However, surface active agents will effect the marking characteristics of an ink.

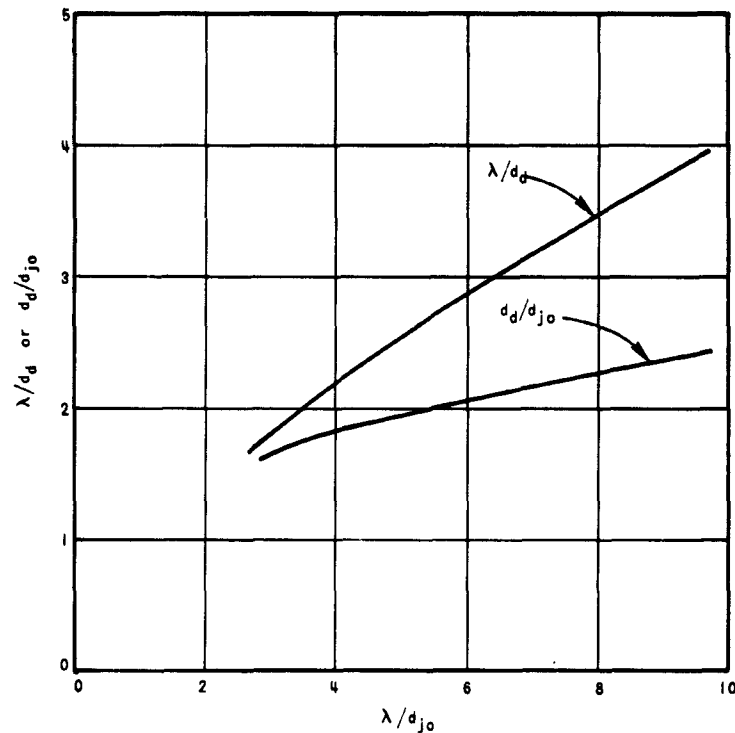


FIG. 32. RELATION BETWEEN JET DIAMETER  $d_{jo}$ , DROP DIAMETER  $d_d$ , AND DROP SPACING  $\lambda$ .

Rayleigh's original analysis assumes that surface-tension forces are opposed by fluid inertia only, and that the effects of viscosity can be neglected. As long as inertial reactions predominate, the only effect of viscosity is to reduce the rate of growth of the disturbance; the wavelength for maximum instability remains the same. If viscous forces predominate, division of a liquid thread tends to occur at points separated by distances very large compared to the stream diameter, as in the case of honey, or molten glass. A tendency for a liquid cylinder to separate into closely spaced drops may thus be taken as evidence that viscosity effects are small.

Equation (3) assumes a sinusoidal disturbance that is small compared with the stream diameter; the equation is not valid near the point of drop separation. Experimentally, drops separate near the computed point, but each drop is sometimes accompanied by an extra, small satellite drop.

The equation neglects electrostatic forces due to surface charges on the jet produced by the signal-input potential. These forces oppose those of surface tension and, if high enough, may delay or even change entirely the jet breakup mechanism [Ref. 14]. For maximum signal-voltage inputs that can be used in the oscillograph, surface charge does not appreciably affect the jet disturbance growth up to the drop-separation point, but the formation of satellites may be encouraged, to a serious extent, by electrostatic forces in the vicinity of the drop-separation point.

Equation (3) also assumes that the jet cross section is circular, and that the flow is laminar, parallel, and uniform across this cross section. Aerodynamic forces are neglected. The characteristics of actual jets are affected by the convergence angle of the nozzle, sharpness of the edge at the nozzle exit, capillary attraction between the fluid and the nozzle material, and any disturbance of streamlined flow upstream from the nozzle.

#### c. Synchronization of Drop Formation

The initial synchronizing disturbance of the jet may be produced by mechanically vibrating the nozzle along the jet axis, or by varying the pressure of the ink at the synchronization frequency. The resulting velocity modulation of the jet causes a periodic downstream "bunching" of the fluid, as in a klystron microwave amplifier tube. In this case, the "beam"-density modulation manifests itself as a variation in cross-sectional area, since the fluid is not compressible.

The instantaneous jet velocity  $v_j$  at the nozzle may be expressed by

$$v_j = v_{j0} + v_n \sin(2\pi f_d t) , \quad (6)$$

where  $v_n$  is the peak amplitude of the alternating component of jet velocity resulting from the synchronizing vibration or pressure variation. For a vibrating nozzle,  $v_n$  is related to the peak vibration amplitude  $z_n$  by

$$v_n = 2\pi f_d z_n . \quad (7)$$

The bunching process may be visualized by considering the fluid issuing from a vibrating nozzle. At the peaks of nozzle displacement, the nozzle velocity is zero, and the jet-fluid velocity is equal to the average (pressure-induced) velocity  $v_{jo}$ . A section of fluid that issues at the instant of negative peak displacement of the nozzle (maximum displacement opposite to jet-flow direction) is preceded by fluid going slower than average, and followed by fluid going faster than average. Downstream, the fluid "piles up" about these sections of the jet that issue once each vibration cycle.

If  $v_n \ll v_{jo}$ , an analysis analogous to that applied to beam bunching in a klystron [Ref. 15] shows that sinusoidal velocity modulation of the stream produces a sinusoidal, growing variation in cross-sectional area that increases linearly with time, and with distance from the nozzle, according to

$$\frac{\Delta A_j}{A_{jo}} = \left( \frac{v_n}{v_{jo}} \right) 2\pi f_d t, \quad (8)$$

where  $\Delta A_j$  is the peak variation in jet cross-sectional area,  $A_{jo}$  is the unperturbed cross-sectional area at the nozzle, and  $\Delta A_j/A_{jo} \ll 1$  [in Ref. 15,  $\Delta A_j/A_{jo}$  corresponds to the ratio of peak klystron fundamental current to the dc current,  $I_1/I_0$ ;  $2\pi f_d t$  to the unperturbed transit angle  $\theta_0$ ; and  $(v_n/v_{jo})2\pi f_d t$  to the "bunching parameter,"  $k$ ]. Equation (8) is a suitable approximation for  $\Delta A_j < 0.5A_{jo}$ . Substituting the approximation given by

$$\frac{\Delta A_j}{A_{jo}} = \frac{(d_{jo} + \Delta d_j)^2 - d_{jo}^2}{d_{jo}^2} \approx \frac{2\Delta d_j}{d_{jo}} \quad (9)$$

into Eq. (8) yields

$$\Delta d_j = d_{jo} \left( \frac{v_n}{v_{jo}} \right) \pi f_d t, \quad (10)$$

where  $\Delta d_j$  is the peak variation in jet diameter.

The rate of disturbance growth due to velocity modulation is constant, while the rate due to surface-tension forces, given by the

exponential relation of Eq. (3), is proportional to disturbance amplitude. The result is a disturbance wave that initially grows linearly, according to Eq. (10), until a critical amplitude is reached; the exponential process expressed by Eq. (3) then "takes over," as illustrated in Fig. 33. This is an approximate analysis, since both surface-tension forces and velocity-modulation effects should be considered simultaneously near the transition point.

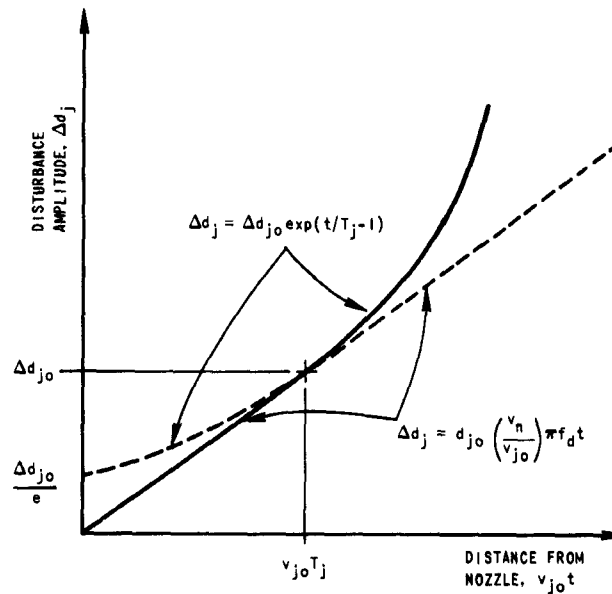


FIG. 33. ENVELOPE OF JET PROFILE SHOWING TRANSITION FROM LINEAR GROWTH TO EXPONENTIAL GROWTH OF DISTURBANCE.

The transition point may be found by equating the derivatives (rates of disturbance growth) of Eqs. (3) and (10) and solving for the time and disturbance amplitude. The results show that the transition occurs at time  $t = T_j$  and the disturbance amplitude  $\Delta d_{jo}$  at this point is given by

$$\Delta d_{jo} = d_{jo} \left( \frac{v_n}{v_{jo}} \right) \pi f_d T_j, \quad (11)$$

where  $T_j$  is the same time constant (associated with disturbance growth due to surface-tension forces) that was defined for Eq. (3). The distance

$z_t$  from the nozzle to the transition point is then equal to

$$z_t = v_{jo} T_j . \quad (12)$$

This value also equals the length of jet, beyond the transition point, in which the disturbance grows by the factor  $e$ . Figure 33 shows that growth beyond the transition point (i.e., for  $t > T_j$ ) follows the exponential relation given by Eq. (3) with  $\Delta d_{jo}/e$  substituted for  $\Delta d_{jo}$ ,

$$\Delta d_j = \frac{\Delta d_{jo}}{e} \exp\left(\frac{t}{T_j}\right) = \Delta d_{jo} \exp\left(\frac{t}{T_j} - 1\right) . \quad (13)$$

The total time to drop separation  $t = T_s$  is the time required for the disturbance to sever the jet. This may be found by setting  $\Delta d_j = d_{jo}$  in Eq. (13) and solving for  $t$ , yielding

$$T_s = T_j \left[ 1 + \ln\left(\frac{d_{jo}}{\Delta d_{jo}}\right) \right] . \quad (14)$$

The distance  $z_s$  to the drop-separation point then equals

$$z_s = v_{jo} T_s . \quad (15)$$

#### d. Evaporation of Drops

Langmuir [Ref. 16] has shown that the evaporation of a small spherical drop in still air may be expressed as a constant rate of change of the surface area  $A_d$ , independent of drop size, according to

$$\frac{dA_d}{dt} = 4\pi D_v \frac{\rho_v}{\rho_i} \quad (16)$$

where  $D_v$  is the diffusion constant of the ink-solvent vapor in air, and  $\rho_v$  is the partial density of the ink-solvent saturated vapor. If the ink solvent is water, the evaporation rate is decreased by the factor  $(1-H)$ , where  $H$  is the relative humidity expressed as a fraction. For water, the evaporation rate in dry air at 20 °C is  $5.2 \cdot 10^{-5} \text{ cm}^2/\text{sec}$ .

The drop velocity, relative to the air, modifies the evaporation rate during transit. The correct value is obtained by multiplying Eq. (16) by an empirically determined correction factor  $k_r$  given by [Ref. 17]

$$k_r = 1 + 0.276 \left( \frac{\mu_a}{D v \rho_a} \right)^{1/3} R_d^{1/2}, \quad (17)$$

where  $R_d = d_d v_{jo} \rho_a / \mu_a$  is the Reynolds number associated with the drop flight,  $\mu_a$  is the air viscosity, and  $\rho_a$  is the air density. For water drops in air at 20 °C,  $k_r = 1 + 0.24 R_d^{1/2}$ .

The fluid loss during flight turns out to be negligible for the parameter magnitudes of interest here, but Eq. (16) is useful in approximating the required record drying time for a record made on a non-absorbent surface at a writing speed high enough so that the individual drops do not merge. The time given by Eq. (16) will be somewhat less than the true value, because evaporation does not take place from the under side of the drop, where it contacts the paper.

## 2. Electrostatic Charging of Ink Drops

The signal voltage is applied between an electrode, capacitively coupled to the ink jet at the point of drop formation, and the continuous conducting jet that extends from the nozzle to this point. Each drop, after it separates from the jet, carries a charge exactly proportional to the signal voltage at the instant of detachment, provided the fluid conductivity is sufficiently high and the capacitance between the separating drop and previously charged drops can be neglected.

### a. Calculation of Drop Charge

Figure 34 shows the drop-charging configuration used in the experimental systems. The charging electrode is physically close to the jet, in order to maximize the coupling capacitance, and is arranged so as to shield the jet between the nozzle and drop-formation point from external fields. Electrical contact to the jet is made through the metal nozzle-supply tubing.

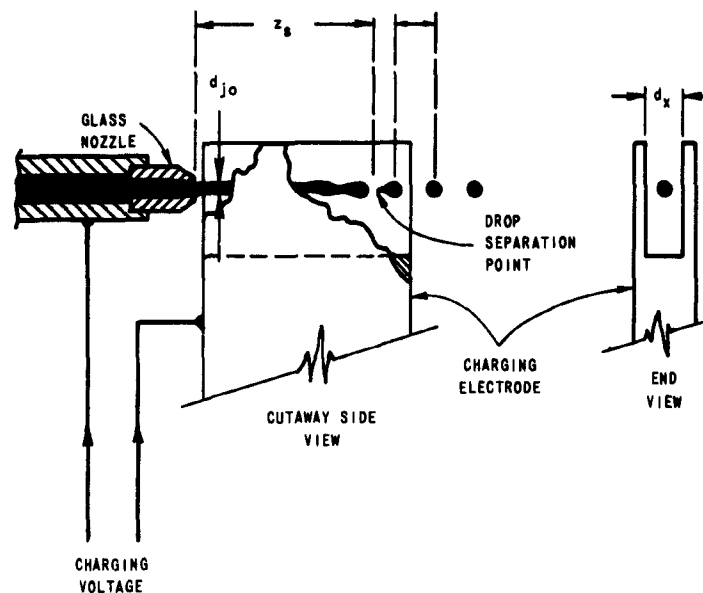


FIG. 34. DROP-CHARGING CONFIGURATION.

The stream of drops extending downstream from the charging point is equivalent to a lumped transmission line with series and shunt impedances that are pure capacitances, as shown schematically in Fig. 35.

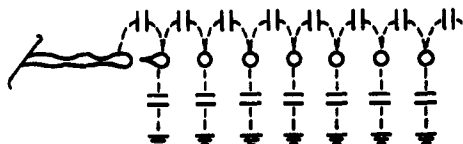


FIG. 35. REPRESENTATION OF DROP STREAM AS A TRANSMISSION LINE.

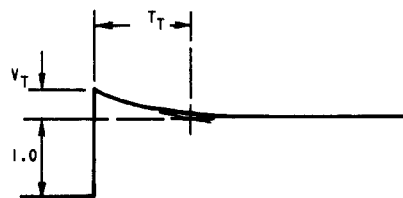
Because of the capacitive coupling between drops, the charge on the drop about to separate is influenced by the charge on the just previously released drop. Charges on drops farther downstream also influence the charge on the separating drop to an extent that decreases rapidly with distance from the charging point.

The drop-to-drop coupling results in a transient-step response having an overshoot, as illustrated in Fig. 36. The overshoot characteristics can be computed if all the capacitances of the equivalent circuit of Fig. 35 are known. This has not been attempted for the

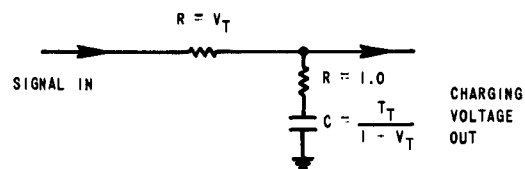
systems described here. The amplitude and time duration of the overshoot are determined experimentally; overshoot amplitude is typically 20 percent, and has a decay time constant of about two drop-repetition periods. Both the magnitude and time duration of the overshoot decrease with decreasing ratio of drop-to-drop capacitance to drop-to-ground capacitance.



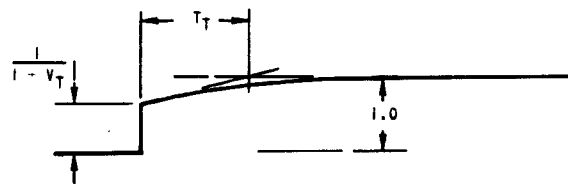
a. Step input signal voltage



b. Uncompensated recorder response



c. Normalized equalizing network



d. Charging voltage for equalized response

FIG. 36. COMPENSATION FOR TRANSIENT OVERTHOOT.

Figure 36 also shows the required signal predistortion for an equalized recorder response and the corresponding equalizing network. Since the charging process is linear, this is the correct equalizing network for any input waveform.

The approximate value of the charge  $q$  induced on the drop about to separate is obtained by neglecting the influence of nearby previously charged drops, giving

$$q = C_i V_i , \quad (18)$$

where  $V_i$  is the potential between charging electrode and nozzle, and  $C_i$  is the capacitance between the charging electrode and the drop being charged.

The charging capacitance  $C_i$  is determined by the geometry of the jet and charging electrode. In the configuration of Fig. 34,  $C_i$  may be approximated by assuming that the jet is the cylindrical center conductor of a transmission line with an outer conductor consisting of two, infinite, parallel plates with spacing  $d_x$ . The capacitance per unit length [Ref. 18] of this configuration is multiplied by  $\lambda$ , the length of the fluid cylinder that forms one ink drop, to obtain an approximate value for the charging capacitance:

$$C_i = \frac{2\pi k_o \lambda}{\ln\left(\frac{4d_x}{\pi d_{jo}}\right)} , \quad (19)$$

where  $k_o$  is the permittivity of free space.

The charging electrode must be symmetrical about any plane through the jet axis. If the system is asymmetric, transverse forces are exerted on the jet which are proportional to the square of the charging voltage, and any resulting deflection produces record distortion.

#### b. Maximum Drop Charge

The maximum achievable drop charge corresponds to the maximum charging voltage for which corona discharge or sparking does not occur in the gap between jet and charging electrode. The surface charge density induced on a separating drop is proportional to the electric field at the drop surface. Because of the small dimensions of a typical charging configuration, electric fields may greatly exceed the usual value determined from data on breakdown of air gaps with spacings on the order of a centimeter.

Similarly, the field at the surface of a very small free drop may be quite high without causing air breakdown. The charge on a free drop remote from neighboring objects is distributed uniformly over the surface, and the resulting radial electric field decreases inversely as the square of the distance from the center of the drop. The field thus drops to one-quarter of its maximum value at one drop radius from the drop surface; although the field lines terminate at points distant from the drop, the air gap over which appreciable field exists is on the order of a drop radius.

The dielectric strength of air is plotted against air gap length in Fig. 37 [Ref. 19]. The data are for parallel electrodes but may be used to estimate maximum fields for the geometries discussed here.

The relation between electric field  $E_d$  at a surface (air dielectric) is a direct consequence of Gauss's law for electrostatics and is given by

$$E_d = \frac{q}{k_o A_d}, \quad (20)$$

where  $A_d$  in this case is the surface area of the ink drop,  $\pi d_d^2$ .

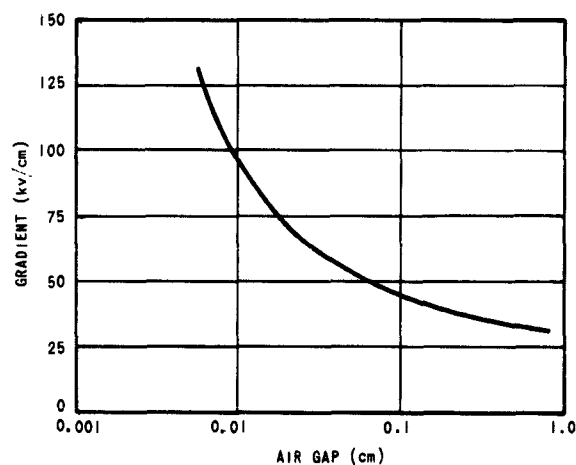


FIG. 37. BREAKDOWN GRADIENT FOR AIR BETWEEN PLANE-PARALLEL ELECTRODES.

The forces due to surface charge on a drop oppose those of surface tension and tend to cause the drop to disintegrate. Rayleigh [Ref. 1] analyzed the situation and determined that the maximum charge, determined by this limitation, is given by

$$q_{\max}^2 = 8 \cdot 10^{-7} \pi^2 k_o d_d^3 \sigma_i . \quad (21)$$

In systems described here, drops are charged as they form, before they attain their final spherical shape. The limiting drop charge must therefore be less than that given by Eq. (21).

c. Drop Charging Time

The continuous column of ink extending from the nozzle to the drop separation point is equivalent to a section of RC transmission line with open-circuit termination. Figure 38 shows the response at the

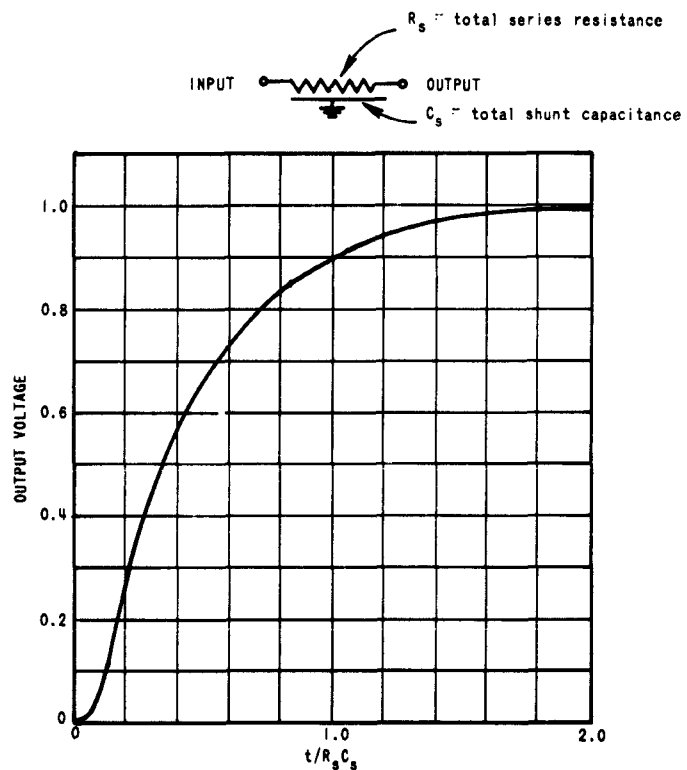


FIG. 38. OPEN-CIRCUIT RESPONSE OF DISTRIBUTED RC TRANSMISSION LINE TO UNIT-STEP INPUT VOLTAGE.

open-circuited end of such a line to a step input. The line is assumed to have uniformly distributed series and shunt impedances that are purely resistive and capacitive, respectively.

The capacitance and resistance of the jet between nozzle and drop-separation point may be computed if the modulation of diameter is neglected and the jet is approximated as a uniform cylinder between two parallel plates. The capacitance of the jet, for the charging configuration of Fig. 34, is then approximately

$$C_s = \frac{2\pi k_o z_s}{\ln\left(\frac{4d}{\pi d_{jo} x}\right)}, \quad (22)$$

where  $C_s$  is the total capacitance between the continuous portion of the jet and the charging electrode, and  $z_s$  is the jet length from nozzle tip to drop-separation point, given by Eq. (15).

Neglecting the resistance of the ink inside the nozzle, the series resistance is expressed by

$$R_s = 4R_i z_s / \pi d_{jo}^2, \quad (23)$$

where  $R_s$  is the total jet resistance between nozzle tip and drop-separation point, and  $R_i$  is the volume resistivity of the ink.

The time  $T_r$  required to charge a drop with a step input from 10 to 90 percent of the final value is, from Fig. 38,

$$T_r = 0.9 R_s C_s. \quad (24)$$

If the full, transient, recording capability of the system is to be achieved without equalization, this time should be short compared with the drop repetition period  $1/f_d$ .

### 3. Deflection of Drops by Electrostatic Field

The trajectories of the charged ink drops between the drop-separation point and the record surface are determined by the initial velocity and by the forces acting on the drops during flight. Ideally, the only appreciable force is that due to a constant electrostatic deflecting field normal to the jet axis. If the field is uniform over the entire

flight path, the trajectories are parabolic and the drop deflection is given by

$$\begin{aligned}
 x &= \frac{1}{2} a_x t_o^2 & (25) \\
 &= \frac{10^7 q E_x z_o^2}{2 m_d v_{jo}^2}
 \end{aligned}$$

where:  $a_x$  is the transverse acceleration of the drop due to the deflecting field

$x$  is the deflection amplitude at the record surface

$q$  is the drop charge, given by Eqs. (18) and (19)

$E_x$  is the value of the deflection field

$t_o$  is the transit time from drop-separation point to record surface

$m_d$  is the drop mass

$z_o$  is the axial distance from drop-separation point to record surface.

For this ideal case, transit time is independent of deflection, since no acceleration of the drops takes place in the direction normal to the record surface. The increased velocity of deflected drops is entirely due to acceleration by the electric field in a direction normal to the jet axis.

The configuration of the actual experimental system is shown in Fig. 39. A high dc potential is established between two parallel deflection plates on opposite sides of the ink stream. It will be shown in Section 5 that fidelity increases with increasing deflection field. The deflection system should, therefore, be designed to establish the maximum field possible across the path traversed by the ink drops. The attainable field is limited to something less than the dielectric strength of air (which is about 30 kv/cm at 1 or 2 centimeters spacing) and the deflection plates are therefore parallel, rather than divergent as in a cathode-ray tube, in order to allow the maximum field to be established through nearly the full length of the system. The minimum clearance between the ends of each deflection plate and the record surface is limited by short circuiting of the field at the record

surface, which may occur through the conducting, recorded trace. The minimum spacing between plates is determined by the requirement that the plates not intercept ink at maximum deflection. For a given deflecting field, the required deflection voltage is proportional to the plate spacing.

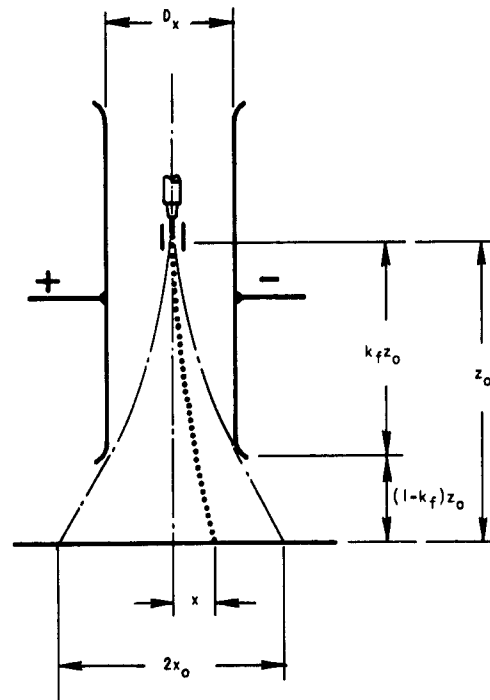


FIG. 39. DEFLECTION-SYSTEM GEOMETRY.

Because the deflection plates do not extend to the record surface, the field is not uniform over the entire flight path. Assuming the field to be uniform between the plates and zero beyond them--that is, neglecting fringing of the field between the ends of the plates and the record surface--Eq. (25) becomes

$$x = \left( \frac{10^7 q E_x z_0^2}{2m v_{jo}^2} \right) k_f (2 - k_f) , \quad (26)$$

where  $k_f$  is the fraction of total flight path from drop-charging point to record surface in the electric field. The maximum peak-to-peak deflection  $2x_0$ , without interception by the deflection system then

exceeds the plate spacing, and is given by

$$2x_o = D_x \left( \frac{2-k_f}{k_f} \right), \quad (27)$$

where  $D_x$  is the deflection-plate spacing.

The continuous free jet between the nozzle tip and the drop-separation point should be shielded from the deflection field to avoid transverse deflection of the jet at the drop-separation point. Such deflection changes the charging geometry and thus introduces nonlinear distortion. Of even more importance is the dependency of this deflection on signal frequency because of the transit time from nozzle tip to drop-separation point; the high-frequency response of the recorder may be appreciably modified if the deflecting field acts on this portion of the jet.

#### 4. Distortion Causes

Additional forces, not considered in the section on deflection, act on the ink drops to produce spurious deflections, or distortion. These forces include mutual electrostatic forces between charged drops and nonuniform aerodynamic forces. Distortion also results from nonuniformities in the deflection field, resulting from fringing effects. A steady force, which acts equally on all drops, does not produce distortion but results in a constant deflection or time delay that can be accommodated in the calibration.

Distortion is analyzed here by first deriving equations for the peak change in drop transit time and deflection resulting from a small perturbing force. The force is assumed to be constant over the flight path taken by a particular drop, but to vary unpredictably in magnitude and direction from drop to drop.

Drop-to-drop variations in aerodynamic and mutual electrostatic forces cannot exceed limits established by the system parameters. Using these maximum force values, limiting expressions are found for the peak spurious deflection.

The effect of deflection-field fringing is discussed, but no analytical treatment is attempted. Finally, in Section 5, the limiting

expressions for spurious deflection are organized so that the effect of system-parameter variation on distortion is evident, and the resulting constraints on system design are discussed.

a. General Small Perturbing Force

Distorting forces on ink drops are assumed to act only in the plane defined by the jet and the deflection axes. Any distorting force may then be resolved into two orthogonal components, which are directed along the jet or  $z$  axis, and along the deflection or  $x$  axis.

The transit time of an ink drop subjected to a constant axial retarding force along the  $z$  axis is given implicitly by

$$z_o = v_{jo} t_o - \frac{1}{2} \frac{F_z}{m_d} t_o^2, \quad (28)$$

where  $z_o$  is the distance from drop-separation point to paper  
 $v_{jo}$  is the initial drop velocity  
 $t_o$  is the transit time from drop-separation point to paper  
 $m_d$  is the drop mass  
 $F_z$  is a retarding force acting along the jet axis, and is constant over the flight path taken by a particular drop, but varies from drop to drop.

Differentiation of Eq. (28) with respect to transit time yields

$$v_{jo} - \frac{F_z t_o}{m_d} - \frac{t_o^2}{2m_d} \frac{\partial F_z}{\partial t_o} = 0. \quad (29)$$

Replacing the differentials by small incremental values yields, for  $F_z \rightarrow 0$ , the approximation

$$\Delta t_o = \frac{t_o^2 \Delta F_z}{2m_d v_{jo}}, \quad (30)$$

where  $\Delta t_o$  represents a small change in total transit time. For small  $F_z$ ,  $z_o \approx v_{jo} t_o$ , and substitution in Eq. (30) yields the desired expression for the change in transit time caused by changing the axial

retarding force from zero to a small constant value  $\Delta F_z$ :

$$\Delta t_o = \frac{z_o^2 \Delta F_z}{2m_d v_{jo}^3} . \quad (31)$$

The deflection of an ink drop subjected to a constant transverse force is given by

$$x = \frac{1}{2} \frac{F_x}{m_d} t_o^2 , \quad (32)$$

where  $x$  is the unperturbed transverse deflection at the record and  $F_x$  is a constant force acting along the deflection axis. Differentiation of Eq. (32) with respect to transit time yields

$$\frac{\partial x}{\partial t_o} = \frac{F_x t_o}{m_d} + \frac{t_o^2}{2m_d} \frac{\partial F_x}{\partial t_o} . \quad (33)$$

Replacing the differentials by small incremental values yields, for  $\Delta t \ll t_o$ , the approximation

$$\Delta x = \frac{F_x t_o \Delta t_o}{m_d} + \frac{t_o^2 \Delta F_x}{2m_d} , \quad (34)$$

where  $\Delta x$  represents a small perturbation in deflection due to a change in transit time  $\Delta t_o$  and an incremental transverse force  $\Delta F_x$ . Combining Eqs. (31), (32), (34), and the relation  $z_o \approx v_{jo} t_o$  yields the desired expression for the change in trace deflection caused by small constant axial and transverse forces  $\Delta F_z$  and  $\Delta F_x$ :

$$\Delta x = \frac{z_o}{2m_d v_{jo}^2} (2x \Delta F_z + z_o \Delta F_x) . \quad (35)$$

Equations (31) and (35) are valid only if the deflecting and perturbing forces are constant during the drop transit time from drop-separation point to paper. Forces that vary during drop flight are not considered here, except that the change in deflection or transit time caused by a small impulsive force is noted to be proportional to the product of

impulse amplitude and flight time after application. It follows that a force acting during the early part of the drop flight causes more deflection than an equivalent force acting near the finish line.

b. Mutual Electrostatic Forces between Drops

Distortion results from mutual square-law attractive or repulsive forces existing between neighboring charged drops. Because of the square-law relationship, mutual forces decrease rapidly with increased drop spacing, and the force on any particular drop may be satisfactorily approximated by considering charges on adjacent drops only.

Maximum distortion occurs when adjacent drops have nearly equal charges. The trajectories of the drops are then similar, and they remain neighbors during the entire journey to the record surface. The smallest spacing between any two drops is equal to  $\lambda$ , the initial drop-to-drop spacing. The maximum force  $F_q$  between two drops is then given by

$$F_q = \frac{10^7 z_o^2 q^2}{4\pi k_o \lambda^2} \quad (36)$$

Equation (36) follows from the force equation for point charges and is an appropriate approximation for spherical drops if the center-to-center spacing exceeds about 1.5 drop diameters. For adjacent drop geometries that are realizable in the oscillograph, Eq. (36) suitably approximates the maximum possible force on a drop.

Assuming that Eq. (36) represents maximum values for simultaneous transverse and axial drop force components  $F_x$  and  $F_z$ , substitution into Eqs. (31) and (35) yields the following limiting values for peak spurious time error and deflection:

$$\Delta t_{oq} = \frac{10^7 z_o^2 q^2}{8\pi k_o m_d \lambda^2 v_{jo}^3} \quad (37)$$

$$\Delta x_q = \frac{10^7 z_o^2 q^2 (2x+z_o)}{8\pi k_o m_d \lambda^2 v_{jo}^2} \quad (38)$$

where the subscript  $q$  indicates effects caused by mutual electrostatic forces. Typical values for these quantities are given in the numerical example in Section 6.

The time and amplitude errors given by Eqs. (37) and (38) are limits that cannot be exceeded. Since the drop displacements resulting from repulsion forces are in a direction to reduce the force, the maximum forces used in deriving the equations are not maintained during the entire transit time. The actual errors are thus considerably less than indicated; they also depend on the geometric relation between the drops during transit, and hence on the signal waveform. The primary value of Eqs. (37) and (38) is their usefulness in relating relative distortion amplitude with variation in system parameters.

Oppositely charged drops attract each other, but this force is opposed by the deflecting field, which acts to separate them. If the deflecting force predominates, the attractive force is appreciable for only a brief interval and the resulting distortion is small. If the attractive force predominates, the drops merge and then follow a trajectory determined by the total resulting charge. Usually, the maximum drop charge is limited to values giving moderate distortion resulting from repulsion effects between drops with like charges. Attractive forces for drops with opposite charges of this magnitude are, in general, then insufficient to produce merging and may be neglected.

Drops should enter the deflecting field immediately after charging, to minimize the merging tendency. For this reason, the charging electrode (see Fig. 34) should not extend appreciably beyond the drop-separation point.

#### c. Aerodynamic Forces

Aerodynamic drag causes an axial deceleration of the ink drops during flight. Because the decelerating force varies from drop to drop, the drop transit time is nonuniform and distortion results. The analysis that follows pertains to the basic system, with no relative motion between the nozzle and ambient air; no analysis is attempted for systems that reduce aerodynamic distortion by utilizing a moving air stream or

rotating nozzle. Qualitative discussions of these distortion-reducing configurations are contained in Section E of Chapter II, and in Appendixes B and C.

For a sphere travelling in still air, the drag force  $F_a$  due to air resistance is given by [Ref. 20]

$$F_a = \frac{1}{8} c_d \rho_a v_{jo}^2 \pi d^2, \quad (39)$$

where  $\rho_a$  is the air density and  $c_d$  is the "drag coefficient," a dimensionless quantity that depends only on the Reynolds number  $R_d$ , given by

$$R_d = d_d v_{jo} \rho_a / \mu_a, \quad (40)$$

where  $\mu_a$  is the air viscosity. Figure 40 is a plot of the empirically determined drag coefficient for spheres over the range of Reynolds numbers of interest in our application [Ref. 20].

In a stream of drops, travelling in single file, deceleration due to air resistance is reduced because each drop follows in the wake of the preceding drop. In recording a fast waveform, the drops in flight at any instant are travelling along appreciably different trajectories. The air resistance on any particular drop is then a function of its position in

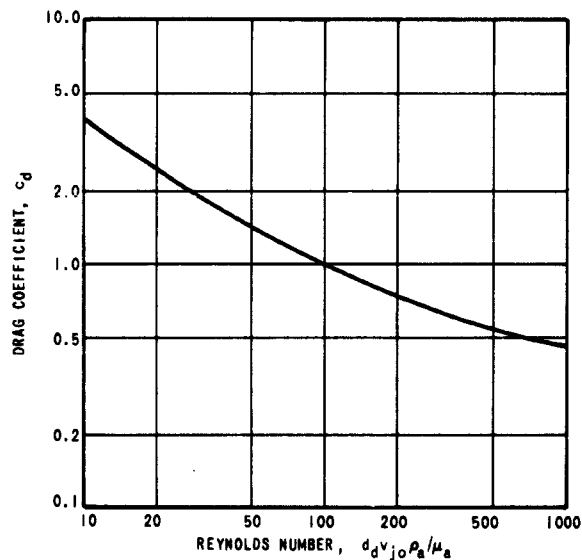


FIG. 40. AERODYNAMIC DRAG COEFFICIENT FOR SPHERE.

the waveform being recorded. For example, in recording a sine wave, the drops near the zero crossings are travelling side by side and are decelerated more than the drops at the peaks, which are travelling in single file. Furthermore, drops just forward of the peaks of the sine wave are more exposed to air drag than those just following the peaks. The result is a bunching of the drops at the peaks, which may eventually result in the touching and coalescence of two or more drops. Figure 41 illustrates the situation.



FIG. 41. DROPS IN FLIGHT FOR SINE-WAVE RECORD, SHOWING REDUCTION IN AERODYNAMIC DRAG NEAR PEAKS.

The difference in force on different drops cannot exceed the value given by Eq. (39). Since this variable force is unidirectional, it represents a peak-to-peak variation; the peak variation from the mean equals one-half of this value and is given by

$$\Delta F_z = \frac{F_a}{2} = \frac{1}{16} c_d \rho_a v_{jo}^2 \pi d_d^2 \quad (41)$$

This force acts along the line of flight. For our analysis the situation is approximated by assuming that the axial component of force  $\Delta F_z$  predominates and that the transverse component  $\Delta F_x$  can be neglected. Substitution of Eq. (41) into Eqs. (31) and (35) then yields the following limiting peak values for spurious time-delay variations and spurious deflections:

$$\Delta t_{oa} = \frac{c_d \rho_a \pi d_d^2 z_o^2}{32 m_d v_{jo}} \quad (42)$$

$$\Delta x_a = \frac{c_d \rho_a \pi d_d^2 x z_o}{16 m_d} \quad (43)$$

where the subscript  $a$  indicates effects caused by aerodynamic forces. Typical values for these quantities are given in the numerical example of Section 6.

Equations (42) and (43) give distortion amplitudes that are much too high because of the drastic assumptions made. They assume that some drops are completely shielded from air resistance and undergo no deceleration, and that others experience the maximum possible aerodynamic drag throughout their entire flight.

Actually, all drops are initially travelling in single file and experience the same minimum (but not zero) aerodynamic force. As signal deflection displaces the drops from the jet axis, some drops become more exposed to aerodynamic drag, and the decelerating force may actually approach the value given by Eq. (40), but only during the latter part of the drop flight. The primary value of Eqs. (42) and (43) is their usefulness in relating the way distortion changes with variation in system parameters. As with mutual repulsion forces, the maximum errors depend on the signal waveform.

#### d. Fringing of Deflection Field

The field in the space between the ends of the deflection plates and the record is nonuniform because of fringing beyond the plate ends. The resulting record distortion is determined entirely by the geometry of the deflection system and the ink-stream trajectory; it is independent of the particular combination of jet velocity, deflection-field magnitude, drop charge, and drop mass, which establishes the trajectory. The field lines intersecting the drop trajectories corresponding to large deflections are concentrated near the plate ends, as illustrated in Fig. 42, and have an axial component which acts to decelerate the drops. The transit time and deflection sensitivity thus increase with deflection amplitude, resulting in both time and amplitude distortion.

For a given deflection-plate configuration and record amplitude, increasing the nozzle to record distance increases the length of uniform field traversed by the drops and hence decreases the distortion from this source.

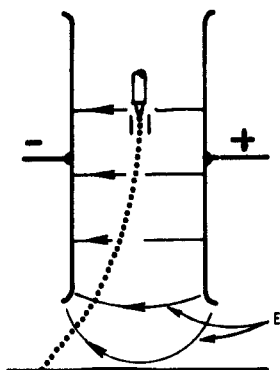


FIG. 42. FRINGING OF DEFLECTION FIELD.

## 5. System Design and Prediction of Performance

Design of an oscillograph involves trade-offs between the desirable characteristics of high-frequency response, high maximum-trace amplitude, low distortion, and small physical size. This section discusses the relations between these characteristics, and presents a rational design approach.

### a. Specification of System Parameters

In specifying parameters for a recording system, one attempts to pick values that provide minimum distortion at the required maximum deflection, a drop-repetition rate sufficient to resolve the maximum input frequency, and an ink-drop size and ink-flow rate that result in a reasonable compromise between trace visibility and resolution at the desired writing speed.

The effect of parameter variation on performance may be clarified by rearranging the limiting distortion equations that were derived in the preceding section. Terms in  $q$ ,  $v_{jo}$ , and  $m_d$  can be eliminated by combining Eq. (25) for deflection (the deflection field is assumed constant over the entire drop path), Eq. (4) for drop-formation frequency, and Eq. (5) for drop mass, with distortion Eqs. (37), (38), (42), and (43), giving

$$\frac{\Delta t_{oa}}{T_d} = \left( \frac{3c_d \rho_a}{16\rho_1} \right) \left( \frac{d_d}{\lambda} \right) \left( \frac{z_o}{d_d} \right)^2 \quad (44)$$

$$\frac{\Delta t_{oq}}{T_d} = \left( \frac{10^{-7} \rho_1}{12k_o} \right) \left( \frac{1}{E_x} \right) \left( \frac{d_d}{\lambda} \right) \left( \frac{d_d}{z_o} \right)^2 (xf_d)^2 \quad (45)$$

$$\frac{\Delta x_a}{x} = \left( \frac{3c_d \rho_a}{8\rho_1} \right) \left( \frac{z_o}{d_d} \right) \quad (46)$$

and

$$\frac{\Delta x_q}{x} = \left( \frac{10^{-7} \rho_1}{6k_o} \right) \left( \frac{1}{E_x} \right) \left( \frac{d_d}{z_o} \right)^3 \left( 1 + \frac{z_o}{2x} \right) (xf_d)^2 . \quad (47)$$

In these equations the peak time errors are expressed as fractions of the drop-repetition period  $T_d$ , and the peak amplitude errors are expressed as fractions of the signal-record amplitude  $x$ . The aerodynamic distortion is for the basic configuration, without relative motion between nozzle and ambient air. As previously explained, actual distortion will be considerably less than indicated by the equations, because of the assumptions made in their derivation.

It is evident from the equations that  $E_x$  and  $\lambda/d_d$  should be as large as possible. The deflection field  $E_x$  is limited by the dielectric strength of air to something less than 30,000 v/cm. The drop-spacing to drop-diameter ratio  $\lambda/d_d$  is limited to values for which drops can be satisfactorily formed; the section on experimental results indicates that the maximum ratio corresponds to a  $\lambda/d_j$  ratio of about 8.0, resulting in a maximum  $\lambda/d_d$  of 3.5 (from Fig. 32). In the following discussion,  $E_x$  and  $\lambda/d_d$  may therefore be considered as constants in the distortion equations.

Values for deflection and drop rate,  $x$  and  $f_d$ , are chosen on the basis of desired system performance. Since fractional distortion increases as the product of these quantities increases, their magnitude is limited by the required system fidelity.

The best jet length  $z_o$  involves balancing the distortion due to the term,  $(1+z_o/2x)$  in Eq. (47), which increases as  $z_o$  increases,

with the distortion due to deflection-field fringing, which decreases with increasing  $z_o$ .

Distortion due to mutual electrostatic drop repulsion increases as the remaining unspecified term  $d_d/z_o$  increases; distortion due to aerodynamic forces decreases as  $d_d/z_o$  increases. Thus, since all parameters except  $d_d$  have been specified, there exists a unique value of  $d_d$  for minimum time or amplitude distortion.

So far, the effect of drop size on trace characteristics has been ignored. Usually, what is wanted is a drop just big enough to produce a distinctly visible dot on the record surface. If the procedure given does not result in a drop near this size, values for  $z_o/2x_o$  and  $d_d/z_o$  will have to be changed somewhat from the previously determined optimum values.

The approximations involved in the distortion equations limit their usefulness to order-of-magnitude estimates in directly determining system performance. The relations are most useful in predicting the effect of changes in a system with experimentally determined performance. If the experimentally determined distortion in a prototype can be correctly divided into electrostatically caused and aerodynamically caused components, and if the contemplated changes are not too large, the performance change caused by a modification of the system should be quite accurately predictable, using Eqs. (44) to (47).

Equations (44) and (46) are not appropriate for making even rough estimates of distortion resulting from aerodynamic effects in systems employing a relative motion between nozzle and ambient air. They may be of some use, however, in predicting the result of parameter changes on aerodynamic effects in these systems.

#### b. Scaling

Any system (including those employing a relative air-nozzle velocity) may be scaled to a larger or smaller size, and the drop trajectories may be predicted exactly on the basis of the prototype performance, if dynamic similarity is maintained. This requires that ratios between air or drop inertia forces  $F_i$  (tendency of mass to resist acceleration), forces due to air viscosity  $F_\mu$ , and electrostatic forces

$F_c$ , not be changed in the scaling process. Gravitational forces may be neglected. It is not necessary to scale fluid-viscosity and surface-tension forces, which affect only the drop-formation process, and not the subsequent drop trajectories. The forces of interest may be generalized by the following fundamental proportionalities:

$$F_i \sim ma \sim (\rho l^3) \left( \frac{l}{t^2} \right) \sim \rho l^2 v^2 \quad (48)$$

$$F_\mu \sim \mu \frac{dv}{dy} A \sim \mu \left( \frac{v}{l} \right) l^2 \sim \mu v l \quad (49)$$

$$F_e \sim Eq \sim \left( \frac{V}{l} \right) (CV) \sim \left( \frac{V}{l} \right) (lV) \sim V^2, \quad (50)$$

where  $l$  or  $y$ ,  $m$ , and  $t$  refer to length, mass, and time;  $A$ ,  $v$ , and  $a$  refer to area, velocity, and acceleration;  $\mu$  and  $\rho$  are gas viscosity and gas or drop density. In the proportionality for  $F_e$ ,  $C$  is the capacitance of some element of the system, which is proportional to linear dimension;  $V$  is potential; and  $E$  is electric field. If the ratios of these forces are to remain constant, the following relations must be satisfied:

$$\frac{l v \rho}{\mu} = \text{Reynolds number} = \text{constant} \quad (51)$$

and

$$\frac{\rho V^2}{\mu^2} = \text{constant}. \quad (52)$$

These relations must hold for any two corresponding points in the scaled system and its prototype, if the systems are to be dynamically similar.

If  $\mu$  and  $\rho$  are not changed, scaling a system by a factor  $r$  involves multiplying all linear dimensions by  $r$ ; jet velocity, air velocity (if an air-flow system is used), and chart velocity by  $1/r$ ; and drop frequency and signal input frequency by  $1/r^2$ . The signal-input voltage and deflection voltage are not changed.

The drop trajectories and recorded traces in the scaled system and its prototype will then be identical, except for scale factor, including perturbations resulting from air drag, mutual electrostatic

drop repulsion, and deflection-field fringing. Frequency responses of the two systems are in the ratio of  $1:1/r^2$ . Scaled electric fields vary as  $1/r$ ; if the deflection field in the prototype is air-breakdown-limited, the deflection field in the scaled system will be less than optimum for  $r > 1$  and will not be realizable for  $r < 1$ .

The scaling concept is particularly valuable in predicting the performance obtainable by reducing the size of an existing system. This is done by measuring the performance of the prototype at reduced fields and voltages appropriate to the contemplated smaller model, and scaling the results.

#### 6. Numerical Example

This section applies the relations derived in this appendix to a typical experimental oscillograph. The basic configuration, which does not provide a relative motion between the nozzle and the ambient air, is used.

##### a. System Specification

The ink (Schaeffer's "Scrip", washable black) is assumed to be a dilute solution in water, with corresponding values of viscosity, surface tension, density, saturated-vapor density, and vapor diffusion coefficient. Temperature and air pressure are taken as 20 °C and 760 mm Hg.

The approximate nozzle profile, somewhat idealized to simplify calculation, and the charging electrode geometry for the experimental system are shown in Fig. 43. The remaining specifications are:

Required peak deflection	$x$	= 0.5 cm
Ink-drop repetition frequency	$f_d$	= 100,000 cps
Drop-spacing-to-diameter ratio	$\lambda/d_{jo}$	= 6.0
Peak nozzle-vibration amplitude	$z_n$	= $5 \cdot 10^{-5}$ cm
Axial distance from ink-drop separation point to record surface	$z_o$	= 2.5 cm
Deflecting field	$E_x$	= 15,000 v/cm
Fraction of ink-drop trajectory exposed to deflection field	$k_f$	= 0.75
Ink-viscosity	$\mu_1$	= 0.01 poise

Ink density	$\rho_i$	=	$1.0 \text{ gm/cm}^3$
Ink surface tension	$\sigma_i$	=	$72.7 \text{ dynes/cm}$
Ink volume resistivity	$R_i$	=	$130 \text{ ohm-cm}$
Partial density of ink-solvent saturated vapor	$\rho_v$	=	$1.73 \cdot 10^{-5} \text{ gm/cm}^3$
Diffusion coefficient of ink-solvent vapor in air	$D_v$	=	$0.239 \text{ cm}^2/\text{sec}$
Air viscosity	$\mu_a$	=	$1.83 \cdot 10^{-4} \text{ poise}$
Air density	$\rho_a$	=	$0.00120 \text{ gm/cm}^3$
Air relative humidity	$H$	=	$0.50 \text{ (50 percent)}$

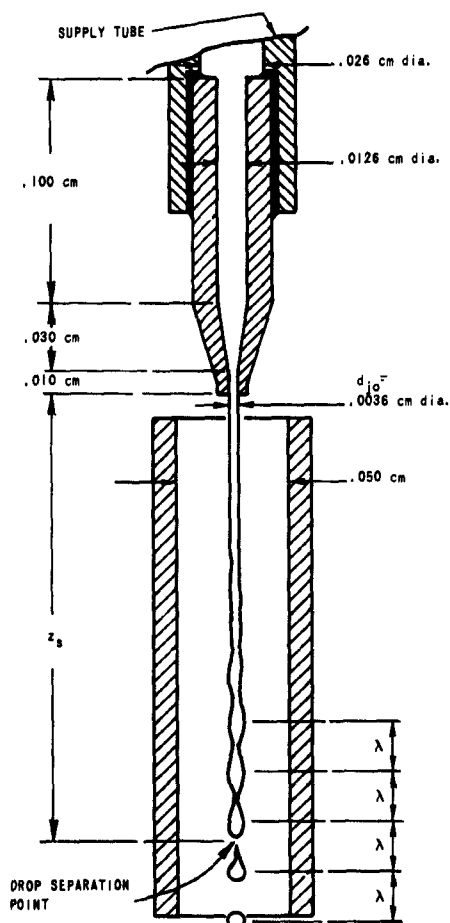


FIG. 43. NOZZLE AND CHARGING-ELECTRODE DIMENSIONS FOR NUMERICAL EXAMPLE. Scale: 35X.

b. Calculated Performance

Initial drop-to-drop spacing	$\lambda$	= 6.0 $d_{jo}$ = 0.022 cm
Initial ink-drop velocity [from Eq. (4)]	$v_{jo}$	= 2200 cm/sec
Ink-drop transit time	$t_o$	= $z_o/v_{jo}$ = 0.00114 sec
Ink pressure [from Eq. (1)] Figure 44 shows how the pressure is divided among friction, surface- tension, and velocity components.	$P_i$	= $32.5 \cdot 10^5$ dynes/cm <sup>2</sup> (47.2 psi)
Peak variation in jet velocity [from Eq. (7)]	$v_n$	= 31 cm/sec
Time constant for jet disturbance growth [from Eq. (3) and Fig. 31]	$T_j$	= $29 \cdot 10^{-6}$ sec
Distance from nozzle to drop separation point [from Eqs. (15), (14), and (11)]	$z_s$	= 0.195 cm
Ink-drop diameter from Fig. 32	$d_d$	= 0.0075 cm
Ink-drop mass from Eq. (5)	$m_d$	= $0.224 \cdot 10^{-6}$ gm

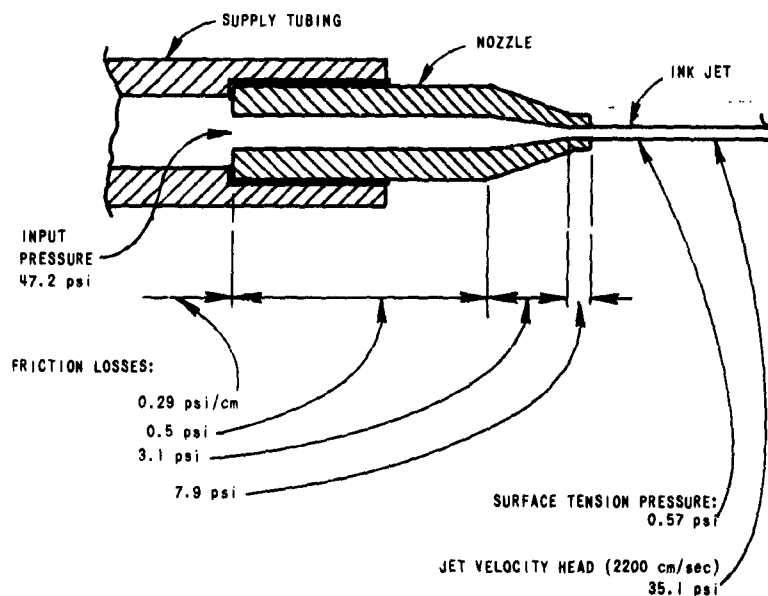


FIG. 44. NOZZLE PROFILE SHOWING CALCULATED INK-PRESSURE COMPONENTS.

Ink flow rate	$m_d f_d = 0.0224 \text{ gm/sec}$ (0.0224 cm <sup>3</sup> /sec)
Ink-drop Reynolds number [from Eq. (40)]	$R = 108$
Initial drop surface area	$A_d = \pi d_d^2$ $= 1.77 \cdot 10^{-4} \text{ cm}^2$
Rate of change of drop surface area in still air [from Eq. (16)]	$dA_d/dt = 2.6 \cdot 10^{-5} \text{ cm}^2/\text{sec}$
Rate of change of drop surface area during flight [from Eqs. (16) and (17)]	$dA_d/dt = 9.1 \cdot 10^{-5} \text{ cm}^2/\text{sec}$
Drop charge for peak deflection [from Eq. (26)]	$q = 1.23 \cdot 10^{-12} \text{ coulomb}$
Electric field at drop surface for above charge [from Eq. (20)]	$E_d = 78,600 \text{ v/cm}$
Charge for which drop disintegrates [from Eq. (21)]	$q_{\max} = 4.62 \cdot 10^{-12} \text{ coulomb}$
Ink-drop "beam current" at peak deflection	$i_j = q f_d$ $= 0.123 \cdot 10^{-6} \text{ amp}$
Drop charging capacitance [from Eq. (19)]	$C_i = 0.00425 \cdot 10^{-12} \text{ farad}$
Input voltage for peak deflection [from Eq. (18)]	$V_i = 290 \text{ v}$
Jet capacitance from charging electrode to continuous jet between nozzle and drop-separation point [from Eq. (22)]	$C_s = 0.0377 \cdot 10^{-12} \text{ farad}$
Jet resistance from nozzle to drop-separation point [from Eq. (23)]	$R_s = 2.49 \cdot 10^6 \text{ ohm}$
Drop charging time [from Eq. (24)]	$t_s = 0.084 \cdot 10^{-6} \text{ sec}$
Summary of drop forces	
Peak deflection force	$F = 10^7 q E_x$ $= 0.185 \text{ dynes}$
Gravitational force	$F = m_d g$ $= 0.00022 \text{ dynes}$
Maximum aerodynamic drag force [from Eq. (39) and Fig. 40]	$F_a = 0.122 \text{ dynes}$
Maximum mutual electrostatic force [from Eq. (36)]	$F_q = 0.028 \text{ dynes}$
Limiting value of peak transit time variation due to aerodynamic forces [from Eq. (44)]	$\Delta t_{oa} = 85 \cdot 10^{-6} \text{ sec}$

Limiting value of peak transit-time  
variation due to mutual electro-  
static forces [from Eq. (45)]

$$\Delta t_{oq} = 32 \cdot 10^{-6} \text{ sec}$$

Limiting value of peak spurious  
deflection due to aerodynamic forces  
[from Eq. (46)]

$$\Delta x_a = 0.075 \text{ cm}$$

Limiting value of peak spurious  
deflection due to mutual electro-  
static forces [from Eq. (47)]

$$\Delta x_q = 0.098 \text{ cm}$$

### c. Experimental Performance

Records made with an experimental system meeting the specifications of Section a. are reproduced in Fig. 45 for sinusoidal input frequencies of 200, 2000, and 20,000 cps. The following system characteristics were measured:

Ink pressure for jet velocity of  
2200 cm/sec

$$P_i = 60 \text{ psi}$$

Time constant for jet disturbance  
growth

$$T_j = 25 \cdot 10^{-6} \text{ sec} \\ (\text{approx.})$$

Peak ink-drop "beam current" for  
deflection of 0.5 cm

$$i_j = 0.17 \cdot 10^{-6} \text{ amp}$$

Drop charging voltage for deflection  
of 0.5 cm

$$V_i = 360 \text{ v}$$

The discrepancy between measured and calculated ink pressures may be attributed to errors made in determining the nozzle profile. Errors in the calculated results, because of approximations made in deriving them, are sufficient to account for the discrepancies with the remaining experimental data.



FIG. 45. EXPERIMENTAL OSCILLOGRAMS FOR NUMERICAL EXAMPLE.

SYMBOLS FOR APPENDIX A

$a_x$	acceleration of ink drop along deflection axis (in $\text{cm}/\text{sec}^2$ )
$A_d$	ink-drop surface area (in $\text{cm}^2$ )
$A_{jo}$	initial ink-jet cross-sectional area (in $\text{cm}^2$ )
$\Delta A_j$	peak variation in ink-jet cross-sectional area (in $\text{cm}^2$ )
$c_d$	aerodynamic drag coefficient for sphere (dimensionless)
$C_i$	capacitance between charging electrode and separating ink drop (in farads)
$C_s$	capacitance between charging electrode and continuous jet between nozzle and ink-drop separation point (in farads)
$d_d$	ink-drop diameter (in cm)
$d_{jo}$	initial ink-jet diameter (in cm)
$\Delta d_j$	peak variation in ink-jet diameter between nozzle and drop-separation point (in cm)
$\Delta d_{jo}$	peak variation in ink-jet diameter at point where exponential jet disturbance growth begins (in cm)
$d_n$	inside diameter of nozzle or nozzle supply tubing (in cm)
$d_x$	ink-drop charging-electrode plate spacing (in cm)
$D_v$	diffusion coefficient of ink solvent vapor in air
$e$	naperian logarithm base ( = 2.7183 )
$E_d$	electric field at drop surface (in $\text{v}/\text{cm}$ )
$f_d$	ink-drop repetition frequency (in drops/sec)
$F_a$	aerodynamic drag force on ink drop (in dynes)
$F_q$	electrostatic force on ink drop, resulting from charges on neighboring drops (in dynes)
$F_x$	force on ink drop along deflection axis (in dynes)
$\Delta F_x$	peak variation in force on ink drop along deflection axis (in dynes)
$F_z$	force on ink drop along jet axis (in dynes)
$\Delta F_z$	small peak variation in force on ink drop along jet axis (in dynes)
$H$	relative humidity (expressed as a fraction)
$I$	ink jet "instability factor" (dimensionless)
$k_f$	fraction of ink-drop trajectory exposed to deflection field
$k_o$	permittivity of free space ( = $8.85 \cdot 10^{-14}$ farads/cm)

SYMBOLS (Cont'd)

$k_r$	correction factor for ink-drop evaporation rate resulting from relative air-drop velocity
$l$	distance measured along length of nozzle or nozzle supply tubing (in cm)
$m_d$	ink-drop mass (in gm)
$P_i$	ink pressure on ink in supply reservoir (in dynes/cm <sup>2</sup> ) (1.0 psi = 68,947 dynes/cm <sup>2</sup> )
$P_f$	ink pressure loss due to friction in nozzle and supply tubing (in dynes/cm <sup>2</sup> )
$q$	ink-drop electrostatic charge (in coulombs)
$R_i$	volume resistivity of ink (in ohm-cm)
$R_d$	Reynolds number (dimensionless) associated with ink-drop velocity ( $= d_d v_{jo} \rho_a / \mu_a$ )
$R_s$	resistance of continuous jet, between nozzle and ink-drop separation point (in ohms)
$t$	time (in sec)
$t_o$	ink-drop transit time, from separation point to record surface (in sec)
$\Delta t_o$	small peak variation in ink-drop transit time, resulting from spurious forces (in sec)
$\Delta t_{oa}$	small peak variation in ink-drop transit time, resulting from aerodynamic drag forces (in sec)
$\Delta t_{oq}$	small peak variation in ink-drop transit time, resulting from mutual electrostatic forces between drops (in sec)
$T_d$	ink-drop repetition period $1/f_d$ (in sec)
$T_j$	time constant for growth of disturbance on ink jet between nozzle and drop-separation point (in sec)
$T_r$	time required to charge ink drop to 90 percent of final value, with step-charging-voltage input (in sec)
$T_s$	ink transit time from nozzle to drop-separation point (in sec)
$v_j$	ink-jet instantaneous velocity at nozzle (in cm/sec)
$v_{jo}$	average ink-jet velocity (equals initial ink-drop velocity) (in cm/sec)
$v_n$	peak variation in ink-jet velocity at nozzle, resulting from velocity modulation (in cm/sec)
$v_p$	ink-flow velocity in nozzle or nozzle supply tubing (in cm/sec)

SYMBOLS (Cont'd)

$V_i$	ink-drop charging voltage between jet and charging electrode (in v)
$x$	ink-drop deflection at record surface along deflection axis (in cm)
$\Delta x$	small peak variation in ink-drop deflection, resulting from spurious forces (in cm)
$\Delta x_a$	small peak variation in ink-drop deflection, resulting from aerodynamic drag forces (in cm)
$\Delta x_q$	small peak variation in ink-drop deflection, resulting from mutual electrostatic forces between drops (in cm)
$z_n$	peak nozzle-vibration amplitude (in cm)
$z_o$	axial distance from ink-drop separation point to record surface (in cm)
$z_s$	length of continuous jet between nozzle and drop separation point (in cm)
$z_t$	distance from nozzle to point where exponential growth of ink-jet disturbance begins (in cm)
$\lambda$	wavelength of disturbance on jet between nozzle and drop-separation point (equals initial spacing between drops in ink-drop stream) (in cm)
$\mu_i$	ink viscosity (in poise) (dyne-sec/cm <sup>2</sup> )
$\mu_a$	air viscosity (in poise)
$\pi$	3.1416
$\rho_i$	ink density (in gm/cm <sup>3</sup> )
$\rho_a$	air density (in gm/cm <sup>3</sup> )
$\rho_v$	partial density of ink-solvent saturated vapor (in gm/cm <sup>3</sup> )
$\sigma_i$	ink surface tension (in dynes/cm)

APPENDIX B. EXPERIMENTAL OSCILLOGRAPH WITH AIR FLOWING COLLINEARLY WITH INK JET

Figure 46 shows the configuration of a recording system in which the ink jet is injected into an air stream that flows in the same direction as the ink. Ideally, the air velocity should match that of the ink drops, thus completely eliminating spurious forces due to aerodynamic drag.

An experimental system has been constructed embodying this principle and is illustrated in the photographs of Figs. 47 through 49. Figure 47 is an overall view of the system. Air, supplied by a vacuum cleaner connected as a blower, enters at the top. The wooden box is a settling chamber that contains transverse silk screens to smooth the air flow. The air then accelerates in the convergent plexiglass enclosure and finally enters a constant-velocity section that has a constant cross-sectional area. The deflecting field is established across this final section, and the ink drops are directed down its axis.

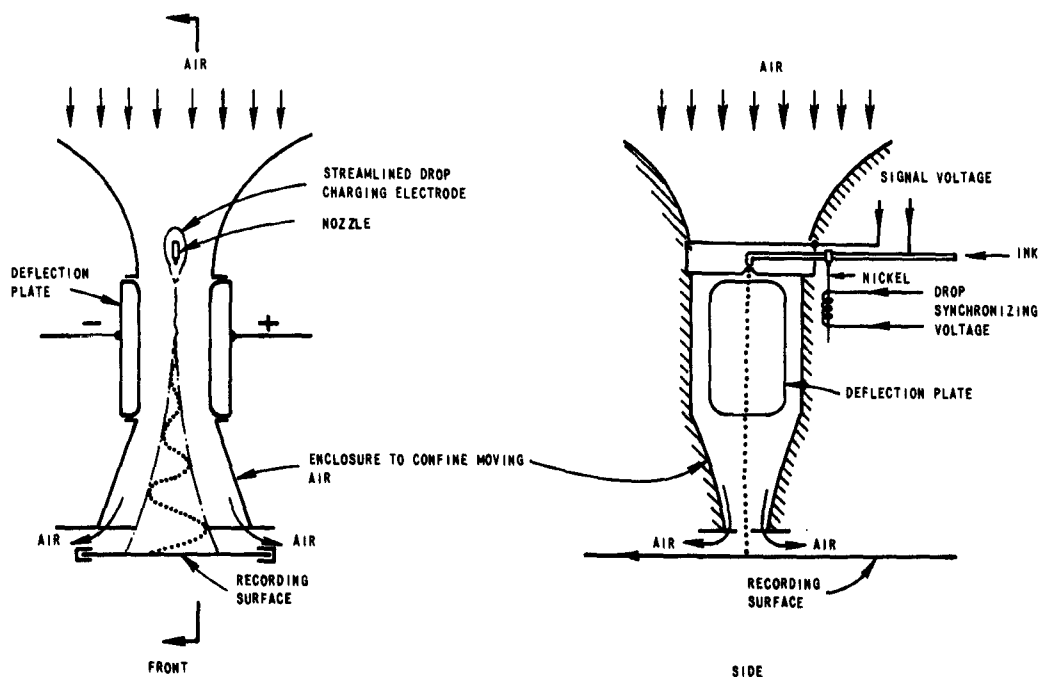


FIG. 46. DIAGRAM OF OSCILLOGRAPH WITH AIR FLOWING COLLINEARLY WITH INK-DROP STREAM.



FIG. 47. EXPERIMENTAL OSCILLOGRAPH WITH AIR FLOWING COLLINEARLY WITH INK-DROP STREAM.



FIG. 48. EXPERIMENTAL OSCILLOGRAPH, PARTIALLY DISASSEMBLED.

The paper transport at the bottom of the photograph advances the record with a variable-speed friction drive.

Figure 48 shows a closeup of the final section of the air enclosure. The hand holds the "ink-drop gun", less charging electrode, which has been separated from the rest of the system. The nozzle is at the end of the tube extending to the left, and points downward; it is vibrated by a nickel magnetostrictive transducer similar to that described in Section A of Chapter II.

Two opposing walls of this section of the air enclosure are formed by the deflection plates. The banana jack extending to the left is the input terminal for one of these plates. The charging electrode for the ink drops is a hollow, metal, streamlined strut positioned across the upper end of the constant-area section of the enclosure; it surrounds the nozzle and drop-formation point when the ink-drop gun is assembled to the system. In Fig. 48 one end of the strut is visible in the enclosure wall that faces the hand.



FIG. 49. CLOSEUP OF EXPERIMENTAL OSCILLOGRAPH.

Figure 49 is a close-up view showing the ink-drop gun assembled to the final section of the air enclosure, the recording paper, and part of the paper guiding and driving system.

Performance of the system at varying air velocities is demonstrated by the oscillograms of Fig. 50. The turbulence of the air stream increases rapidly with air velocity and produces significant random deflections of the ink drops at high air speeds. The optimum air velocity for minimum distortion thus turns out to be considerably less than that of the ink; the resulting relative velocity between the moving air and ink drops causes aerodynamic forces that, although appreciably less than the still-air value, still produce significant distortion.

This system has not been thoroughly evaluated. Work on it was suspended when preliminary tests demonstrated the superiority of a system (described in the body of this report) using air flowing perpendicular to the jet axis. The perpendicular-air-flow system may operate with a lower air velocity; a nonturbulent flow is therefore more easily achieved. Also, the strut enclosing the nozzle in the collinear-air-flow system produces a turbulent wake in the air flowing past it; in the perpendicular-air-flow system, this obstruction in the airway is not necessary.



a. Air velocity: zero



b. Air velocity: 1020 cm/sec



c. Air velocity: 1580 cm/sec



d. Air velocity: 1920 cm/sec

FIG. 50. OSCILLOGRAMS SHOWING EFFECT OF AIR VELOCITY.

For all records:

Ink-drop frequency: 100 kc  
Input signal: 1000-cps sine wave  
200 v peak-to-peak  
Ink-drop velocity: 1880 cm/sec  
Jet length, drop-separation point to paper: 8.0 cm

### APPENDIX C. EXPERIMENTAL OSCILLOGRAPH WITH ROTATING NOZZLE

Figure 51 shows the configuration of a recording system in which the jet-forming nozzle rotates about an axis perpendicular to the jet axis; the record is made on the inside of a cylindrical surface that advances along the rotation axis. Opening up and flattening the record after recording produces the raster display illustrated in Fig. 52. The nozzle rotation results in a different trajectory for each succeeding drop, regardless of signal deflection. Aerodynamic drag is thus constant for all drops, since a drop cannot follow in the wake of another drop, and distortion from this source is eliminated. An additional advantage of this system is the high writing speed obtained along the time axis of the record without the necessity for high paper-transport speeds.

Figure 53 is an overall view of the experimental model. The variable-speed drive motor for rotating the nozzle assembly is located at the bottom of the photograph. Rotation speed is typically 50 rps (3000 rpm).

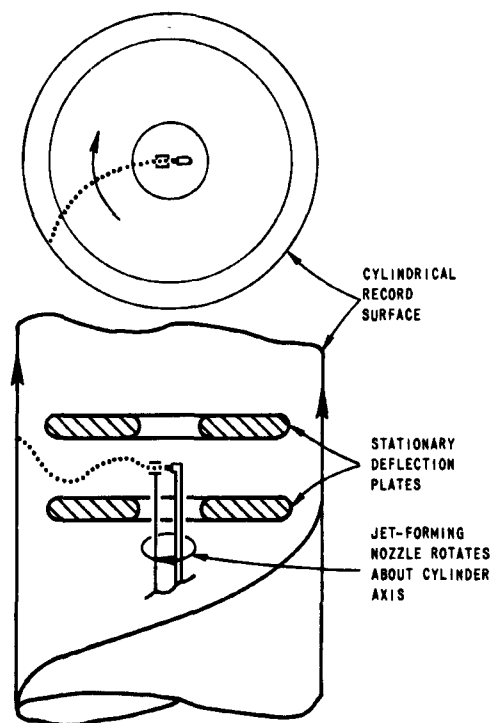


FIG. 51. OSCILLOGRAPH WITH ROTATING NOZZLE AND CYLINDRICAL RECORD SURFACE.

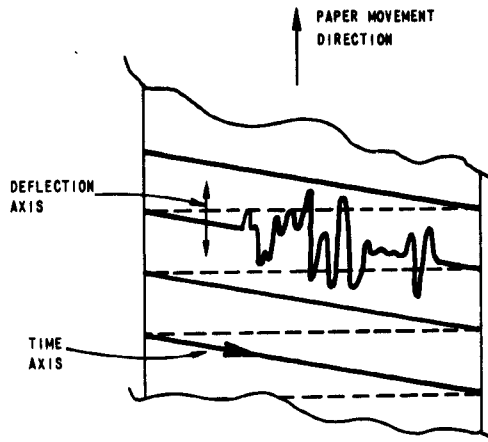


FIG. 52. RASTER PRESENTATION MADE BY ROTATING-NOZZLE OSCILLOGRAPH.



FIG. 53. EXPERIMENTAL OSCILLOGRAPH WITH ROTATING NOZZLE.

Ink, under pressure, is fed through a rotating joint at the lower end of the hollow motor shaft. A cylindrical section of record paper, partially cut away, is in recording position and surrounds the deflection plates and rotating nozzle. The record paper cylinder is 8.25 cm (3-1/4 in.) in diameter. The paper passes inside a cylindrical paper guide that also serves to intercept the ink when no recording paper is present.

Figure 54 shows the recorder with the record paper and outer paper guide removed. The large vertical cylinder serves as an inner paper guide and also houses the rotor that carries the "ink-drop gun". Signal-input and nozzle-vibrator power are supplied through the slip rings near the bottom of the photograph. The rotating nozzle and charging electrode are located midway between the deflection plates, which are two stationary disks visible near the top of the photograph.

Recordings are made on short lengths of paper having a maximum width of 26 cm, which is about 1 cm less than the guide-cylinder circumference.



FIG. 54. EXPERIMENTAL OSCILLO-  
GRAPH WITH OUTER PAPER GUIDE  
REMOVED.

During recording, the paper forms a cylinder having a longitudinal 1-cm gap; the support members for the recorder components inside the paper cylinder pass through this gap. The gap in the record results in the loss of a small fraction of the recorded signal for each nozzle revolution. A record is made by molding the paper to the guide cylinder by hand, and sliding it upward until it is engaged by the rotating friction-drive rollers. The motor-driven rollers then advance the paper at a constant speed.

Figure 55 is a photograph of the paper-drive system, inner paper guide, and lower deflection plate. Two rubber-covered drive rollers engage the paper on opposite sides of the guide cylinder and are geared to rotate in opposite directions. The drive rollers press against idler rollers mounted in the inner guide assembly. Two drive motors are provided, one for high and one for low speeds. The unused motor is uncoupled during operation.

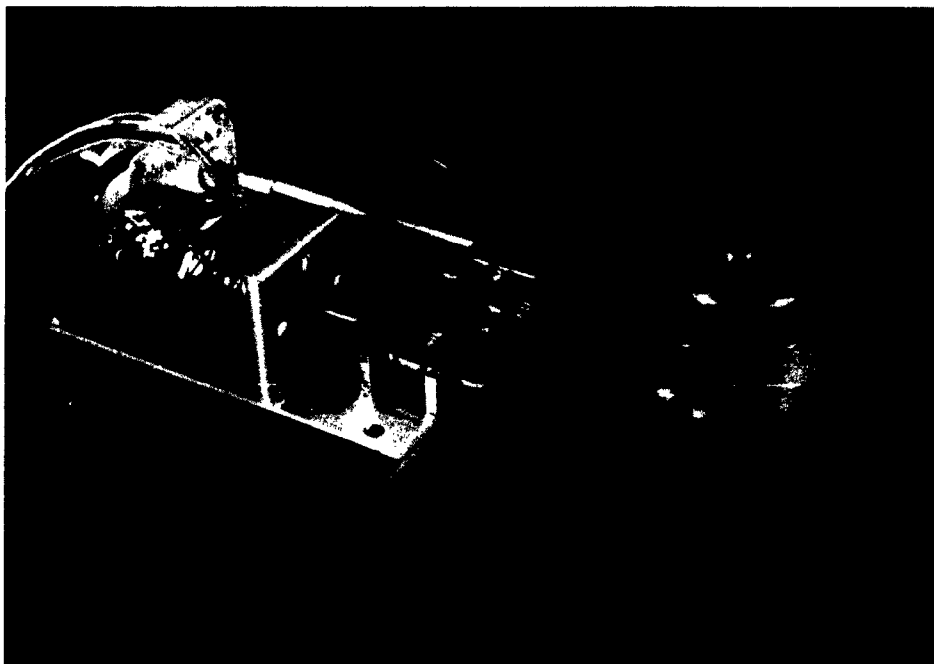


FIG. 55. PAPER TRANSPORT AND INNER PAPER GUIDE.

Figure 56 is a photograph of the rotor and ink-drop gun with the housing (inner paper guide) and deflection plates removed. The ink jet passes between two thin washers (at the top of the photograph) which form the charging electrode. Figure 57 shows the ink-drop gun with cover plate and charging electrode removed. The nozzle points to the right in the photograph and is vibrated by a nickel magnetostrictive transducer similar to that described in Section A of Chapter II.

A section of a record made with this system is reproduced in Fig. 58. The chart velocity (perpendicular to the trace direction) is 50 cm/sec. The effective chart velocity along the trace is due to the nozzle rotation and is 1200 cm/sec. The input signal is a 3750-cps damped sine wave.

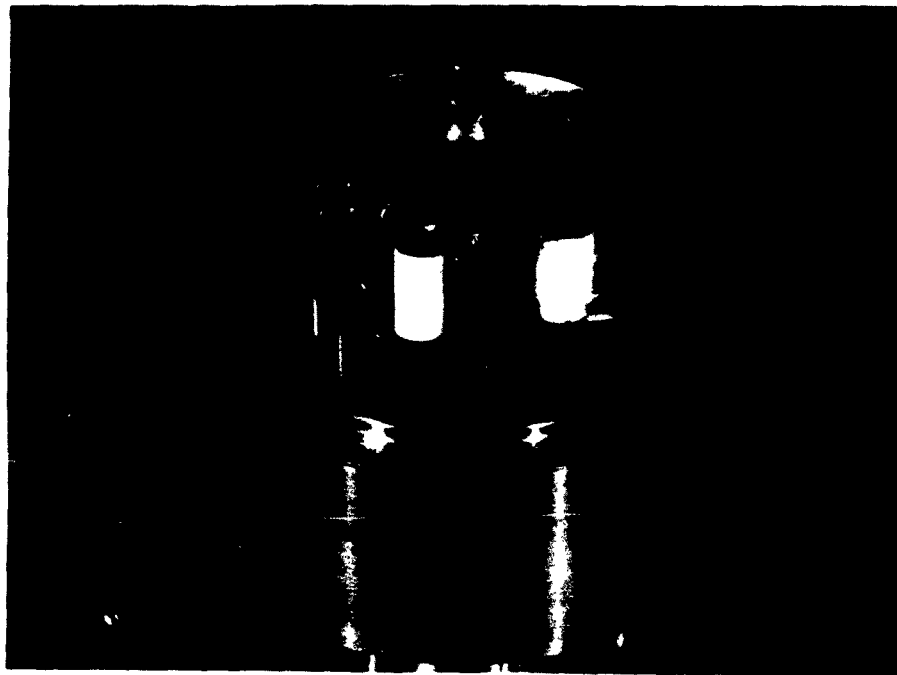


FIG. 56. ROTATING INK-DROP GUN.

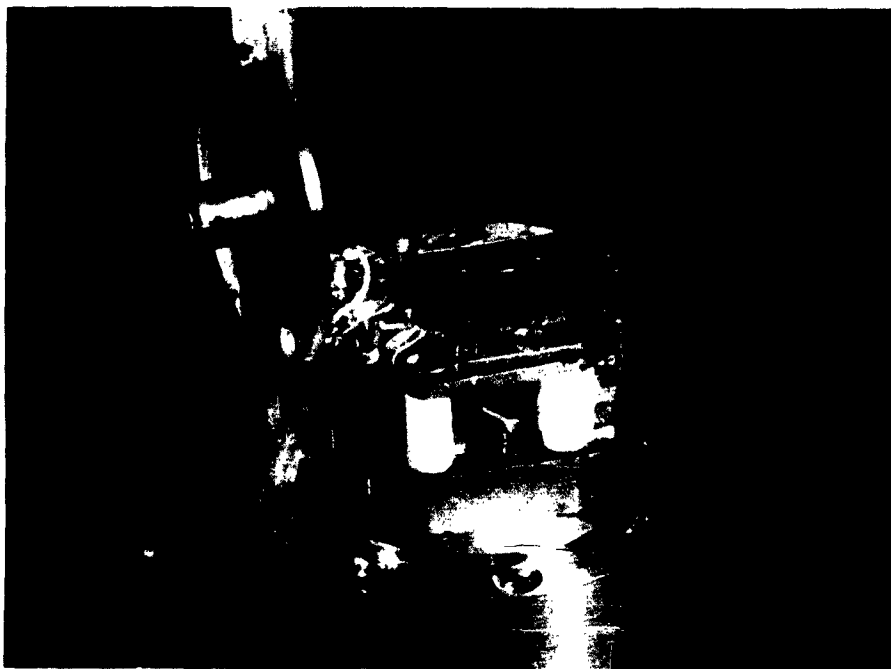


FIG. 57. ROTATING INK-DROP GUN WITH CHARGING ELECTRODE AND COVER  
PLATE REMOVED.

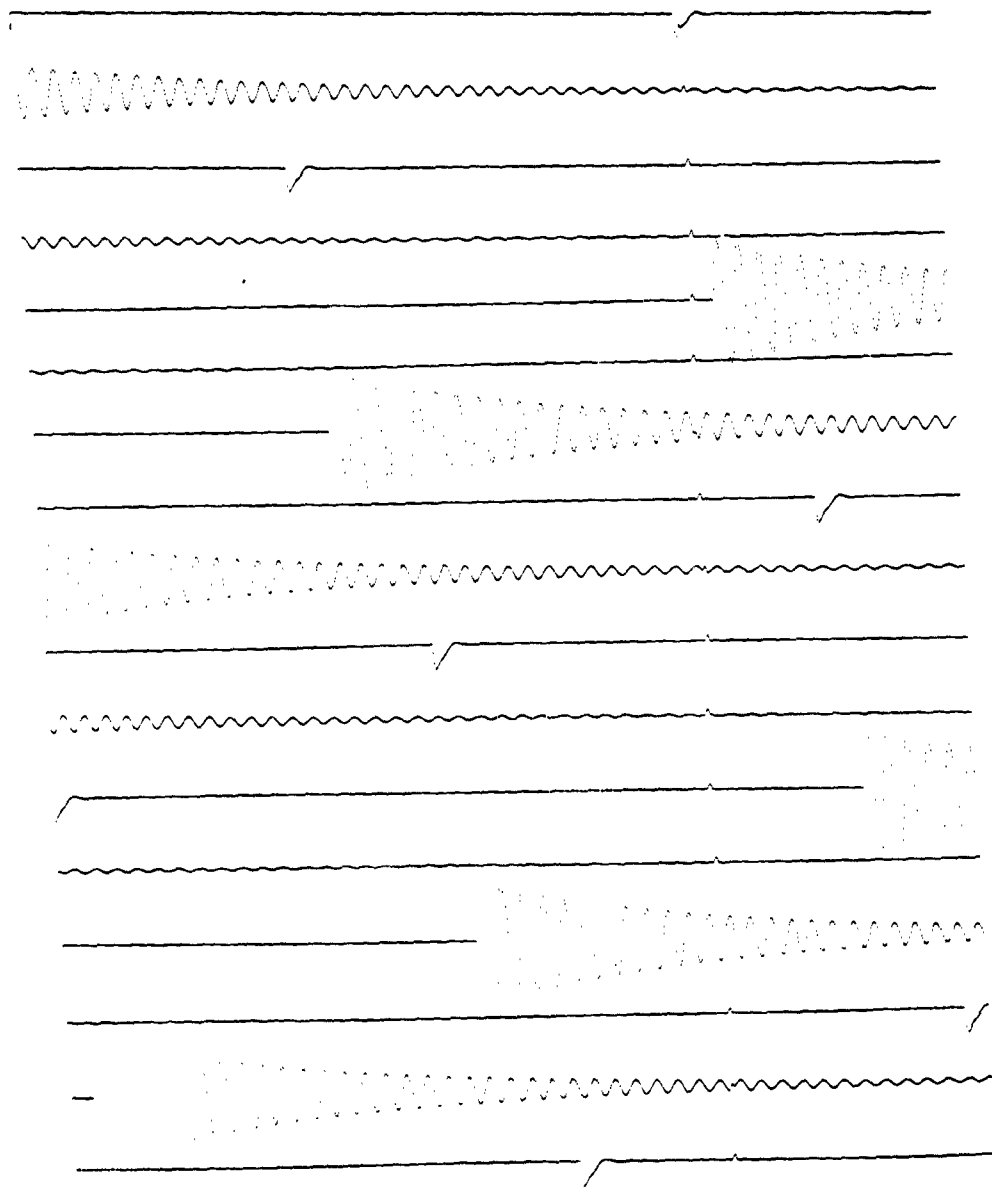


FIG. 58. OSCILLOGRAM MADE WITH ROTATING-NOZZLE OSCILLOGRAPH.

#### APPENDIX D. INK-DROP RATE CONTROL SYSTEM

This is a description and analysis of the system (discussed in Section F of Chapter II) which provides an ink-flow rate proportional to the instantaneous writing speed. The writing speed of the oscillograph is equal to  $[v_x^2 + v_y^2]^{1/2}$ , where  $v_x$  is the component of velocity along the deflection axis, determined by the signal derivative, and  $v_y$  is the chart speed. Ideally, ink drops should be delivered to the record at a rate proportional to this expression.

The system described here adequately approximates the ideal relationship by providing an ink-drop delivery rate which is proportional to the absolute magnitude of the signal derivative plus a constant. The constant is made proportional to the chart speed, and determines the minimum ink delivery rate.

The ink is charged by a pulse voltage that is amplitude modulated by the input signal to be recorded. Each pulse charges one ink drop for the record trace. The ink-drop delivery rate to the record is then proportional to the pulse repetition frequency, as explained in Section F of Chapter II; this frequency is made proportional to the time derivative of the signal voltage plus a constant.

Figure 59 is a block diagram for accomplishing the foregoing. The electronic switch closes whenever its control voltage exceeds a preset threshold. After each switch closure, the next "ink-drop trigger" initiates a pulse in synchronism with an ink drop, which is then amplitude modulated by the input signal. A reset pulse is also generated with each output pulse, which returns the switch control voltage to zero through coupling diodes D3 and D4, and clamping diodes D5 and D6. The pulse repetition frequency of the drop-charging waveform thus equals the switch cycling rate.

If no signal is present, the time required for the control voltage to close the switch is determined by the rate at which C1 or C2 is charged by the dc current  $i_c$ . The value of  $i_c$  thus sets the minimum signal drop frequency, and is made proportional to the chart speed.

Control of the switch by the signal derivative is accomplished by supplying signal voltages of opposite polarity to capacitors C1 and

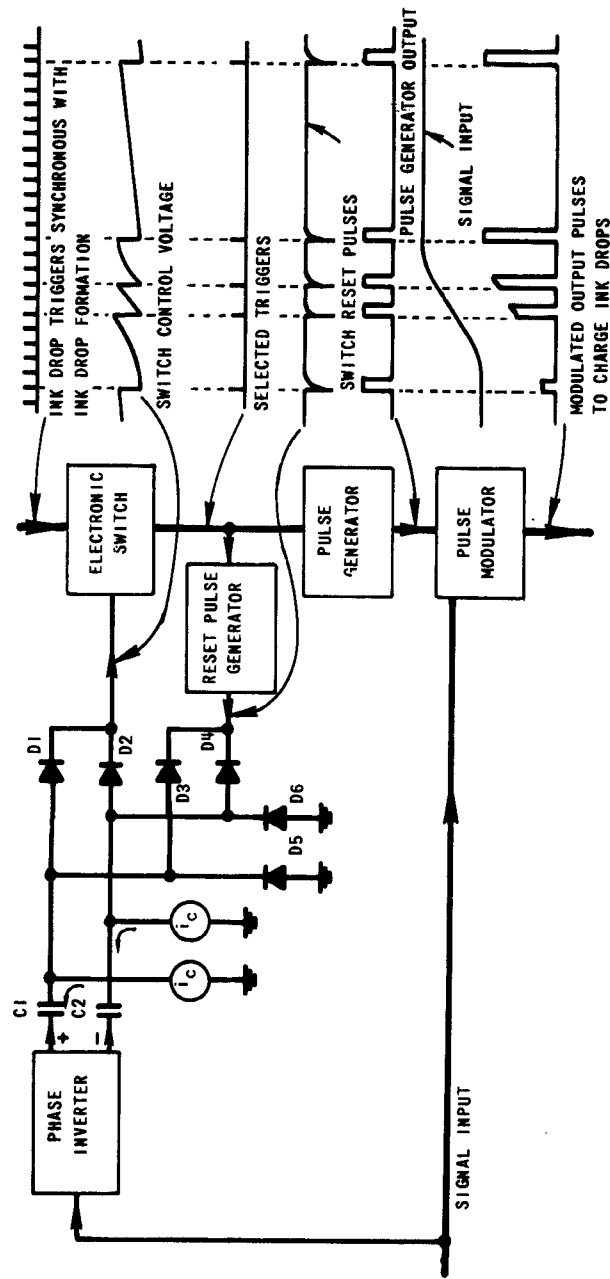


FIG. 59. BLOCK DIAGRAM OF INK-DROP-RATE CONTROL SYSTEM.

C2 via the phase inverter. A positive-going switch-control voltage results from the signal coupling through C1 and D1 (for positive-going input signals), or through C2 and D2 (for negative-going input signals). If the effect of  $i_c$  is neglected, the switch is thus actuated each time the signal voltage changes in either direction by an amount equal to the switch threshold, and the resulting signal pulse rate (up to the limit of the ink-drop repetition frequency at the nozzle) is approximately proportional to the magnitude of the signal derivative. Including the effect of  $i_c$  makes the pulse rate approximately proportional to the signal derivative magnitude plus a constant, which is the desired result. The relation is approximate because a pulse is not initiated at the instant of switch closure; the actual switch-cycling period is increased by the small random time interval between switch closure and the next "ink-drop trigger". The approximation is thus best at low drop-charging pulse rates.

#### REFERENCES

1. Lord Rayleigh, The Theory of Sound, 2nd ed., vol. II, Ch. XX, "Capillarity," Dover Publications, Inc., New York, 1945.
2. C. V. Boys, Soap-Bubbles, their Colours and the Forces which Mould Them, Ch. titled "Liquid Cylinders and Jets," Dover Publications, Inc., New York, 1959, pp. 62-84.
3. B. M. Oliver, J. R. Pierce, and C. E. Shannon, "The Philosophy of PCM," Proc. IRE, **36**, Nov 1948, pp. 1324-1331.
4. H. M. Waage, "Demonstration Experiments with Streams of Water Drops" (abstract), Am. J. Physics, **24**, Sep 1956, p. 478.
5. R. H. Magarvey and B. W. Taylor, "Apparatus for the Production of Large Water Drops," Rev. Sci. Instr., **27**, Nov 1956, pp. 944-947.
6. R. H. Magarvey and B. L. Blackford, "Experimental Determination of the Charge Induced on Water Drops," J. Geophys. Res., **67**, Apr 1962, pp. 1421-1426.
7. F. Schroter, "Signal Recording," U.S. Patent 1,882,043, 11 Oct 1932. Jet recorder, using signal-controlled magnetic field to deflect a fine stream of marking fluid. Deflecting force may be due to magnetic properties of the jet fluid, or field may act on an electric current which is passed through a continuous conducting jet.
8. C. W. Hansell, "Recorder," U.S. Patent 1,941,001, 26 Dec 1933. Jet recorder, using signal-controlled electrostatic field to deflect a fine stream of marking fluid.
9. R. Elmqvist, "Measuring Instrument of the Recording Type," U.S. Patent 2,566,443, 4 Sep 1951. Jet recorder, using a fine stream of marking fluid which emerges from a nozzle attached to the moving coil of a galvanometer movement. Systems using this principle are manufactured as "Mingograf Cardirex" recorders by Elema-Schönander, Industrivägen 23, Stockholm-Solna, Sweden; and as "Oscillomink" oscillographs by Siemens und Halske Aktiengesellschaft, Wernerwerk für Messtechnik, Karlsruhe, West Germany.
10. C. W. Jacob, "Electronic Signal Controlled Recording System and Apparatus," U.S. Patents 2,577,894 and 2,676,868, 11 Dec 1951 and 27 Apr 1954. Facsimile recorder using electrostatically charged spray or mist of marking fluid. Mist is directed through a duct to the recording surface, and turned on and off by electrostatic deflection and precipitation on a wall of the duct.
11. C. H. Richards, "Apparatus for Producing a Stream of Electrically Charged Multimolecular Particles," U.S. Patent 2,600,129, 10 Jun 1952. Method of producing a fine stream of liquid charged droplets by electrostatic forces which act on a liquid surface at the mouth of a nozzle or on the liquid coating a pointed electrode which projects above the free surface of a fluid in a container. Richards suggests subsequent deflection of the drops by signal-controlled electrostatic fields.

12. W. Kaiser, "Oscillomink Direct-Writing Jet Oscillograph," Siemens Review, 26, Aug 1959, pp. 191-194.
13. W. N. Bond and H. O. Puls, "The Change of Surface Tension with Time," Phil. Mag., 24 (supplement), Nov 1937, pp. 864-888.
14. R. H. Magarvey and L. E. Outhouse, "Note on the Break-up of a Charged Liquid Jet," J. Fluid Mech., 13 (Part 1), May 1962, pp. 151-157.
15. K. R. Spangenberg, Vacuum Tubes, Ch. 17, "Velocity-Modulated Tubes, or Klystrons," McGraw-Hill Book Co., Inc., New York, 1948.
16. I. Langmuir, "The Evaporation of Small Spheres," Phys. Rev., 12, Nov 1918, pp. 368-370.
17. N. Frössling, "Über die Verdunstung Fallender Tropfen," Beiträge zur Geophysik, 52, 1938, pp. 170-216. Treatment of the evaporation of falling drops. The article includes an abstract in English.
18. Reference Data for Radio Engineers, "Characteristic Impedance of Transmission Lines," 4th ed., International Telephone and Telegraph Corp., New York, 1956, p. 592.
19. J. D. Cobine, Gaseous Conductors, Par. 7.11, "Spark-Breakdown Field Strength," Dover Publications, Inc., New York, 1958, pp. 173-174.
20. L. Prandtl and O. G. Tietjens, Applied Hydro- and Aeromechanics, Dover Publications, Inc., New York, 1957, pp. 99-101.

SYSTEMS TECHNIQUES DISTRIBUTION LIST  
February 1964

Commanding Officer  
USAEIADL  
Fort Monmouth, N.J.  
1 Attn: SELRA/LNR  
1 Attn: SELRA/DR  
1 Attn: SELRA/NRR  
1 Attn: SELRA/SN  
1 Attn: SELRA/SA  
1 Attn: SELRA/BRD  
1 Attn: SELRA/SEA  
1 Attn: SELRA/SEJ  
1 Attn: SELRA/SES  
1 Attn: SELRA/SEE  
1 Attn: SELRA/SE  
1 Attn: SELRA/ADT  
1 Attn: SELRA/ADO

Commanding Officer  
USAEIADL, Evans Area  
Belmar, N.J.  
1 Attn: Chief, Adv. Tech. Br. SEA

Commanding General, USASCS  
Fort Monmouth, N.J.  
1 Attn: H. Allem, EW Div.

Commanding General  
U.S. Army Missile Command  
Redstone Arsenal, Ala.  
1 Attn: AMSMI-YRT

Commanding Officer  
U.S. Army Signal Missile  
Support Agency  
White Sands Missile Range, N.M.  
1 Attn: SIGWS-MEW  
1 Attn: SIGWS-FC

Commanding General  
U.S. Army Electronics  
Proving Ground  
Fort Huachuca, Ariz.  
1 Attn: Tech. Library

Army Electronics Lab Liaison  
Office-MIT  
77 Mass. Ave., Rm 26-131  
Cambridge 39, Mass.  
1 Attn: RLE Document Room

Army Research Liaison Office  
Lincoln Lab-MIT  
1 Lexington 73, Mass.

Commanding Officer  
Office of Naval Research  
Br. 011.  
1000 Geary St.  
San Francisco, Calif.  
1 Attn: Mr. J. Froman

Director, U.S. Naval Res. Lab  
Washington 25, D.C.  
1 Attn: Code 2027  
1 Attn: Code 5430  
1 Attn: Code 2000

Chief of Naval Operations  
Electronic Warfare Systems Br.  
Washington 25, D.C.  
1 Attn: Code Op-352  
2 Attn: Code Op-0774

Commanding Officer and Director  
U.S. Naval Electronics Lab.  
San Diego 52, Calif.  
1 Attn: Library  
1 Attn: 3060  
1 Attn: 3260  
1 Attn: 3320

Commander  
U.S. Naval Missile Ct.  
Pt. Mugu, Calif.  
1 Attn: N03022

Commanding General  
U.S. Army Materiel Command  
Washington 25, D.C.  
1 Attn: AMCRD-DE-E  
1 Attn: AMCRD-RS-PE-E

Bureau of Naval Weapons  
Dept. of the Navy  
Washington 25, D.C.  
1 Attn: RAAV-11  
1 Attn: RAAV-6

Navy Department  
U.S. Naval Avionics Facility  
Indianapolis 18, Ind.  
1 Attn: Station Library

Director of Res. and Tech.,  
USAF  
Washington 25, D.C.  
1 Attn: AFRT-EE

Chief of Naval Research  
Dept. of the Navy  
Washington 25, D.C.  
2 Attn: Code 463  
1 Attn: Code 427

Chief, Bureau of Ships  
Dept. of the Navy  
Washington 25, D.C.  
1 Attn: Code 362C  
1 Attn: Code 680

Commander, ASD  
Wright-Patterson AFB, Ohio  
1 Attn: ASNPRO  
1 Attn: ASRNR-21, (Mr. Bayliss)  
1 Attn: ASRNR-32  
1 Attn: ASNRR  
1 Attn: ASNPRS-5

Air Force Avionics Laboratory  
Research and Technology Div.  
AFSC, USAF  
Wright-Patterson AFB,  
Ohio, 45433  
2 Attn: AVWW, Capt. J. S. Butto

FTD  
Wright-Patterson AFB, Ohio, 45433  
1 Attn: TDEE  
1 Attn: TDCE, Mr. T. M. Hay, Jr.

Executive Director  
Air Force Office of Scientific  
Res.  
Washington 25, D.C.  
1 Attn: SREE

APGC (PGAPI)  
1 Eglin AFB, Fla.

Commander  
Air Force Missile Dev. Center  
Holloman AFB, N.M.  
1 Attn: MDR

Commander, RADC  
Griffiss AFB  
Rome, N.Y.  
1 Attn: RAWCL  
1 Attn: RAALD, Doc. Lib.  
1 Attn: RALS, J. Fallik  
1 Attn: RALSS, M. Diab  
1 Attn: RAWEC, T. J. Domurat  
1 Attn: RAWED, L. Sues  
1 Attn: RAWE, Haywood Webb  
1 Attn: RAWED

Operations Analysis, SAC  
Offutt AFB, Nebr.  
1 Attn: Mr. E. A. Jackson

Commander, AFSC  
L. G. Hanscom Field  
Bedford, Mass.  
1 Attn: Dr. L. M. Hollingsworth  
Electronic Res.  
Directorate

AF Command and Control Dev't  
Div.  
L.G. Hanscom Field  
Bedford, Mass.  
1 Attn: CCSIL

Commander  
AFCL-ARDC  
L.G. Hanscom Field  
\* Bedford, Mass.  
1 Attn: CRCPV

Hq. USAF (AFRDR-NU-3)  
Rm 4D-335, The Pentagon  
Washington 25, D.C.  
1 Attn: Mr. Harry Mulky

Hq. AFSC  
Andrews AFB  
Washington 25, D.C.  
1 Attn: SCSEI

Department of Defense  
Defense Communications Agency  
Washington 25, D.C.  
1 Attn: 121A, Tech. Library

Director  
Weapons Systems Evaluation Group  
Rm 1E875, The Pentagon  
1 Washington 25, D.C.

Central Intelligence Agency  
\*\*\*2 Washington 25, D.C.

Advisory Group on Electron  
Devices  
346 Broadway  
New York 13, N.Y.  
2 Attn: Harry Sullivan

Advisory Group on Reliability  
of Electronic Equipment  
Office of Asst. Secy. of Def.  
The Pentagon  
1 Washington 25, D.C.

DDC (TISIA)  
Cameron Station  
10 Alexandria, Va.

U.S. Army Materiel Command  
Harry Diamond Labs  
Connecticut Ave. and Van Ness  
St., N.W.  
Washington 25, D.C.  
1 Attn: Library

Director  
U.S. Nat'l Bureau of Standards  
Washington 25, D.C.  
1 Attn: G. Shapiro, Sec. 14.1

Director  
National Security Agency  
Ft. George G. Meade, Md.  
2 Attn: C 3/TDL  
1 Attn: R 304, W. R. Boenning  
1 Attn: C 15  
1 Attn: R 42

Systems Techniques 2-64

Chief  
U. S. Army Security Agency  
Arlington 12, Va.  
1 Attn: IACON

University of California  
Dept. of Electrical Engineering  
Los Angeles, Calif.  
\*1 Attn: C. T. Leondes  
\*1 Attn: R. S. Elliott

University of California  
Laurence Radiation Lab  
P.O. Box 808  
Livermore, Calif.  
1 Attn: Clovis G. Craig, TID

Columbia Radiation Lab  
Columbia University  
536 W. 120th St.  
New York 27, N.Y.  
\*1 Attn: D. L. Harrow

University of Chicago  
Labs for Applied Sciences  
Museum of Science and Industry  
Chicago 37, Ill.  
1 Attn: Librarian  
1 Attn: Central Doc. Control-199

Illinois Institute of Tech.  
3301 S. Dearborn St.  
Chicago 16, Ill.  
1 Attn: Security Officer  
Electronics Res. Lab.

Carlyle Barton Labs  
Johns Hopkins University  
Charles and 34th Streets  
Baltimore 18, Md.  
1 Attn: Librarian

MIT Electronic Systems Lab  
Cambridge 39, Mass.  
1 Attn: J. E. Ward

University of Michigan  
Cooley Electronics Lab  
Electrical Engineering Dept.  
Ann Arbor, Mich.  
1 Attn: Dr. B. F. Barton

Director  
Research Division  
New York University  
New York, N.Y.  
1 Attn: R. F. Cotellessa

The Ohio State University  
Res. Foundation  
1314 Kinnear Rd.  
Columbus, Ohio 43212  
1 Attn: R. A. Fouty

Stanford Research Institute  
Menlo Park, Calif.  
\*1 Attn: External Reports, G-037

ERL, SURC  
P.O. Box 26, University Station  
Syracuse, N.Y.  
1 Attn: T. F. Curry

Defense Systems Lab  
Syracuse University Res. Corp.  
P.O. Box 26, University Station  
Syracuse, N.Y.  
1 Attn: Mr. B. E. Simmons

Defense Research Lab  
P.O. Box 8029  
University of Texas  
1 Austin, Texas

Systems Techniques 2-64

Military Physics Res. Lab.  
University of Texas  
P.O. Box 8036, University  
Station  
Austin 12, Texas  
1 Attn: Mrs. O. G. Williams

Alderman Library  
University of Virginia  
\*Charlottesville, Va.  
1 Attn: J. C. Wyllie

Aerospace Corp.  
P.O. Box 95085  
Los Angeles 45, Calif.  
1 Attn: Dr. Roy Ward

Airborne Instruments Lab  
Walt Whitman Rd.  
Melville, N.Y.  
1 Attn: Librarian

American Electronics Labs., Inc.  
P.O. Box 552  
Lansdale, Pa.  
1 Attn: Librarian

Cornell Aeronautical Labs  
4455 Genessee St.  
Buffalo 21, N.Y.  
1 Attn: D. K. Plummer  
1 Attn: J. P. Desmond, Librarian

Fairchild Semiconductor  
Res. and Dev. Labs  
4001 Junipero Serra Blvd.  
\*Palo Alto, Calif.  
1 Attn: Dr. Grinich

General Electric Co.  
Research Labs  
P.O. Box 1088  
Schenectady, N.Y.  
1 Attn: R. L. Shuey, Mgr.

The Hallcrafters Co.  
4401 W. 5th Ave.  
Chicago 24, Ill.  
1 Attn: Security Librarian

HRB-Singer, Inc.  
1 State College, Pa.  
1 Attn: Conrad L. Welch  
2 Attn: Richard Mollo

Hughes Aircraft Co.  
Documents Center  
Bldg. 6, Rm C2048  
Florence at Teale St.  
Culver City, Calif.  
1 Attn: Tech. Library

ITT Corporation  
ITT Labs Div.  
492 River Rd.  
Nutley, N.J.  
1 Attn: J. LeGrand

ITT Corp.  
ITT Fed. Labs Div.  
500 Washington Ave.  
Nutley, N.J.

Tech. Reports Center  
IBM Corp.  
Space Guidance Center  
Federal Systems Div.  
1 Owego, N.Y.

Jansky and Baily, Inc.  
1339 Wisconsin Ave., N.W.  
Washington 7, D.C.  
1 Attn: Mr. J. Renner

Lockheed Aircraft Corp.  
Scientific Tech. Info.  
Dept. 72-34  
1 Marietta, Ga.

Loral Electronics Corp.  
825 Bronx River Ave.  
New York 72, N.Y.  
1 Attn: Louise Daniels,  
Librarian

Melpar, Inc.  
3000 Arlington Blvd.  
Falls Church, Va.  
1 Attn: Librarian

Motorola, Inc.  
1450 N. Cicero Ave.  
Chicago 51, Ill.

Motorola, Inc.  
Semiconductor Products Div.  
5005 E. McDowell Rd.  
Phoenix, Ariz.  
1 Attn: Military Marketing Dept.

North American Aviation, Inc.  
Engineering Tech. Library  
Los Angeles 45, Calif.  
1 Attn: D. R. Bracha

Packard Bell Electronics  
P.O. Box 337  
1 Newbury Park, Calif.

Packard Bell Electronics  
12333 W. Olympic Blvd.  
Los Angeles 64, Calif.  
1 Attn: Security Officer

Radio Corp. of America  
75 Varick St.  
New York 13, N.Y.  
1 Attn: G. Muligano

Radio Corp. of America  
DEP and DSD Eng. Library, 304/3  
8500 Balboa Ave.  
Van Nuys, Calif.  
1 Attn: L. R. Hund, Librarian

The RAND Corp.  
1700 Main St.  
Santa Monica, Calif.  
1 Attn: Librarian

Raytheon Co.  
406 E. Gutierrez Ave.  
P.O. Box 636  
1 Santa Barbara, Calif.

Revere Copper and Brass, Inc.  
Foil Div.  
196 Diamond St.  
Brooklyn 22, N.Y.  
1 Attn: Vincent B. Lane

Sanders Assoc., Inc.  
95 Canal St.  
Nashua, New Hampshire  
1 Attn: Mr. G. Steeg

Scope, Inc.  
121 Fairfax Dr.  
1 Falls Church, Va.

Smyth Res. Associates  
3555 Aero Court  
San Diego 11, Calif.  
1 Attn: Security Officer

Sperry Gyroscope Co.  
Division of Sperry Rand Corp.  
Great Neck, N.Y.  
1 Attn: Mail Sta F-7  
(Mr. K. H. Barney)

Sperry Microwave Electronics Co.  
P.O. Box 1828  
Clearwater, Fla.  
1 Attn: Dr. J. E. Pippin

Lockheed Electronics Co.  
Military Systems  
U.S. Highway No. 22  
Plainfield, N.J.  
1 Attn: C. L. Optiz

Commanding Officer  
U.S. Army Signal Electronic Res. Unit  
P.O. Box 205  
1 Mt. View, Calif.

Sylvania Electronic Systems  
Waltham Labs  
100 First Ave.  
Waltham 54, Mass.  
1 Attn: Librarian

Systems Development Corp.  
2500 Colorado Ave.  
Santa Monica, Calif.  
1 Attn: Library, R. Lunney

Ohio University  
College of Applied Sciences  
\*Athens, Ohio  
1 Attn: H. L. Hoffee

Hughes Aircraft Co.  
\*Culver City, Calif.  
1 Attn: Dr. N. I. Hall  
Vice President, Engineer

Space Systems Division  
Air Force Systems Command  
Air Force Unit Post Office  
Los Angeles 45, Calif.  
1 Attn: SSD/S:TRG  
Capt. Robert D. Eaglett

\* Unclassified Reports Only  
\*\* Quarterly Status Reports Only  
\*\*\* Via - Opal Cook